AN ON-THE-BOTTOM SEA GRAVIMETER

by

CHARLES GODDARD WING

B.A., Bowdoin College
(1961)

SUBMITTED IN PARTIAL FULFILLMENT
OF THE REQUIREMENTS FOR THE
DEGREE OF DOCTOR OF
PHILOSOPHY

at the

MASSACHUSETTS INSTITUTE OF
TECHNOLOGY

June 1966

Signature of the Author .....
Department of Geology and Geophysics

Certified by .....
Thesis Supervisor

Accepted by .....
Chairman, Departmental Committee
on Graduate Students

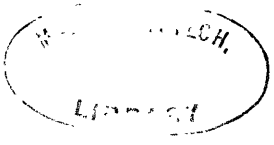

ABSTRACT

AN ON-THE-BOTTOM SEA GRAVIMETER

by

C.G. Wing

Submitted to the Department of Geology and Geophysics on June 1, 1966, in partial fulfillment of the requirement for the degree of Doctor of Philosophy.

90% of the ocean floor lies beyond the reach of present marine gravimeters. For features with dimensions of the same order as the water depth, resolution demands an on-the-bottom profile.

An inertial guidance component, the American Bosch Arma Lot D vibrating string accelerometer was adapted to measure gravity automatically in a free-fall, on-the-bottom vehicle. By special techniques, an accuracy in the range 1-2 mgal was obtained under preliminary operating conditions.

Outlines are presented for two new gravimeters using the vibrating string.

Thesis Supervisor:
Title: Professor of Oceanography

TABLE OF CONTENTS

LIST OF FIGURES

PART ONE

PART TWO

page

PART THREE

APPENDICES

LIST OF TABLES

PART ONE

Part I is a condensation of the thesis, intended primarily for publication.

AN EXPERIMENTAL DEEP SEA BOTTOM GRAVIMETER

Charles G. Wing

Department of Geology and Geophysics

Massachusetts Institute of Technology

Cambridge, Massachusetts 02139

ABSTRACT

An experimental automatic sea bottom gravimeter has been developed using an inertial guidance accelerometer. Operation of the instrument in its various modes should provide criteria for future bottom gravimeters as well as significant geophysical information. Initial tests indicate the useful accuracy is limited by the free-air and latitude corrections.

INTRODUCTION

With the successful adaptation of land gravimeters to surface-ship gravimetry the applications of deep sea bottom gravimetry have been largely neglected. These applications derive from the bottom gravimeter's higher accuracy and closeness to the source of the anomaly.

Due to the Eötvös effect, the surface-ship gravimeter is capable of ± 2 mgal precision only with precise navigational aids. Since precise navigation is the exception rather than the rule, the usual precision for surface-ship gravimetry is more nearly ± 10 mgal. Bottom gravimetry is not subject to the Eötvös effect and is therefore limited by navigation only through the less critical latitude correction. Open ocean "base stations" for the correction of surface gravity profiles might be established with bottom gravimeters. In addition there are large areas of the ocean over which free-air gravity anomalies are nearly constant. Free-air anomalies for these areas established with few accurate bottom measurements would be of particular value to geodesy.

Dean (1958) pointed out the attenuation of gravity anomaly magnitudes with distance from the source. In the 2 - dimensional case, depth H to a structure of width L acts as a linear filter with frequency response $e^{-H\pi/L}$ on the gravity anomaly. For structures with horizontal dimensions less than the depth, the magnitude reduction can be an order of magnitude. The 3 - dimensional filtering is even more severe. Among such small bottom structures are the proposed Sigsbee Deep salt domes (Ewing, Worzel, and Ewing, 1962) and the suspected Laborador Sea dikes (Godby, et al., 1966). Surface and bottom gravity profiles for hypothetical models of these structures are shown in Figure 1. The signal to noise ratios demonstrate the greater information content of the bottom profiles in each case. The filtering of the alternate dike structure anomalies would probably result in an incorrect structure interpretaion.

Downward continuation with and without smoothing has shown that the operation of continuation using surface-ship quality data is no effective substitute for bottom measurements over such small features.

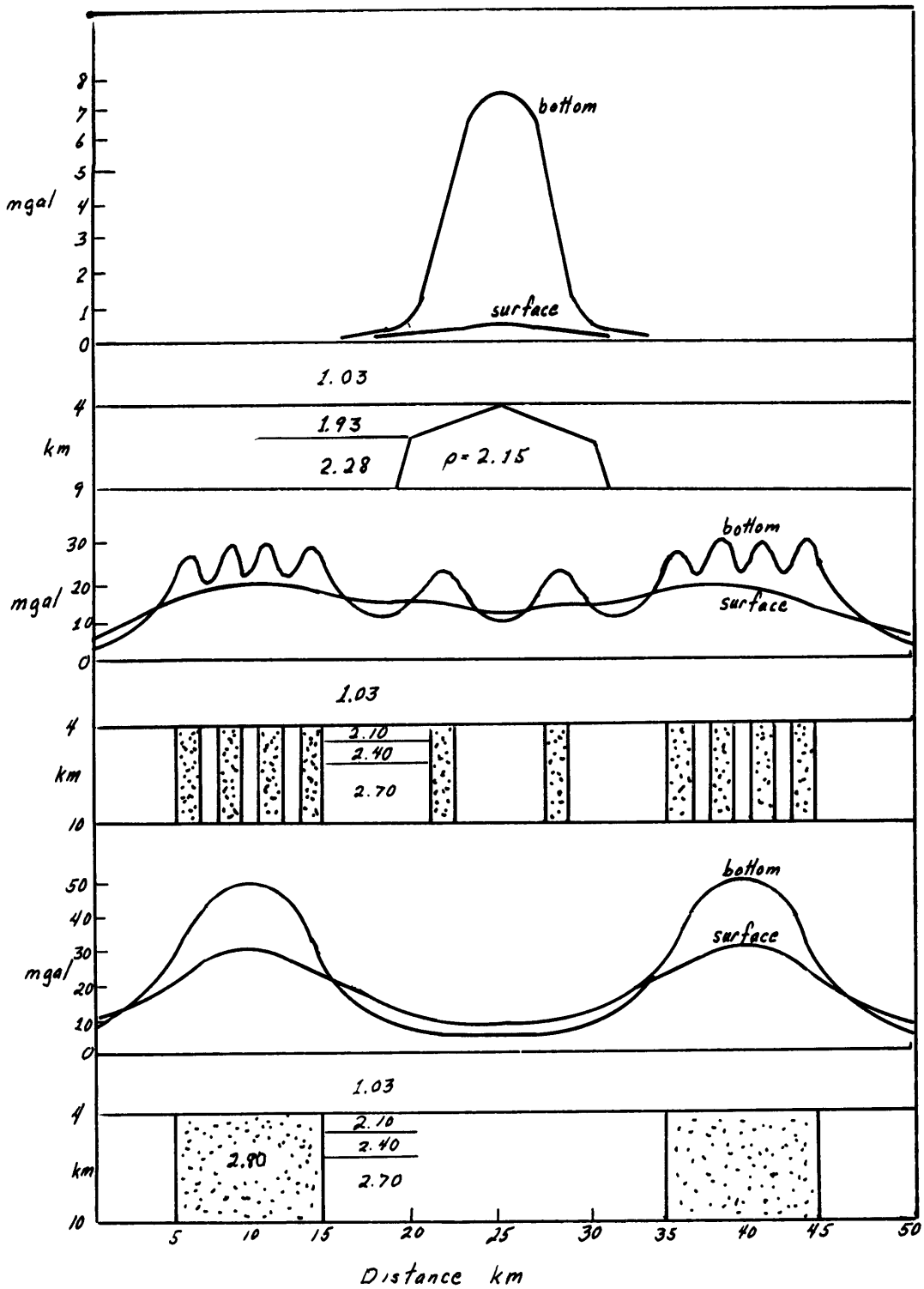

Fig. 1. Surface and bottom gravity profiles over hypothetical models of: a) Sigsbee Deep salt dome, b) Laborador Sea dikes, c) variation of Laborador Sea dikes.

Past Work. Excepting the use of diving bells and deep subersibles, sea-bottom gravimetry to date has been with remotely operated versions of land gravimeters. A depth of 904 m has been achieved by Beyer, et al., (1966) with a modified LaCoste-Romberg underwater gravimeter on a 13 conductor cable. The same method could probably be used at increased depths but Beyer et al. indicate that much greater depths would require substantial gravimeter modification to either single conductor or fully automatic operation.

Deep sea gravimetry on a cable might prove impractical for either of 2 reasons: 1) the difficulty of maintaining the instrument, sensitive to accelerations of 10^{-5} cm/sec^2, at rest on a 5,000 m cable in moving water, or 2) the length of time required in lowering and raising the gravimeter. For these reasons the preset gravimeter was designed to have 3 possible operational modes: 1) remote readout on a cable, 2) fully automatic on a cable, 3) free-fall. The last two modes are presently operational; the first requires the addition of an electrical feed-through only.

THE INSTRUMENT

With reasonable effort, any of the land gravimeters now in use could be fully automated. An automatic digital version of the Worden gravimeter has been developed and the vibrating string borehole meters described by Goodell and Faye (1964) and Howell, Heintz and Barry (in press) would be particularly simple to automate. At the initiation of this project, none of the above instruments had appeared. W. S. von Arx suggested that inertial guidance accelerometers be considered. Many inertial guidance accelerometers have sensitivities in the range of small gravity variations. Considering size, power consumption, and simplicity the American Bosch Arma vibrating string accelerometer (hereafter VSA) was the most appealing. The choice of sensor was generously settled by the loan of a Lot D VSA from the U. S. Air Force.

The Vibrating String. The resonant frequency of vibration of a vertical string with a suspended mass has been derived by Rayleigh (1945).

$$f = 1/2L \sqrt{T/m} \left[1 + x/L \sqrt{\frac{ES + T}{T}} \right]$$

where: T = string tension

L = string length

m = string mass per unit length

x = radius of gyration of the string about mid-plane

E = string modulus of elasticity

S = string cross-section.

In the usual case the term in brackets is <0.01 and a useful approximation is:

$$f = 1/2L\sqrt{T/m}$$

When the string is clamped at both ends, T consists of 2 terms:

T_o = prestress, due to clamping lower end,

Mg = force of gravity on the suspended mass.

The resonant frequency varies with the acceleration of gravity. The frequency - gravity relationship may be expressed as a MacLaurin's series:

$$F = K_0 + K_1 g + K_2 g^2 + \cdots$$

If a current is passed through a conducting string in the field of a magnet, a displacing force is produced in the string. The resulting motion of the string induces a voltage across the string. The voltage may be regenerated through a stable high gain amplifier and fed back to the string. The string and amplifier circuit is analogous to a parallel resonance tank. Proper design of the feedback circuit allws maintainance of a very stable oscillation. In addition, the high gain amplifier buffers the sensitive string from the measurement circuitry.

Previous Use. The first patent for a vibrating string gravimeter was filed by Hayes (1935) in 1928. Gilbert (1949) was the first to attempt vibrating string gravity measurements at sea. His first cruise yielded an rms error of only 4 mgal. A slightly improved borehole gravimeter followed (Gilbert, 1952). Lozinskaya (1959) of the USSR constructed a nearly identical apparatus. Tomoda and Kanamori (1962) were the first to apply preset counting, considerably speeding data acquisition. They also used a digital filter in separating

sea surface accelerations from that due to gravity. Goodell and Faye (1964) constructed the first deep borehole meter with a precision of about 1 mgal. Howell, Heintz, and Barry (in press) have achieved a precision of 0.01 mgal in a borehole meter by substantial improvements in design.

American Bosch Arma VSA. The requirements for inertial guidance accelerometry differ from those of gravimetry on 3 ways:

1) a greater range of acceleration is to be sensed,
2) both positive and negative accelerations occur,
3) linearity is greatly stressed.

To meet these requirements the Arma VSA differs from previous strings in several particulars. As in Figure 2, separate but equal masses, joined by a soft isolating spring, are suspended by identical beryllium copper strings. Let the accelerometer input vector coincide with the gravity vector and let g represent the acceleration of gravity. Expressing the frequency of each string as a MacLaurin's series:

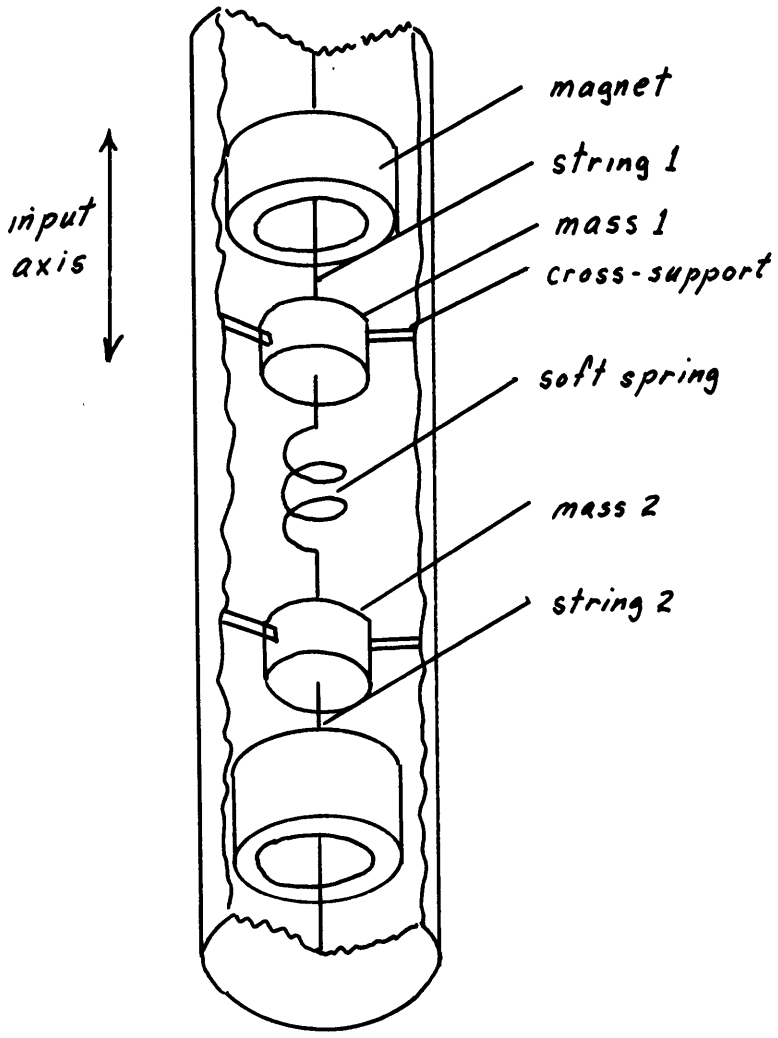

Fig. 2. American Bosch Arma Vibrating String Accelerometer.

$$F_1 = K_{01} + K_{11}g + K_{21}g^2 + K_{31}g^3 \ldots$$

$$F_2 = K_{02} - K_{12}g + K_{22}g^2 - K_{32}g^3 \ldots$$

The negative terms in series 2 are a result of the inverse relationship between gravity and tension in the lower string. Subtracting the series to obtain the difference frequency:

$$\Delta F = F_1 - F_2 = (K_{01} - K_{02}) + (K_{11} + K_{12})g + (K_{21} - K_{22})g^2 + \ldots$$

If the strings were identical, all even order terms would be zero.

The largest part of the string instability occurs in the null factor $(K_{01} - K_{02})$. In the present gravimeter a simple technique is employed to eliminate this component. Let the subscript +g indicate a measurement made with the accelerometer input axis coinciding with the positive gravity vector and a subscript -g indicate the inverse. Then:

$$F_{1,+g} = K_{01} + K_{11}g + K_{21}g^2 + K_{31}g^3 + \cdots$$

$$F_{2,+g} = K_{02} - K_{12}g + K_{22}g^2 - K_{32}g^3 + \cdots$$

$$F_{1,-g} = K_{01} - K_{11}g + K_{21}g^2 - K_{31}g^3 + \cdots$$

$$F_{2,-g} = K_{02} + K_{12}g + K_{22}g^2 + K_{32}g^3 + \cdots$$

$$F_{+g} = (F_1 - F_2)_{+g} = (K_{01} - K_{02}) + (K_{11} + K_{12})g + (K_{21} - K_{22})g^2 + \cdots$$

$$F_{-g} = (F_2 - F_1)_{-g} = (K_{02} - K_{01}) + (K_{12} + K_{11})g + (K_{22} - K_{21})g^2 + \cdots$$

$$F_{+g} + F_{-g} \qquad 0 \qquad + 2(K_{11} + K_{12})g + \qquad 0 \qquad + \cdots$$

Measuring in opposite orientations and summing the results identically eliminates the even order terms of the expansion, chief of which is the unstable null factor. The major portion of the residual drift is linear in time and can be interpolated as in Figure 3.

The construction of the VSA is such as to reduce its temperature coefficient. The aluminum housing expands with temperature, increasing the tension; the beryllium-copper strings expand with temperature, reducing the tension; the isolating spring expands with temperature, reducing the tension. In addition, the string elastic modulus decreases with temperature. At the operating temperature of $0^{\circ}C$ a temperature

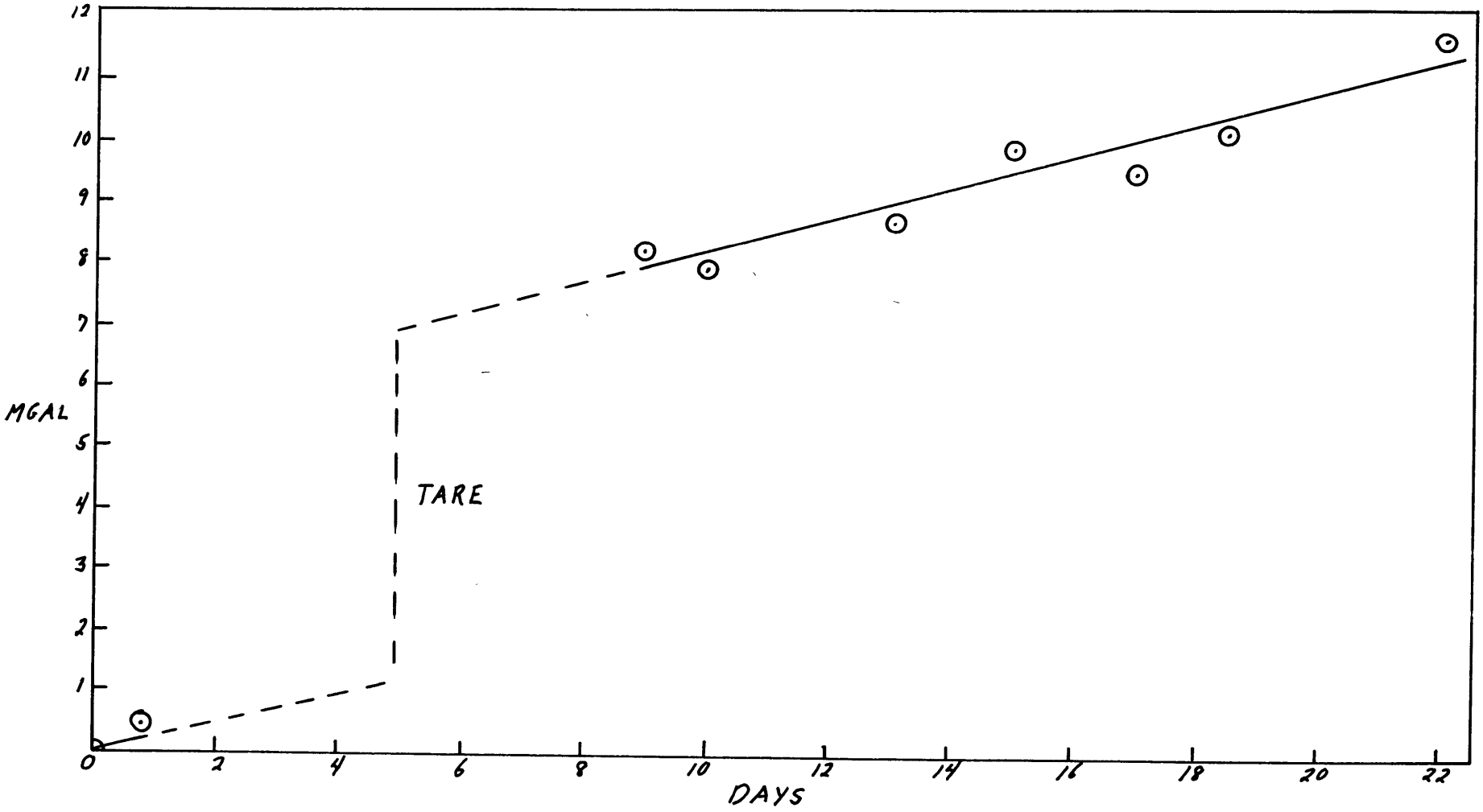

Fig. 3. Accelerometer scale factor drift showing interpolation.

coefficient of +5 mgal/C^{o} is found. String frequency is also influenced by the amplitude of the string vibration and the phase shift in the amplifier. Automatic gain control holds a constant amplitude, but a small (+1.8 mgal/volt) phase shift dependence on supply voltage is ~~also~~ found.

The instrument and pressure case are shown in Figure 4. Figure 5 is a cross-sectional view. The VSA with a copper thermal shroud is rigidly mounted inside a Plexiglas cylinder with aluminum end caps. The cylinder floats in glycerine within a plastic sphere (C) with a minimum clearance of 0.4 cm. Mercury in cavity (A1) gives the cylinder a pendulosity of 66 X 10^{3} gm-cm, causing it to float vertically. The shape of the cavity can be modified from the outside by adjustment screws to achieve the vertical within $\pm$ 1'. Vertical is indicated by circular level bubbles inside windows (B). When the cylinder is tipped $>$ 90^{o}, the mercury flows through tubes to cavity (A2), causing the cylinder to seek the opposite vertical. This automatic levelling system is stable and reproducible to $<$ $\pm$ 1'.

Fig. 4. The automatic gravimeter in its pressure case (second mode of operation).

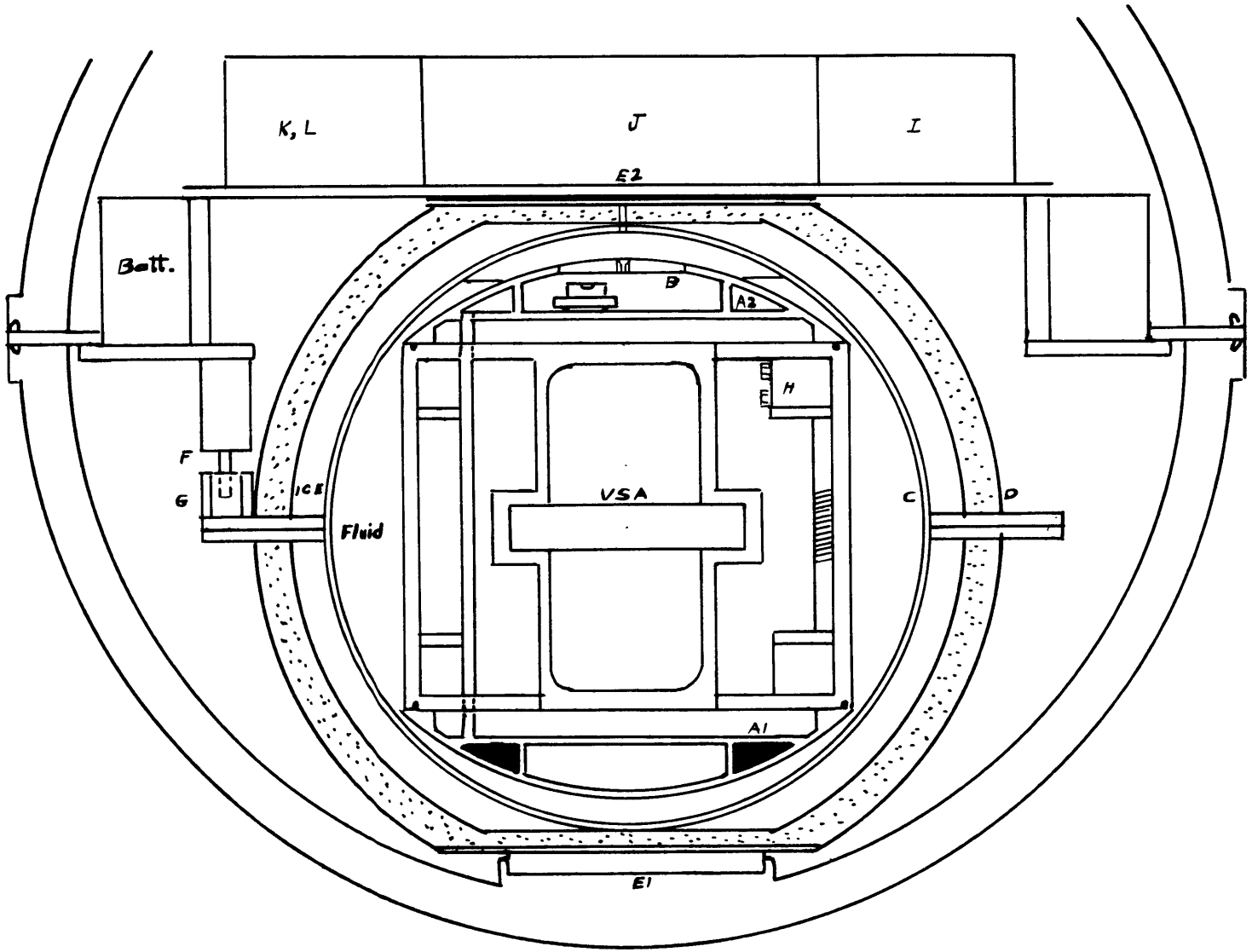

Fig. 5. Cross-section drawing of the automatic gravimeter.

Sphere (D) is mounted on axis (E1,E2) with a stainless power spring at end (E1) and a hollow bearing at (E2). A solenoid plunger projects to shock-mounted stops (G) on the equator of the fiber glass sphere. Activation of the solenoid allows rotation of the spheres through 180° to the next stop. Viscous drag in the glycerine rotates the cylinder through nearly the same angle as the sphere. When the cylinder angle exceeds 90° the mercury flow completes the inversion to 180°± 1'.

The power supply for the VSA is a battery of 22 silver-cadmium rechargeable cells in series (H). Voltage is constant over 60% of the 60 hour discharge cycle and is sufficiently smooth otherwise to allow interpolation within ± 0.05 volt over several hours. The voltage is measured and the battery recharged through the hollow bearing (E2) with a watertight coaxial probe.

To avoid restraints on the self-leveling mechanism, the difference frequency from the VSA (~64 Hz) is transmitted as an amplitude modulated radio signal. The signal is demodulated by a commercial transistor radio and fed into a preset counter (J). The counter, assembled

from Digital Equipment Corp. modules, has a preset capacity of 16 binary bits and a counting capacity of 16 bits. Time base is provided by a 125 kHz Manson Laboratories, Inc. oscillator with a stability of 10^{-8}/day. With a preset number of 3072, the least significant bit of the counter is equivalent to about 0.1 mgal. The 16 bit counter register has a maximum capacity of about 65,000, so the ordinary range of the gravimeter is 6,500 mgal. However, the preset number can be set as high as 57,344 giving a least significant bit equivalence of about 0.005 mgal and a range of 325 mgal.

Upon completion of each measurement the 16 counter bits are recorded directly with incandescent lamps on a Kodak Instamatic film (K), driven by the shaft of a sequence timer (L). The sequence timer controls the 9 operations necessary for a complete gravity measurement. In addition, the sequence timer motor is wired through 2 mechanical timers allowing control of the interval until measurement and the number of measurements to be made.

The instrument is housed in a 7075-T6 aluminum sphere with a 19" id and a 1" wall. Test depth in sea water is 8,500 m with a safety factor of 1.36.

Modes of Operation. The first and second modes, remote readout and automatic on a cable, differ in one significant respect: the remote readout eliminates the *in situ* uncertainty in measurement quality. In the second mode there is no indication of motion on the bottom until film retrieval. Although not included in this design, a conducting cable would also allow the keying of a transducer on the gravimeter from a precision graphic recorder as an aid in depth determination.

The third mode, automatic free-fall, has the greatest chance of success. It has the advantages of independence of water depth and current conditions and a greater speed in deep water. It shares the disadvantage of all free oceanographic instruments - difficulty in retrieval.

FREE-FALL VEHICLE

The vehicle, Figure 6, is a modified fiber glass FOIF (Free Oceanographic Instrument Float) borrowed from the Woods Hole Oceanographic Institution. The original gasoline flotation has been replaced by 7 - 10" and 1 - 16" Corning glass spheres. The aluminum sphere is mounted in a harness of nylon webbing attached to the vehicle with shock cord. The elastic suspension allows the vehicle to stop instantaneously from an axial velocity of 5m/ sec without exceeding the accelerometer limit of 30 g.

The vehicle descends weightedby 2 - 20 kg cast iron balls, 1 at the nose and the other separated by a 5m length of light chain. When the ball on the chain reaches bottom the vehicle assumes a lower terminal velocity, thereby suffering minimal damage on a hard bottom. At the bottom the vehicle lies on its side for greater stability with a negative buoyancy of 10 kg. The iron balls are released at a preset time by a Van Dorn magnesium weight release (Van Dorn, 1953) modified to fit flush inside the vehicle nose. Ascent is nose-first and the vehicle rides vertically with 30 cm above the sea surface.

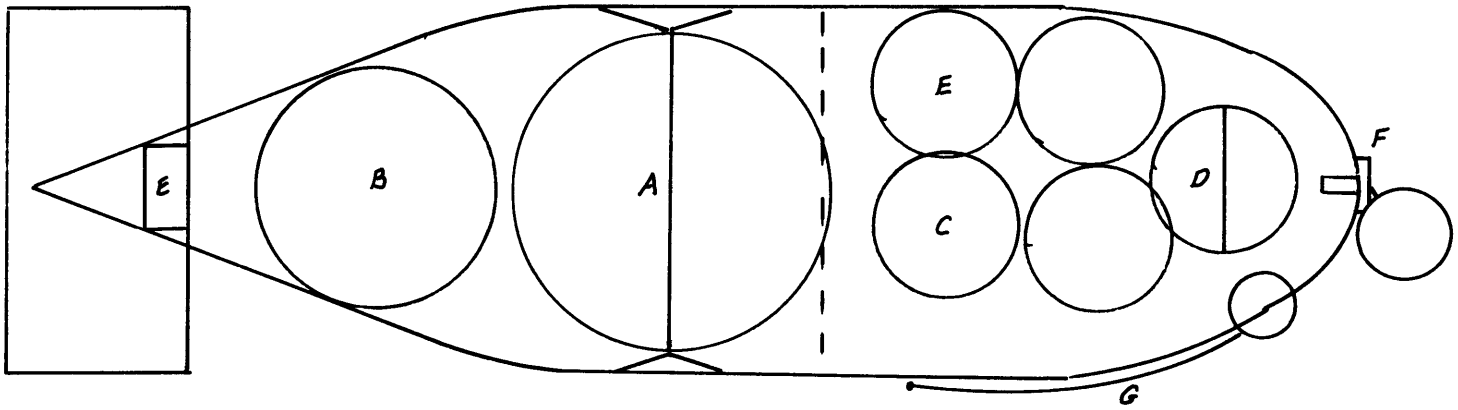

A	19" I.D.	instrument sphere
B	16"	glass sphere
C	10"	glass spheres
D	9"	Benthos sphere, radio, strobe
E	"	" " Webb pinger
F	Mg	weight release
G	C.B.	radio antenna

Fig. 6. The free-fall vehicle, a modified FOIF (Free Oceanographic Instrument Float).

Location. Determination of the instrument location on the bottom in the free-fall mode is accomplished with range-rate techniques identical to those used in tracking Swallow floats. The vehicle has a 40 acoustic watt precision time base pinger in its tail. Lines of position for the pinger may be obtained by towing 1 hydrophone and watching the Doppler shift in repetition rate on the strip chart of a precision graphic recorder (PGR) or by towing 2 hydrophones and observing the arrival time differences on a PGR or dual beam oscilloscope. With the precisely timed repetition rate of the pinger and a PGR record discrimination of ± 0.002 sec, the relative position may be resolved to within ± 300 m by either of the 2 methods.

Depth of the instrument on a level bottom is most easily determined by echo sounding over the instrument position. For small-scale geophysical investigations only relative depths are needed, but when surface free-air anomalies are sought, absolute depth must be obtained by a combination of echo sounding and in situ sound velocity profiling.

Bottom relief may result in false fathogram depths since first arrivals are not necessarily from the depth of the instrument. For investigations in areas of rough bathymetry the vehicle has a pair of conventional protected and unprotected reversing thermometers. When not subjected to the extreme vibrations of a hydrographic wire, the thermometer pair is capable of a ± 0.1% precision in depth (Folsom, 1963).

A more convenient way to measure the depth of a free-fall vehicle would be with a pressure transducer. With a frequency output, a vibrating string pressure transducer would be directly compatible with the present data system. However, the accuracies achieved with commercial vibrating string pressure transducers to date are not sufficient for the purpose of deep sea gravimetry.

Recovery. Recovery of the vehicle is facilitated by the following aids:

1. Day Visual. The international orange color of the vehicle allows visual sighting at ranges depending upon conditions and height of eye.

2. Night Visual. A Benthos, Inc. 1 joule strobe flash in the translucent nose aids in the closer stages of recovery at night.

3. Acoustic. The 40 acoustic watt 4.2kHz pinger has a range of up to 30 km in deep water and up to 2 km surfaced, depending upon wave noise.

4. Radio. A 1 watt citizens' band radio transmitter may be located by direction finding at up to 8 km.

ERROR ANALYSIS

There are 5 sources of error, classified as either instrument errors (1,2) or field errors (3,4,5):

1. Drift is shown in Figure 3. Over a 2 week period the maximum deviation of a set of closely spaced measurements from the straight line drawn through the end points was 0.8 mgal. The standard deviation was 0.5 mgal.

2. Instrument repeatability contains the errors of accelerometer off-level, temperature coefficient, voltage phase shift and counter trigger error. The standard deviation is 0.2 mgal.

Field errors arise in the computation of anomalies through the uncertainty in the gravity meter coordinates. Gravity anomalies are computed relative to the gravitational field at the geoid expressed by

the international gravity formula:

$$g(\phi) = 978.0490(1 + 0.0052884\sin^2\phi - 0.0000059\sin^2 2\phi) \text{ gal.}$$

3. The depth error occurs in the correction for vertical disance of the gravimeter from the geoid. The sum of the free-air correction and the Bouguer correction for the attraction of the water mass is approximately 0.223 mgal/m. Assuming a standard deviation in depth of 2m the depth error is 0.4 mgal.

4. Position relative to the ship, with a standard deviation of about 300 m, results in a gravity error of about 0.2 mgal at mid-latitudes.

5. With some of the latest navigational systems the open ocean precision in ship's position approaches 0.2 km. For example, GEON (Gyro Erected Optical Navigation) has a standard deviation of about 0.2 km, resulting in a gravity error in mid-latitudes of about 0.2 mgal.

The standard deviation for a measurement containing all 5 of the above errors is 0.7 mgal. Each of the individual errors could be reduced with further effort. Drift could be reduced to 0.1 mgal/month by changes in the accelerometer. Repeatability could be reduced to as

little as 0.01 mgal by increasing the counting time and by using proportional temperature control and a mercury cell power supply. The error in relative depth could be reduced to less than ± 1 m (0.2 mgal) with a refined vibrating string pressure transducer or by inverted echo sounding. The position relative to the ship could be reduced to less than ± 100 m by triangulation techniques such as used in the Thresher search. Satellite navigation should provide the ship's position within ± 0.1 km. The maximum effort represented by all of these improvements would result in a standard deviation for a gravity measurement corrected to the surface of 0.2 - 0.3 mgal.

FIELD TEST

The performance of the gravimeter in the second mode (automatic on a cable) was evaluated during the week of 6 April - 13 April, 1966. The accelerometer was run continuously during this period with calibrations on the 6th and 13th. On the 12th, stations 20, 22, 53, 49, 48, and 2 of the Rhode Island Sound Area Gravity Meter Operational Check Range (Fanning and Garoutte , 1962) were reoccupied with the gravimeter. The 6 stations are shown in Figure 7. The range consists of 36 bottom stations established with a LaCoste-Romberg underwater gravity meter. Grid spacing is about 5 km and the accuracy of the established values is about ± 0.1 mgal. The bottom is smooth and the depth averages 72 m.

Operation. The gravimeter was caligrated after running 24 hours on 6 April. Three consecutive readings were taken to ± 0.01 mgal with a laboratory preset counter and averaged. After the field test the gravimeter was recalibrated to determine the drift correction. During the week, 4 days were run at 20°C and 3 days at 0°C. The 7 day drift of +2.5 mgal was exactly as predicted by the previously determined

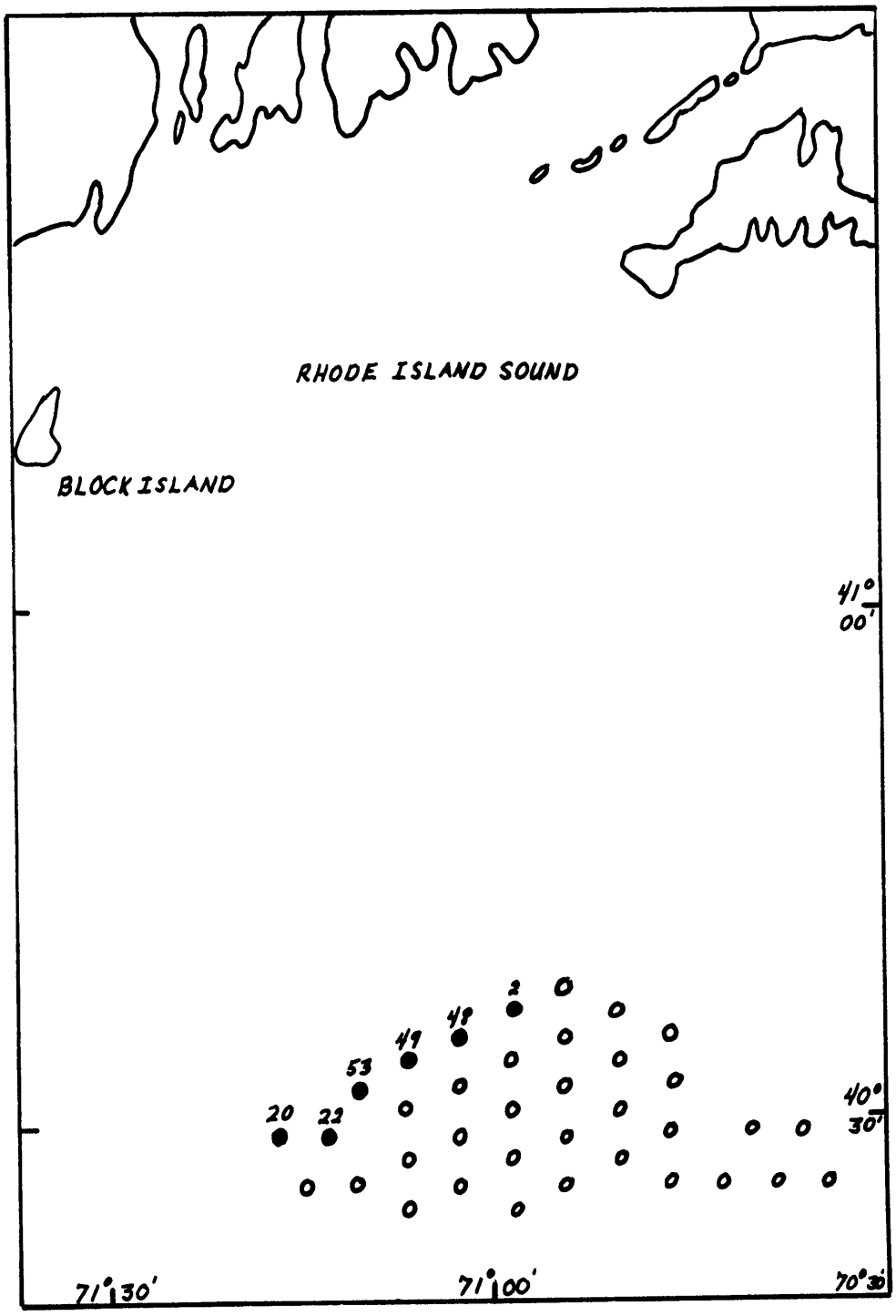

Fig. 7. Stations occupied in the Rhode Island Sound area gravity meter operational check range.

drift rates of +1.5 mgal/week at 0°C and +3.0 mgal/ week at 20°C.

A small steel tugboat owned and operated by the Blount Marine Corp., Warren, Rhode Island, was used for the test. Navigation was by Loran stations 1H4 and 1H5. Depths were measured with a Bendix fathometer. The ship's hoisting gear consisted of an electric capstan with an over-the-stern block and a fixed boom with block and tackle. The capstan proved adequate but the short scope of the boom resulted in the gravimeter striking the rolling ship during lowering and raising operations. Because the gravimeter was out of its shock-mounted vehicle, these shocks were probably as large as would ever be normally encountered. No string tares occured even though the rotating inner sphere was twice jarred from its bearings.

Six stations had previously been chosen as the minimum number allowing any statistical inference. The number of stations should not be taken as an indication of the time required per measurement. After handling became routine the on-station time was reduced to 45 minutes,

including lowering and raising. For an accuracy of±1 mgal a single reading would suffice, reducing the on-the-bottom time to 5 minutes, A change of sequence timer would allow 3 readings in 15 minutes.

Results. Of the 6 stations, 5 were considered successful. The bad station (48) resulted from poor handling. After lowering, the instrument was dragged across the bottom, rotating the flip axis to a vertical orientation. The result was 6 +g measurements with no inversions. A straight-forward correction using the +g measurements and the string scale factors resulted in an error of +2.9 mgal. The necessity of inversion is apparent.

The readings were compared directly to the range bottom values. The fathometer could be read to ± 1 m, but no deviation from the published depths larger than this was found. It should be noted, however, that the depth uncertainty of ± 1 m is equivalent to a gravity correction uncertainty of ± 0.22 mgal. An estimated uncertainty in navigation of ± 0.22 km N-S causes an uncertainty in latitude correction of ± 0.17 mgal.

The uncertainty in real gravity values due to location error is thus ± 0.39 mgal.

The results for the 6 stations are listed in Table 1. The error caused by bottom conditions (mud) has no characteristic pattern, but taking the mean of 3 observations reduces the scatter of differences and is recommended in the case of a soft bottom. Too much weight should not be given an rms value on a sample space of 5 points, but the rms difference of 0.43 mgal without correction for the true gravity uncertainty is within the accuracy predicted on the basis of laboratory tests.

FUTURE WORK

To obtain the technically feasible precision discussed above, extensive modification to the apparatus would be required. However, we now have an instrument capable of ± 1 mgal measurements to a depth exceeding 8,000 m. This precision allows gravitational investigations

TABLE 1

Results of the field test.

Station	Lat.	Long.	Depth	Range g	Measured g	Difference
20	40°28.7'	71°16.9'	73 m	980.2274 gal	980.2276 gal	+0.2 mgal
22	40-28.8	71-12.9	75	.2292	.2288	-0.4
53	40-31.7	71-10.8	70	.2328	.2326	-0.2
49	40-33.4	71-07.0	69	.2341	.2347	+0.6
48	40-34.7	71-02.9	72	.2423	.2452	+2.9
2	40-36.3	70-58.6	67	.2484	.2490	+0.6

RMS Difference without #48	0.43 mgal
Mean Difference without #48	+0.14 mgal
Uncertainty due to difference in location	±0.39 mgal

Calibration

Base station MIT	April 6	980.3832	980.3807
	April 13	980.3832	980.3832 by definition
Drift	7 days		+2.5 mgal
Drift at 0°C	7 days		+1.5 mgal
Drift correction	12 hours		+0.1 mgal

of anomalies heretofore undetected by surface-ship gravimeters. Use of the instrument in its various modes will provide valuable information on the procedures necessary for practical deep sea bottom gravimetry as well as design criteria for future bottom gravimeters.

ACKNOWLEDGEMENTS

This work was performed under Office of Naval Research contract Nonr 1841 (74). Machine computations were done at the Computation Center of the Massachusetts Institute of Technology.

The accelerometer was loaned by the U. S. Air Force. Invaluable aid was rendered by the accelerometer manufacturer, Arma Division, American Bosch Arma Corp., in the person of Dr. Robert Bock.

Dr. William S. von Arx and Dr. Frank Press cleared the path of several difficult obstacles. Valuable suggestions were made by many fellow graduate students, particularly Mr. George Beardsley and Mr. Thomas Sanford.

PART TWO

ON-THE-BOTTOM GRAVIMETRY

by

C.G. Wing

Abstract

Sea-surface and sea-bottom gravity anomalies associated with typical oceanic structures are examined with a view toward providing criteria for when bottom measurements are necessary. Downward continuation is evaluated as a possible substitute. Real structures are used whenever practical.

1. Introduction

Sea level is the ideal surface for geodetic gravimetry. For geophysical interpretation, however, it is often far from ideal. The sources of gravity anomalies at sea are obviously separated from the surface by at least the water depth. In the case of small-scale structures or structures with sharp features, attenuation of the anomaly with vertical distance can be a very limiting factor.

Dean (1958) has shown that the attenuation factor (peak anomaly at surface/peak anomaly at bottom, depth h) is e^{-hu} where u is the frequency (2π /length of the structure). The attenuation can be shown by comparing the computed surface and bottom gravity profiles for the proposed structure. Profiles are easily computed with the two and three-dimensional algorithms of Talwani, Worzel and Landisman (1959) and Talwani and Ewing (1960). These algorithms and their Fortran II listings are given in Appendices A and B.

In addition, surface profiles with varying degrees of precision are downward continued and compared with actual bottom profiles in

order to point out limitations. A Fortran II program for downward continuation, with or without error function smoothing, is given in Appendix C.

2. Structures

Two considerations argue against surface gravimetry over small features: 1) the low precision obtained with the surface gravimeter, 2) the large attenuation of the small-scale anomaly with vertical distance.

For these reasons, oceanic structures studied gravimetrically in the past have all been of large scale. On-the-bottom gravimetry would make possible the investigation of a number of smaller features, heretofore sensed only by seismic profiling. We will investigate six structures, ranging in width from 400 km down to 1 km. For convenience, anomalies will, in the majority of cases, be presented as "gravity effects" (Grant and West, 1965). The gravity effect is the difference in gravity caused by the density contrast between the structure and the surrounding medium.

2.1 Puerto Rico Trench

The Puerto Rico Trench, Figure 2.1, has a structure wavelength of about 400 km and a maximum depth of about 8.5 km. The maximum attenuation factor, e^{-hu}, based upon these figures is 0.984. The maximum free-air anomaly over the trench is about -350 mgal (Talwani, Sutton and Worzel, 1959). With the above attenuation factor, the difference between surface free-air anomalies and free-air anomalies obtained from bottom measurements would be about 6 mgal. Of course small scale features near the bottom could cause a larger difference, but this must be considered noise regarding the gross structure. Six mgals is less than the mismatch between measured anomalies and anomalies calculated on the basis of seismic work (Talwani, et al. 1959; Bunce and Fahlquist, 1962). In the presence of the mismatch of up to 50 mgal, 6 mgal loses significance.

2.2 Mendocino Escarpment

Much of the discussion on the Puerto Rico Trench applies to the Mendocino Escarpment, Figure 2.2. The wave length

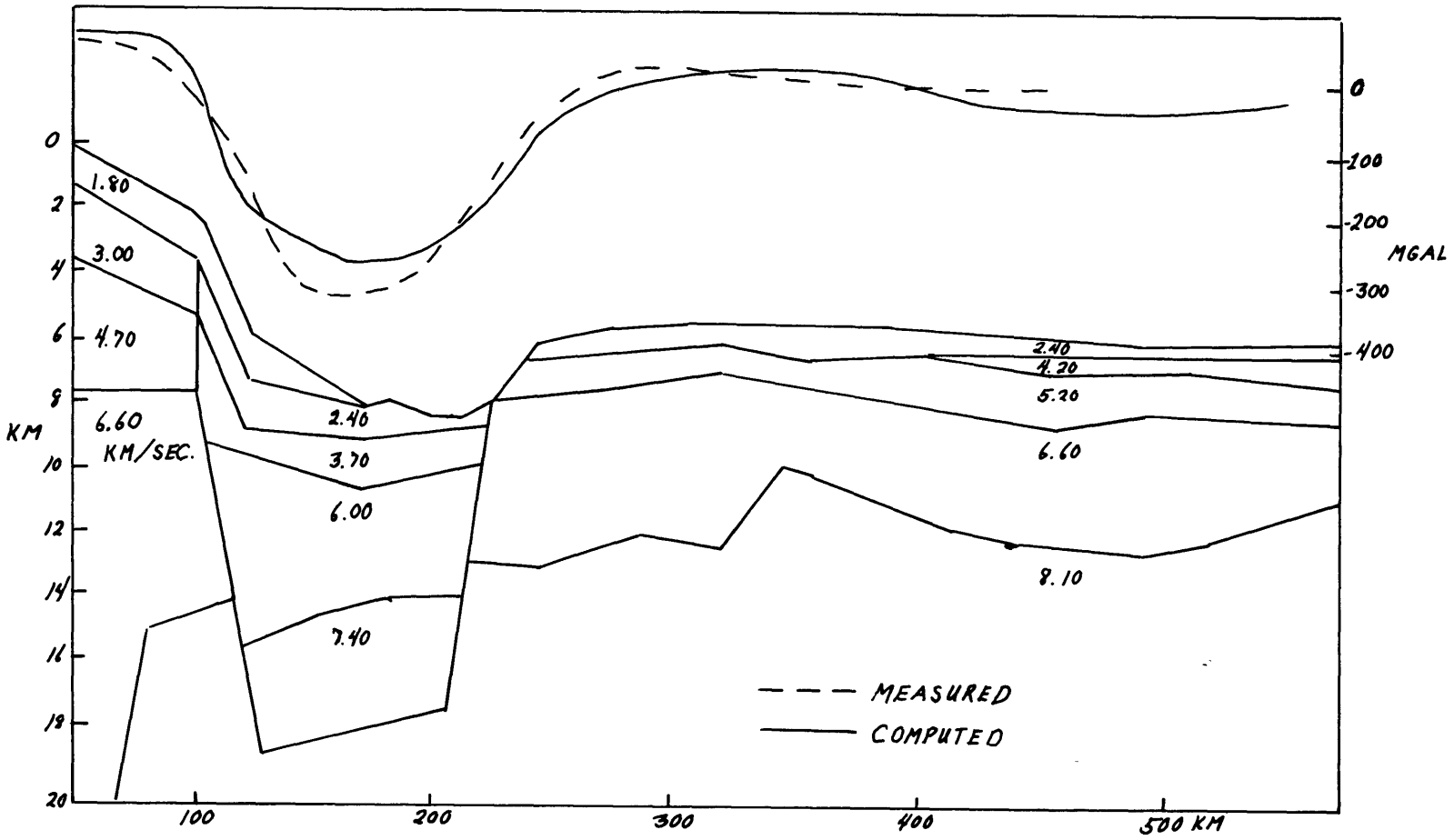

Fig. 2.1. Puerto Rico Trench (after Bunce and Fahlquist)

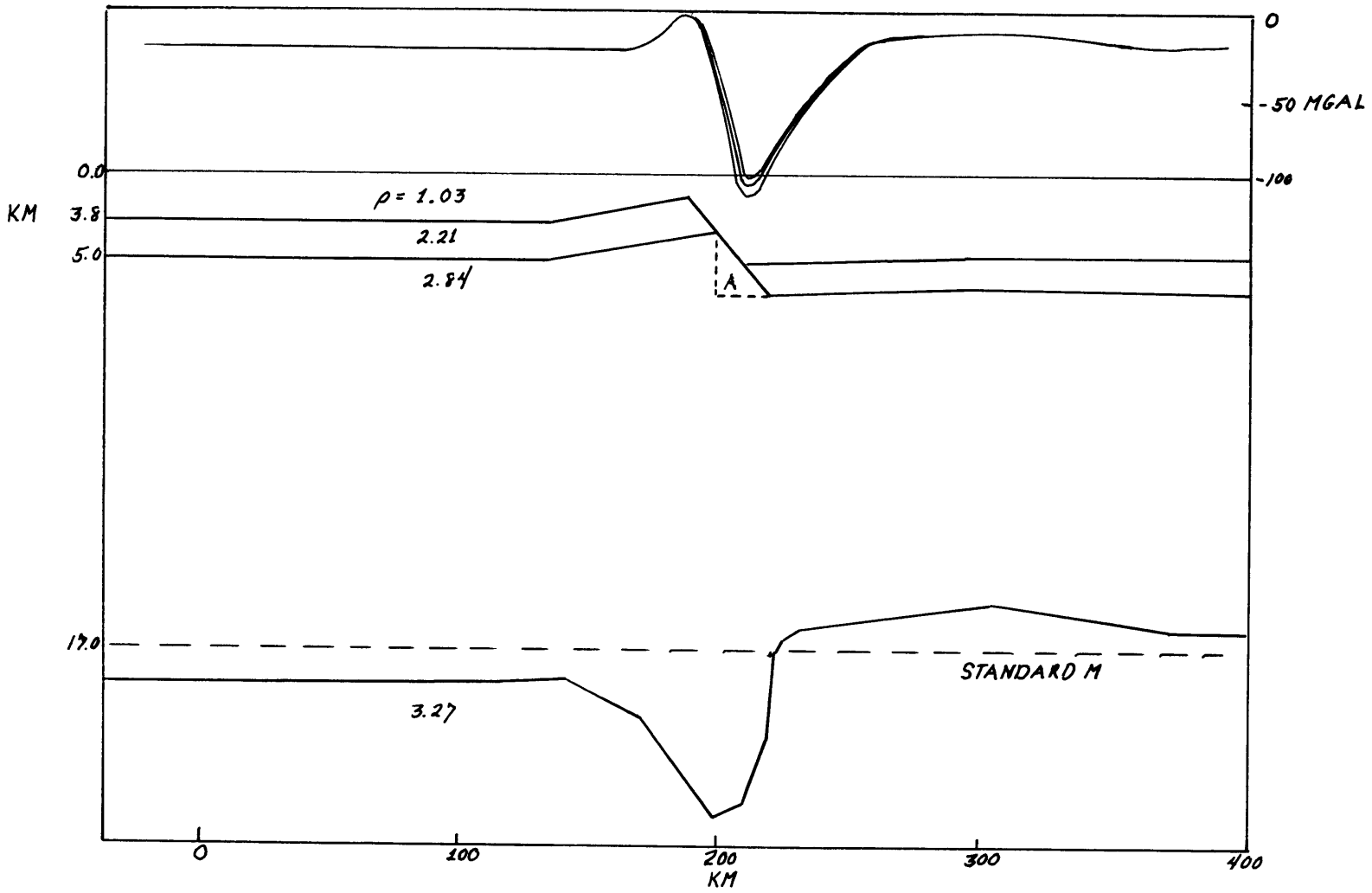

Fig. 2.2 Mendocino Escarpment (after Talwani et al., 1959).

in this case is about 60 km. and the depth 4 km. resulting in an attenuation factor of 0.90. Total relief in the surface anomalies after correction for the water depth is 80 mgal and the maximum amplification to be expected by using bottom values is about 8 mgal.

Figure 2.2 also shows the gravity effect of a modification (A) to the structure. This is the smallest modification which would have any geophysical significance. At the same time, it is the largest which could not be unambiguously defined by seismic measurements. Its maximum gravity effect is -14 mgal on the bottom and -6.7 mgal at the surface. After the bottom uncertainties introduced by topography and the attraction of the upslope mass (slope $\sim 6^{o}$), the surface profile would probably contain more useful information.

Once again, the surface change of -6.7 mgal is smaller than the calculated measured mismatch of 10 mgal (Talwani et al., 1959).

2.3 Pickett Peak Seamount

Pickett Peak Seamount was investigated by Shurbet and Worzel (1955) in order to determine its composition. The magnitude of the

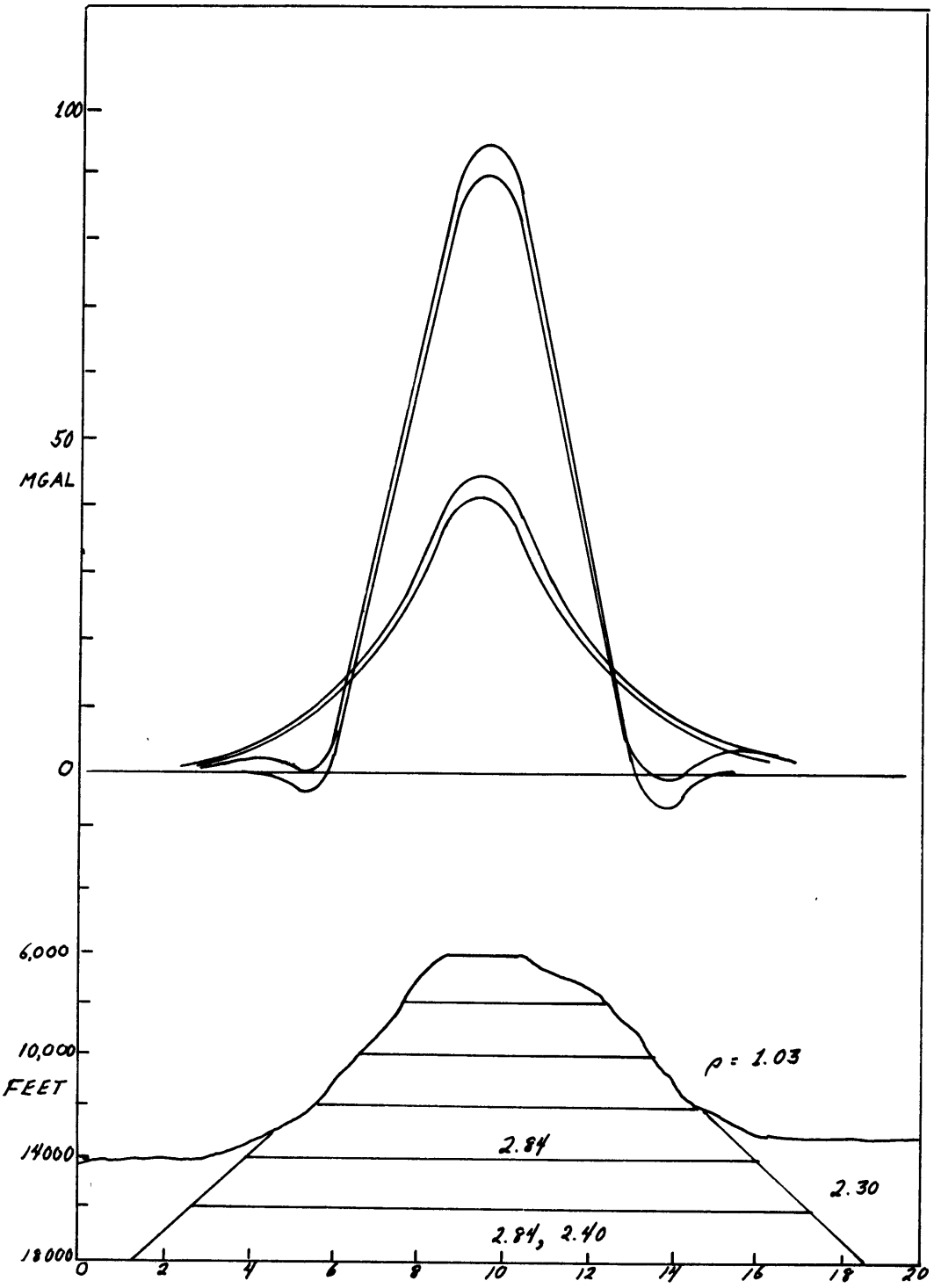

Fig. 2.3 Pickett Peak Seamount.

surface anomaly varies directly as the seamount density. Vertical variations in density are difficult to distinguish from changes in mean density based upon surface measurements alone. However, the gravity effect on the bottom varies more strongly with density structure.

Figure 2.3 shows surface and bottom gravity effects obtained first with a model similar to Shurbet and Worzel's and second, with the density of the bottom layer changed to 2.40. The change is equivalent to raising the bottom of the seamount 2,000 feet or to decreasing the adjacent unconsolidated sediment thickness by 2,000 feet.

The most obvious difference between the surface and bottom profiles is the greater magnitude on the bottom. Secondly, the gradient in the bottom profile is larger. Thirdly, the bottom profile has an edge effect where the gravity effect actually changes sign. The reversal occurs at the point on the slope where the upward attraction of the upslope mass is greater than the attraction of the layers below.

We now change the density of the bottom layer (16,000 - 18,000 ft.) to 2.40 gm./cm.^{3}. With a wavelength of 180,000 feet, the attenuation of the gravity effect of the bottom layer change at the surface relative to a depth of 6,000 feet is theoretically 0.75. Figure 2.3 is in good agreement with an actual attenuation of 0.76. Except for an overall magnitude change of about-3 mgal, the surface bell-shaped profile is vertically unchanged. However, a magnitude change of-4 mgal makes the edge effect of the bottom profile much more noticeable. The edge effect depends upon the slope of the seamount as well as the internal density structure and so its usefulness in practice depends upon the accuracy of bathymetry and location of the gravimeter.

2.4 Buried Peaks

Not all volcanic peaks are topographically expressed. One suspects that there might be several peaks in the Bermuda-New England seamount arc which are buried beneath the continental slope (Northrop, Frosch and Frassetto, 1962). Using a model similar to Pickett Peak buried in Atlantic deep basin sediments, we investigate the gravitational

effects of slightly varying structure parameters, Figure 2.4.

Model (a) has a slope of 11° and just breaks the surface. The maximum bottom effect is 27.5 mgal, while the surface effect is less than 4 mgal. The attenuation factor, 0.15, is large.

Model (b) has a gentler 9° slope and its top lies 0.4 km. beneath the floor. The maximum bottom and surface effects are 21.5 and 7 mgals respectively. The effect of burying the seamount with 0.4 km. of sediment has been a reduction of the attenuation factor, while the gentler slope results in a broader anomaly.

Model (c) shows the increased sensitivity of the bottom profile to vertical density changes in the seamount. The bottom layer has been eliminated, the second layer density contrast raised to 0.7 gm/cm^3, and the slope decreased to 6.5°. The maximum difference between the surface profiles in models (b) and (c) is only 0.25 mgal, but the bottom profile difference is up to 4 mgal.

The half-width of a gravity profile is an often used interpretational parameter. The half widths of the surface profiles vary

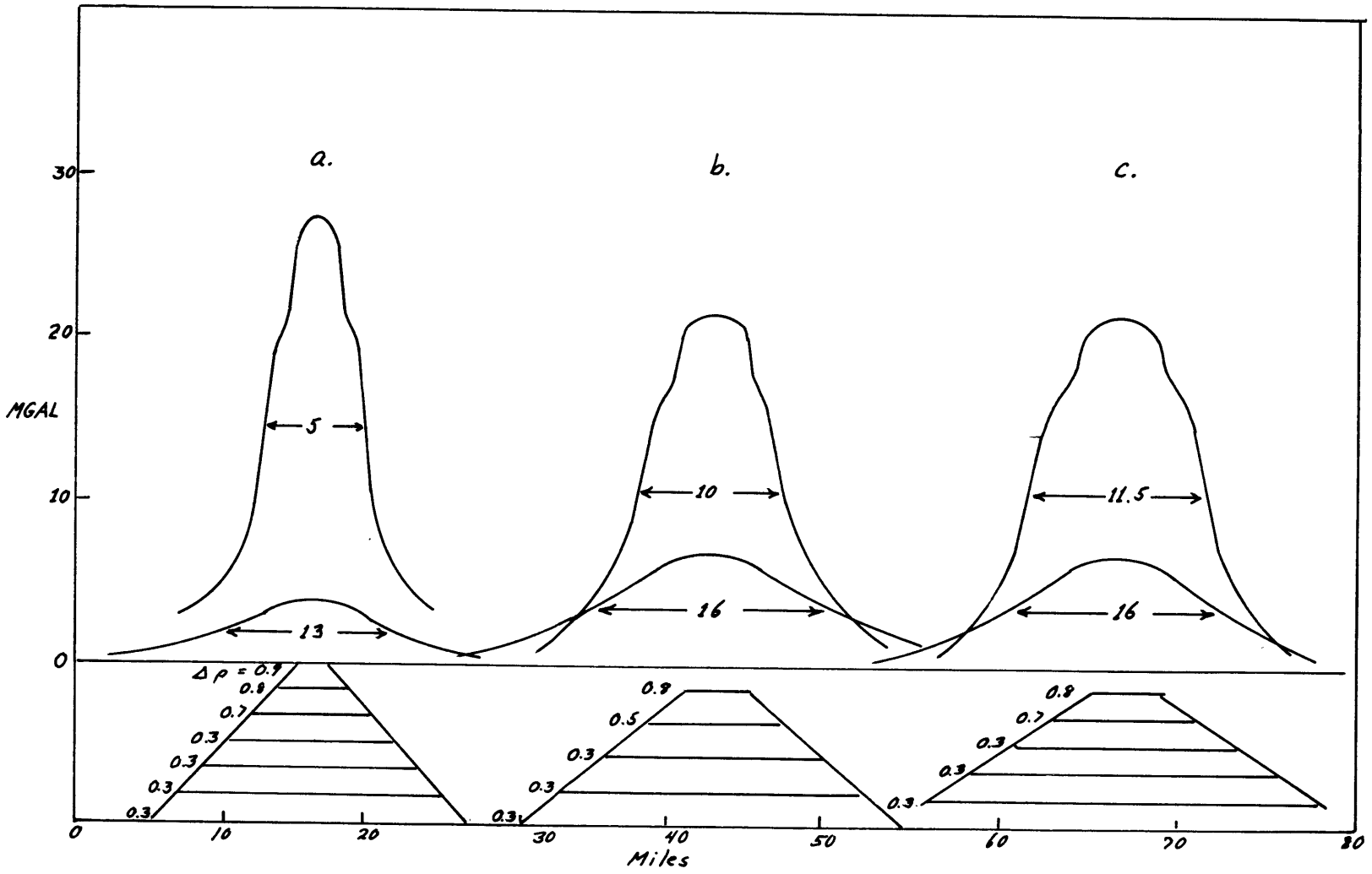

Fig. 2.4. Buried Peaks.

little (13, 16, 16 km.), but the half widths of the bottom profile vary markedly (5, 10, 11.5 km.).

2.5 Salt Domes

Salt domes are perfect structures for gravitational interpretation. They are usually symmetric in plan, have a known density, and possess no magnetic anomaly. Large, deep water salt domes have been discovered in the deep basin of the Gulf of Mexico (Ewing, Worzel and Ewing, 1962). The well-known Sigsbee knolls on the abyssal plain of the Sigsbee deep (3.7 km.) are apparently the surface expressions of salt domes rising from a deep extension of the Louann salt bed. The tops of at least 21 such domes have been delineated by continuous seismic profiling.

There is little question of the size, shape and density of the domes. The size and shape may be guessed closely by seismic studies and the density of the salt is invariably 2.15 - 2.20 gm/cm^3.

One of the most interesting questions in the area of the salt domes is the average density of the sediments. Using seismic

refraction and reflection data and the Nafe-Drake curve, Ewing et al. find an expected free-air anomaly of -225 mgal. Actual measurements show a free-air anomaly of only -25 mgal. The discrepancy could be accounted for by a large deviation in average sediment density from the Nafe-Drake curve.

Given the size and density of a salt dome, its gravity effect would be a very accurate indication of the surrounding sediment densities.

Figure 2.5-a shows a typical dome proposed by Ewing et.al. We divide the dome into ten slabs by eleven equi-spaced polygons. Model 1 uses sediment densities drawn from the Nafe-Drake curve. In model 2 all densities are increased by 0.33 gm./cm.^{3} in order to account for the free-air anomaly discrepancy. The bottom profiles show a maximum difference of 12.5 mgal between the two models while the surface difference is only 1.5 mgal. The surface information is obviously lost in the noise.

Figure 2.5-b shows a more rounded and typical dome shape. In

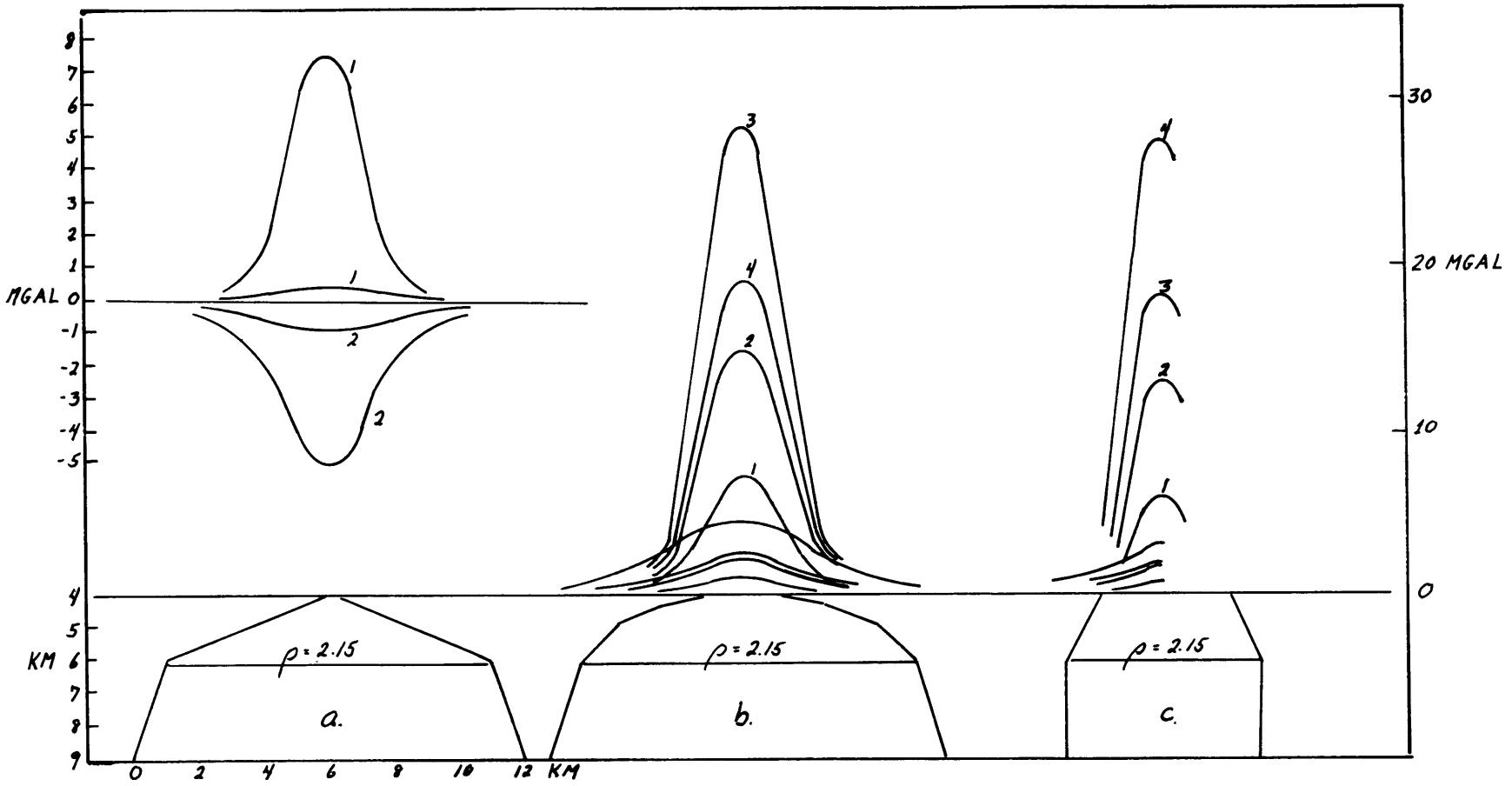

Fig. 2.5 Salt Domes

model 1 the sediment densities are minimum values from the Nafe-Drake curve while model 2 uses the corresponding maximum densities. Models 3 and 4 use the same densities as 1 and 2 respectively, but replace the top 1 km. of the dome with a cap rock of density 2.50 gm./cm.^{3}

The eight profiles are similar in shape but once again, the signal-to-noise ratios are far larger (7/1, 15/1, 19/1, 27/1) in the bottom profiles than in the surface profiles (1/1, 2.5/1, 3/1, 4.5/1). The difference between models with and without the cap rock is+8 mgal on the bottom and+2 mgal at the surface.

Figure 2.5-c shows a more typical-sized salt dome. All densities and depths are identical to the four models of Figure 2.5-b respectively. Reducing the horizontal dimension ("wavelength") of the dome has resulted in an attenuation of the maximum anomalies at the surface by 28%. The bottom profile, being much closer to the source is attenuated only 6%.

2.6 Outer Ridge Basement Relief

Seismic profiles on the Outer Ridge north of Puerto Rico show three principal structures (Bunce and Hersey, in press). The first structure consists of flat-lying 2.1 km./sec. beds. The second structure, with velocity 4.2 km./sec., is partly continuous and partly broken. The third structure is basement with a relief of 0.5 sec. travel time.

Near 21°30' N. and 66°30' W. the basement outcrops a nearly flat-lying floor. Only the density of the topmost layer is known with any certainty. If an outcrop of the basement could be dredged, the density of the second layer might be determined by the gravity effect of the basement and second layer density contrast.

Figure 2.6 shows basement relief in the area 21°30' N., 66°30' W. The basement outcrops. The topography is approximated quite well, but the density structure is oversimplified by assuming a density of 2.85 gm./cm.^{3} in the basement and 2.40 gm./cm.^{3} for all of the sediments.

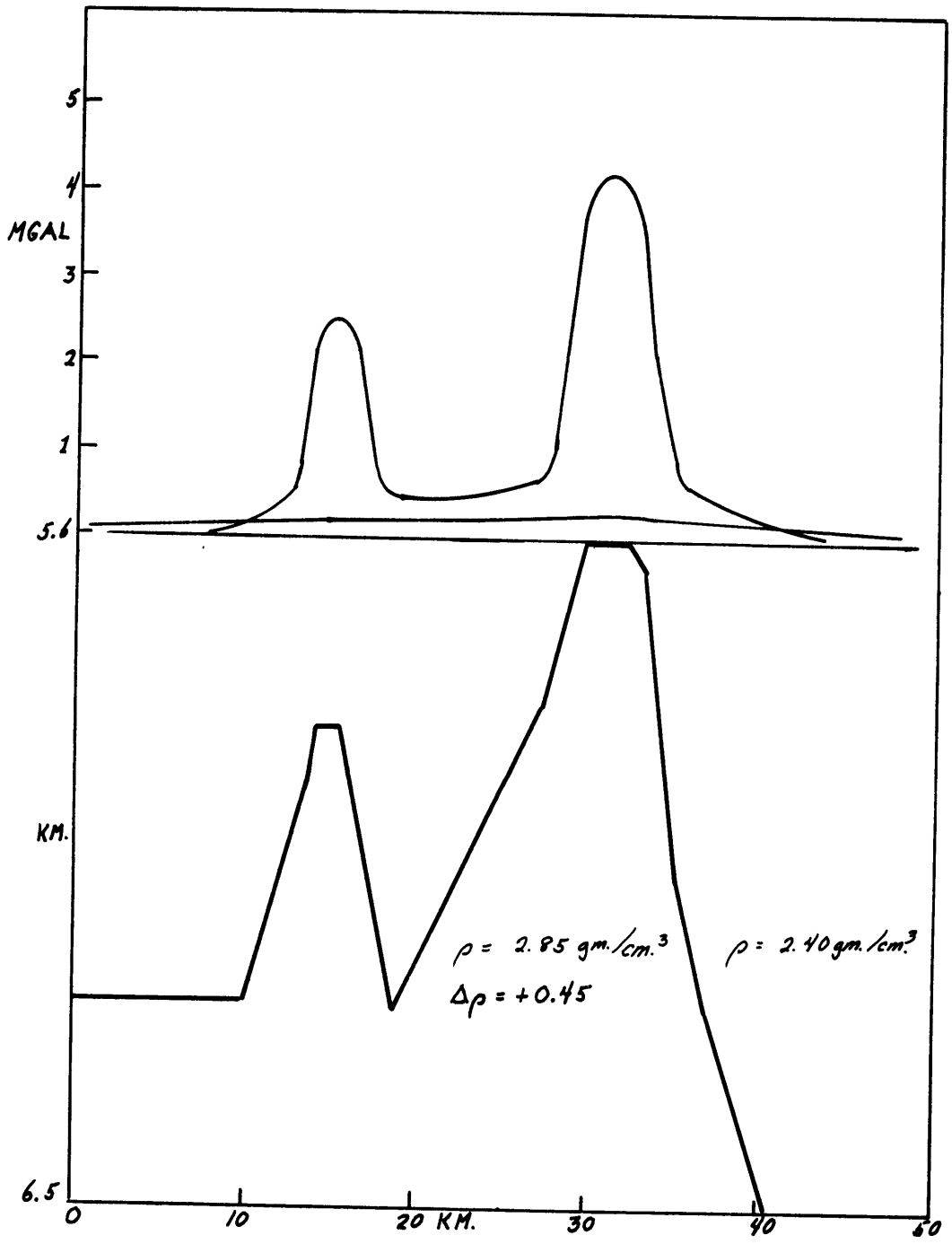

Fig. 2.6. Outer Ridge Basement Relief.

The surface anomaly, having a maximum value of 0.25 mgal is undetectable. The bottom profile, although not spectacular, clearly differentiates the two peaks with a signal to noise ratio of 4/1.

2.7 Dikes

Large dikes are known or suspected in several deep water areas. The Red Sea dikes have been studied with both gravity and magnetics. More recently a magnetic survey in the Laborador Sea has indicated the presence of a series of large dikes (Godby et al., 1966).

Using the typical dimensions and spacing suggested for the Laborador dikes by Godby et al. (1966) , we construct a gravity model, Figure 2.7-a. Some exception may be taken to either the density contrasts or the vertical extent of the dikes but the present argument will not be affected except for a magnitude change.

Both the bottom and surface profiles indicate the presence of the dikes clearly. The bottom profile has a maximum anomaly ratio of 8.7 compared to 2.9 for the surface. The relief (maximum-minimum) is 46 mgal on the bottom and 21 mgal at the surface.

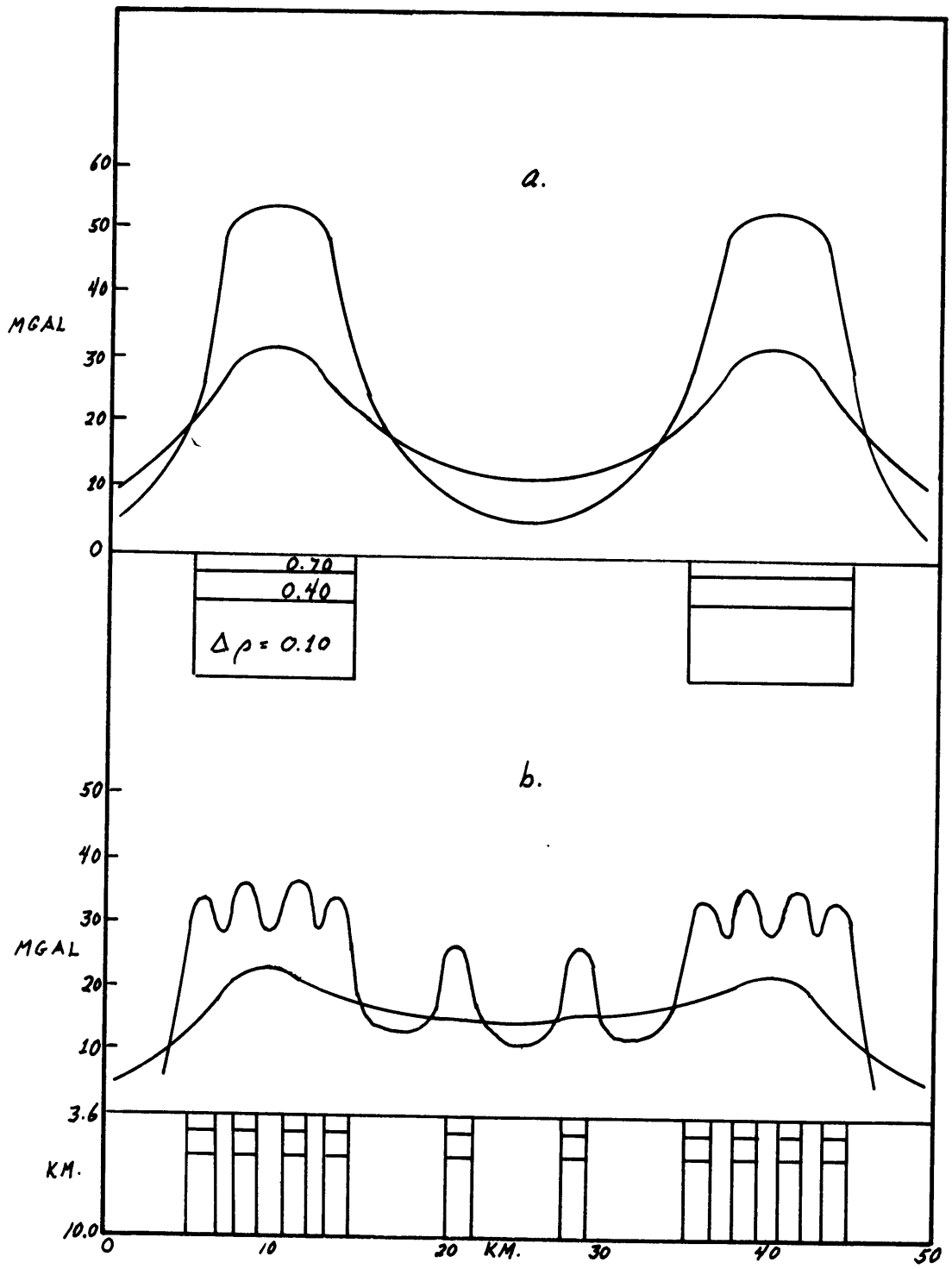

Fig. 2.7 Laborador Dikes and Variation

An interesting variation on the proposed structure is presented in Figure 2.7-b. We replace the two wide dikes with a pattern of narrower dikes, retaining density contrasts and depths. The surface anomalies show a profile similar to the previous case. The relief is not so great, but differentiation of the individual narrow dikes is impossible with the surface profile. Such a profile would probably be ascribed to two wider dikes. The bottom profile clearly delineates individual narrow dikes.

3.1 Downward Continuation

A program of downward continuation has been carried out using an analytic body (horizontal cylinder) in order to show the limitations of such techniques. Given the precision of present day surface ship gravity data, the conclusion must be that downward continuation is no substitute for bottom measurements of the same precision.

Much work has been done on downward continuation of conservative fields by oil exploration groups (Dean, 1958; Nettleton, 1954; Peters, 1949; Swartz and Sokoloff, 1954).

Downward continuation is based upon the principle that specification of a harmonic function over a closed surface determines the harmonic function over any other closed surface in the same free space.

In the case of the gravity potential field the continuation for the first derivative, g, may be written:

$$F_z(x,y,z) = -\frac{1}{2\pi}\int_{-\infty}^{\infty}\int_{-\infty}^{\infty} F_z(x-a,\ y-b)\ \frac{z}{(z^2+a^2+b^2)^{3/2}}\ da\ db$$

where F_z is the vertical component of gravity and integration is performed over the infinite x-y plane. For machine computation in two dimensions the above integral is approximated:

$$G_{bottom}(m\Delta x) = \sum_{n=-N}^{+N} W_n\ G_{surface}\ (m\Delta x - n\Delta x)$$

where the W_n are weighting coefficients.

Dean shows that the operations of upward and downward continuation are exactly analogous to the operation of a linear electric filter. The "frequency response" is the Fourier transform of the weighting function:

$$\frac{-z/2}{(z^2+a^2+b^2)^{2/3}}$$

The frequency response of downward continuation is:

$$e^{+h\sqrt{u^2+v^2}}$$

where: h = distance of continuation

$u/2\pi$, $v/2\pi$ = frequencies in cycles/unit length.

In two dimensions the frequency response reduces to $e^{+h/u/}$.

It can be seen by inspection that the operation of downward continuation is unstable as e^{hu} diverges more rapidly than any finite polynomial in u. The problem then reduces to one of data precision. Any high frequency noise in the data will be amplified with continuation until it masks the desired signal.

The weighting coefficients, W_n, of the weighting function may be found by orthogonal series relations. The mathematical details and a Fortran II program based upon Dean's approach are given in Appendix C.

3.2 Calculations

Dean demonstrated the instability of downward continuation by the extreme case of a step function. Mathematically, this is a

convenient example as it contains much high frequency power. We have here chosen the horizontal cylinder as being more representative in terms of frequency.

The analytic solution for the vertical gravitational anomaly of an infinite horizontal cylinder is given by Nettleton (1940). In order to evaluate downward continuation we propose an infinite horizontal cylinder as in Figure 3.2. The vertical gravity anomaly profiles are calculated at depts 0.0, 0.1, 0.5, 1.0, 1.5, 2.0, 2.5, 3.0, 4/0 and 5/0 km. with a 1 km. horizontal data point spacing. The precision of these profiles is ±0.01 mgal. Random (in magnitude and sign) values of maximum magnitude 0.10 and 1.00 mgal are then superposed on the 0.01 mgal data to obtain three surface profiles with ±0.01, ±0.10, ±1.00 mgal data precision.

The surface profiles are downward continued to the depths listed and compared with the analytic profiles. Normal error curve smoothing (e^{-au^2}) is then introduced into the continuation frequency response and the surface profiles are again downward continued.

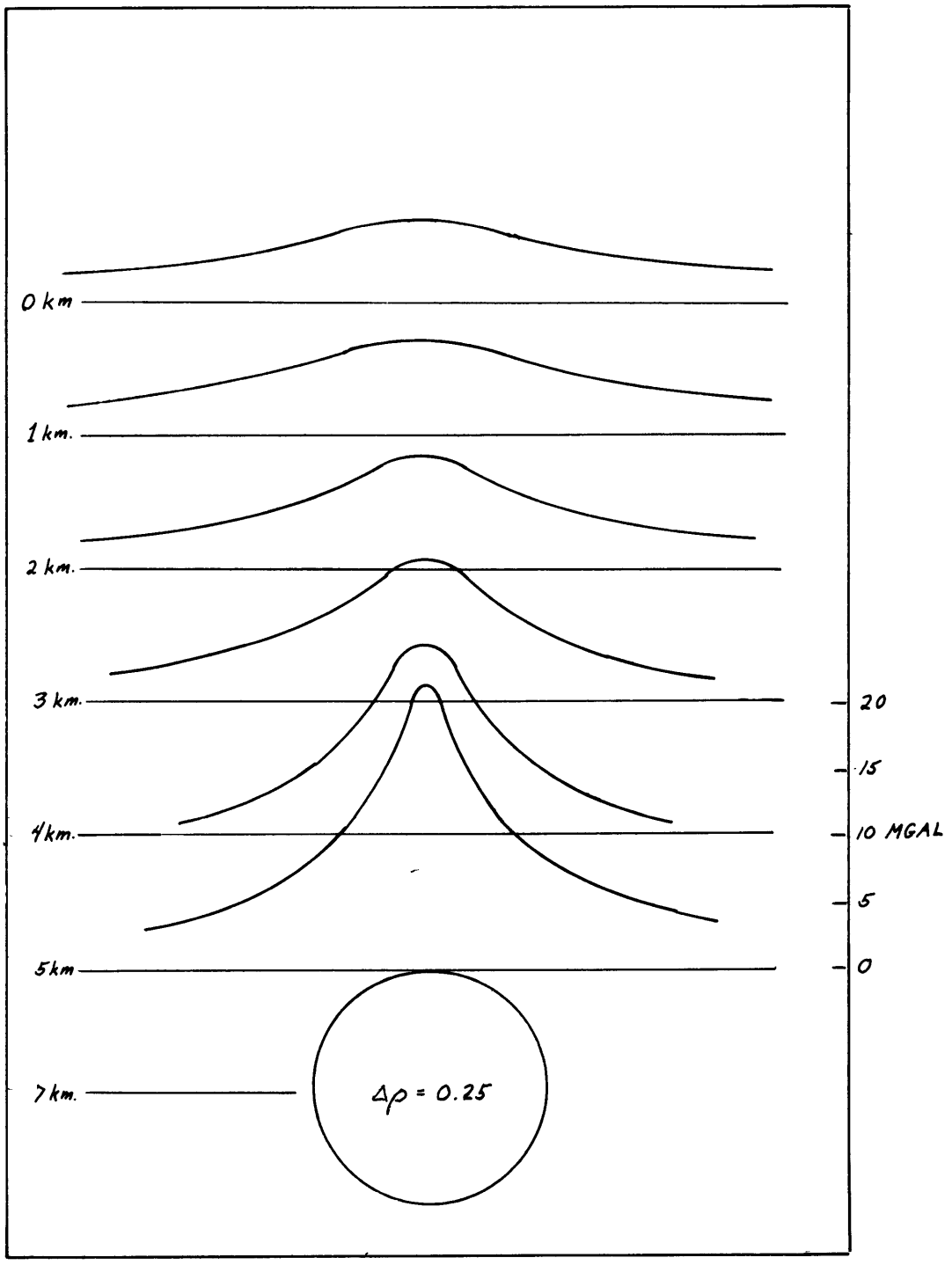

Fig. 3.2. Gravity Effect of a Horizontal Cylinder.

3.3 Results (Figures 3.31 - 3.34)

3.31 ±0.01 mgal

With 3-decimal data and no smoothing continuation is possible to a depth of about 1.5 km. Instability and a magnitude error of 0.12 mgal become apparent at 2.0 km. Smoothing allows continuation to 4.0 km. before instability. Even the 5.0 km. profile contains significant information but the magnitude error has jumped from 2.5 mgal to 5 mgal and oscillations of 2 mgal are present.

3.32 ±0.10 mgal

The 2-decimal data allows continuation to a depth of only 0.5 km. At 1.5 km. the cutoff frequency oscillation (1 cycle/2km.) has an amplitude larger than the real anomaly maximum. Smoothing allows continuation to about 3.0 km. but an instability of 3 mgal occurs at 4.0 km.

3.33 ±1.00 mgal

As might be expected the ±1.00 mgal noise makes continuation to any depth impossible. Here, the action of smoothing is apparent.

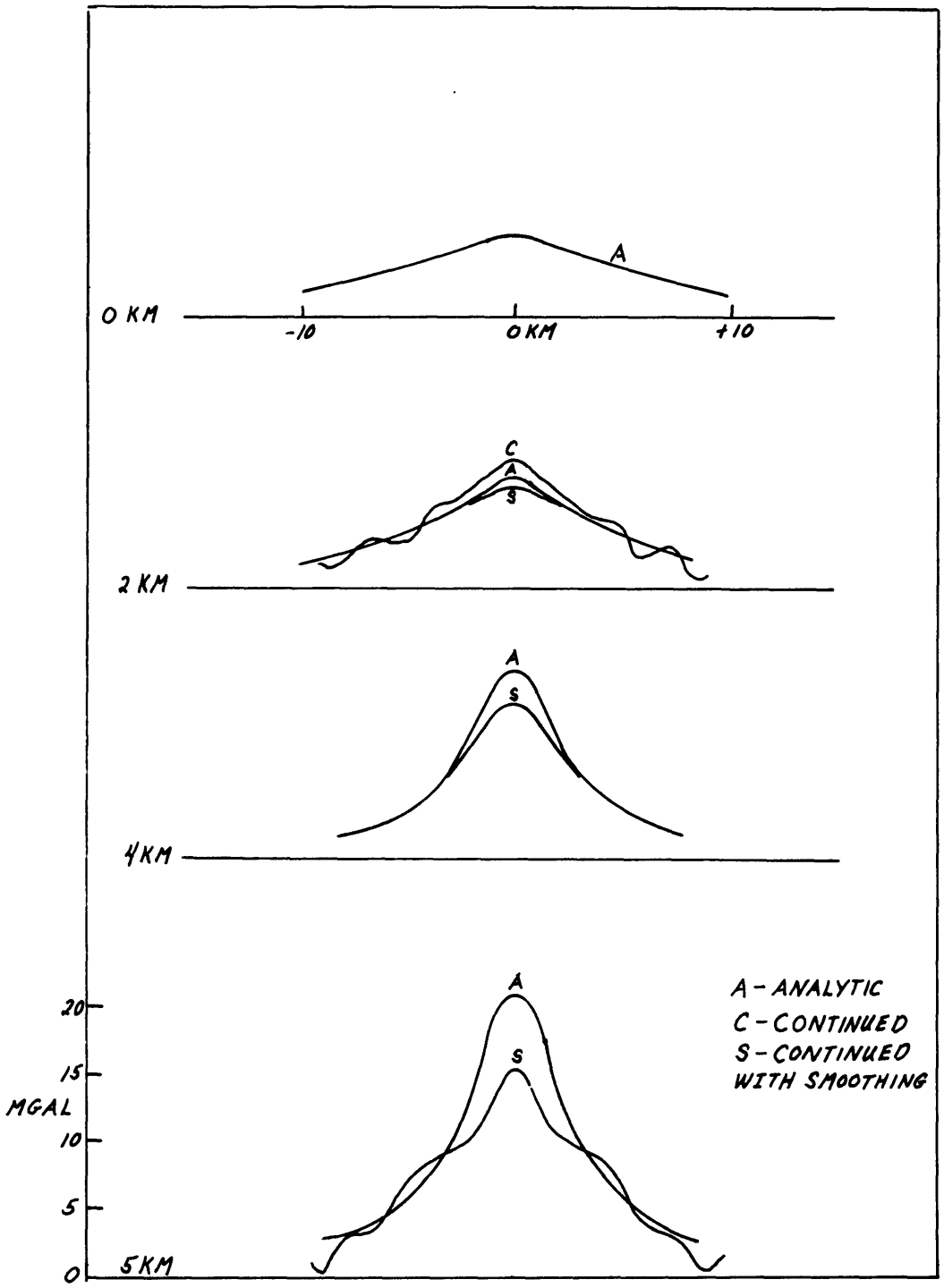

Fig. 3.31. Downward continuation, 0.01 mgal data.

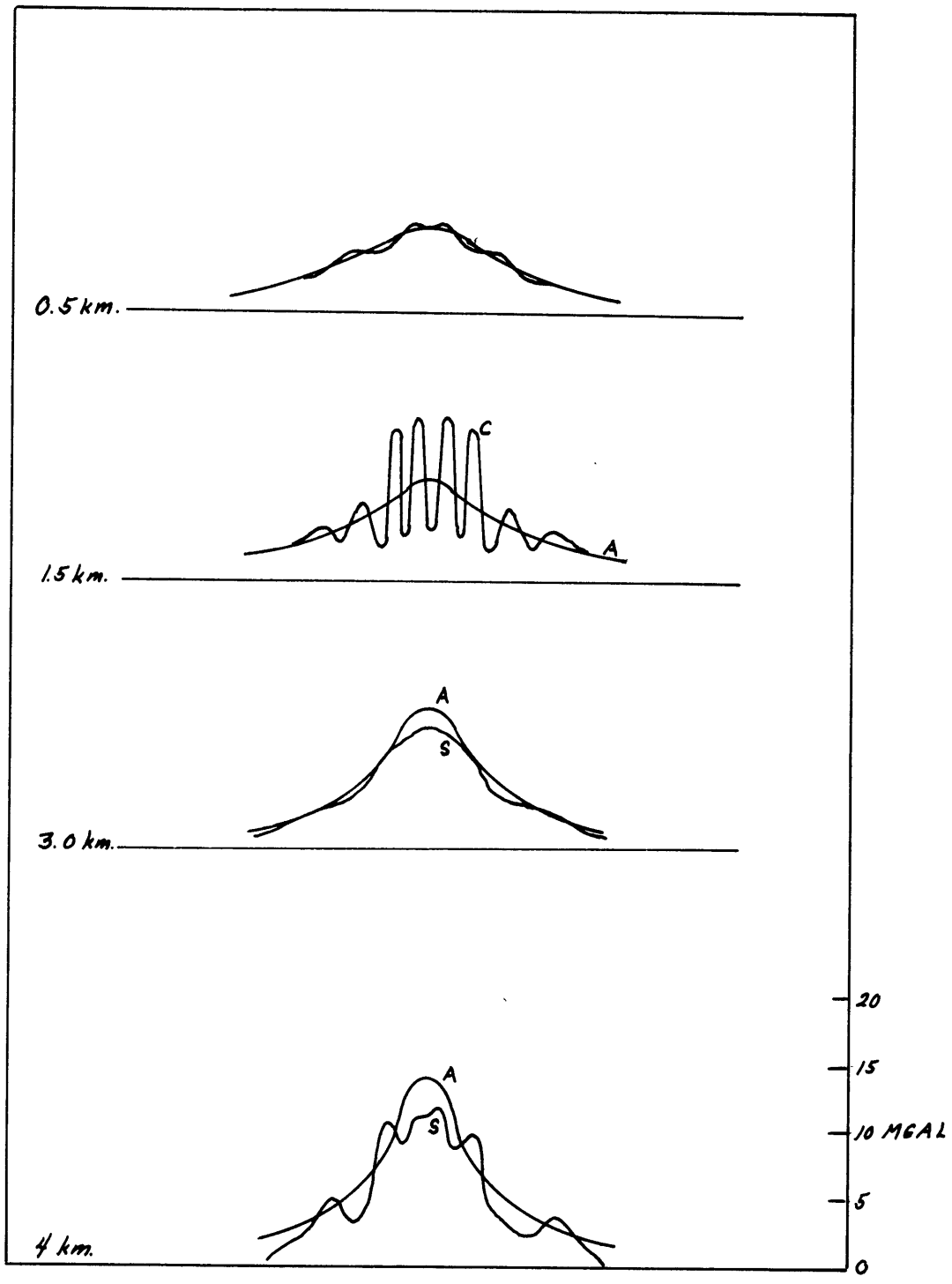

Fig. 3.32. Downward continuation, 0.10 mgal data.

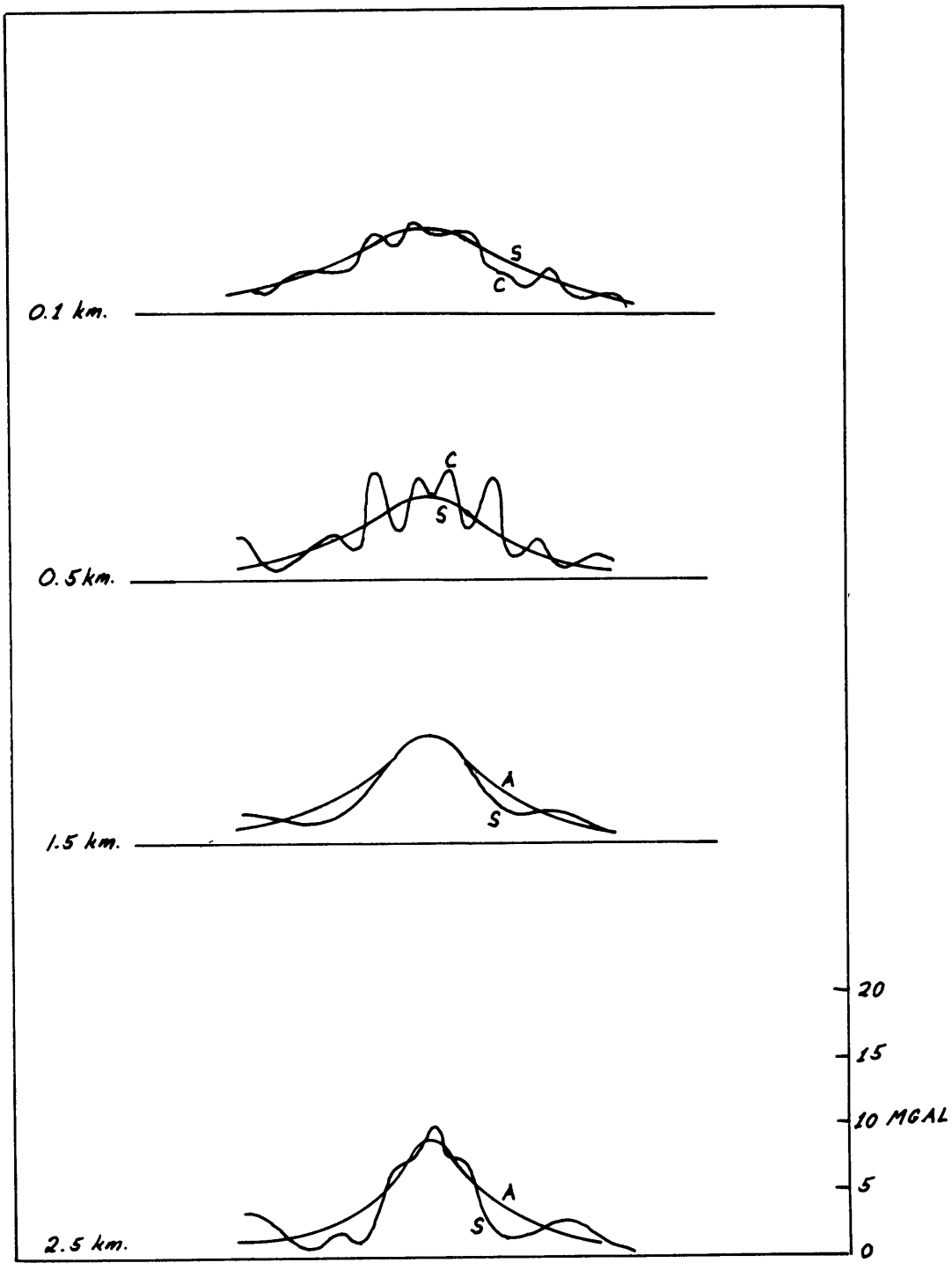

Fig. 3.33. Downward continuation, 1.00 mgal data.

Smoothing of the weighting function coefficients has the same effect as smoothing the input data. The continued and smoothed profile at 1.0 km. is smoother than the input data. The smoothed profile blows up at about 2.0 km.

3.34 Smoothing by eye

The ±1.00 mgal data was smoothed by eye before being fed into the computer. The ordinary continuation blows up first at 1.0 km., showing that the data was not read from the smooth curve to ±0.01 mgal precision.

When the smoothed input is further smoothed in the continuation, the continuation is possible to about 4.0 km. However, the second error inherant in smoothing becomes apparent. The maximum anomaly has been shifted (bias shift) 2 km. and a disymmetry is present.

Least-squares fitting of polynomials of low degree to the input data would allow further continuation in every case presented. However, least-squares smoothing is not a universal panacea. With no prior knowledge of the structure causing the anomaly there

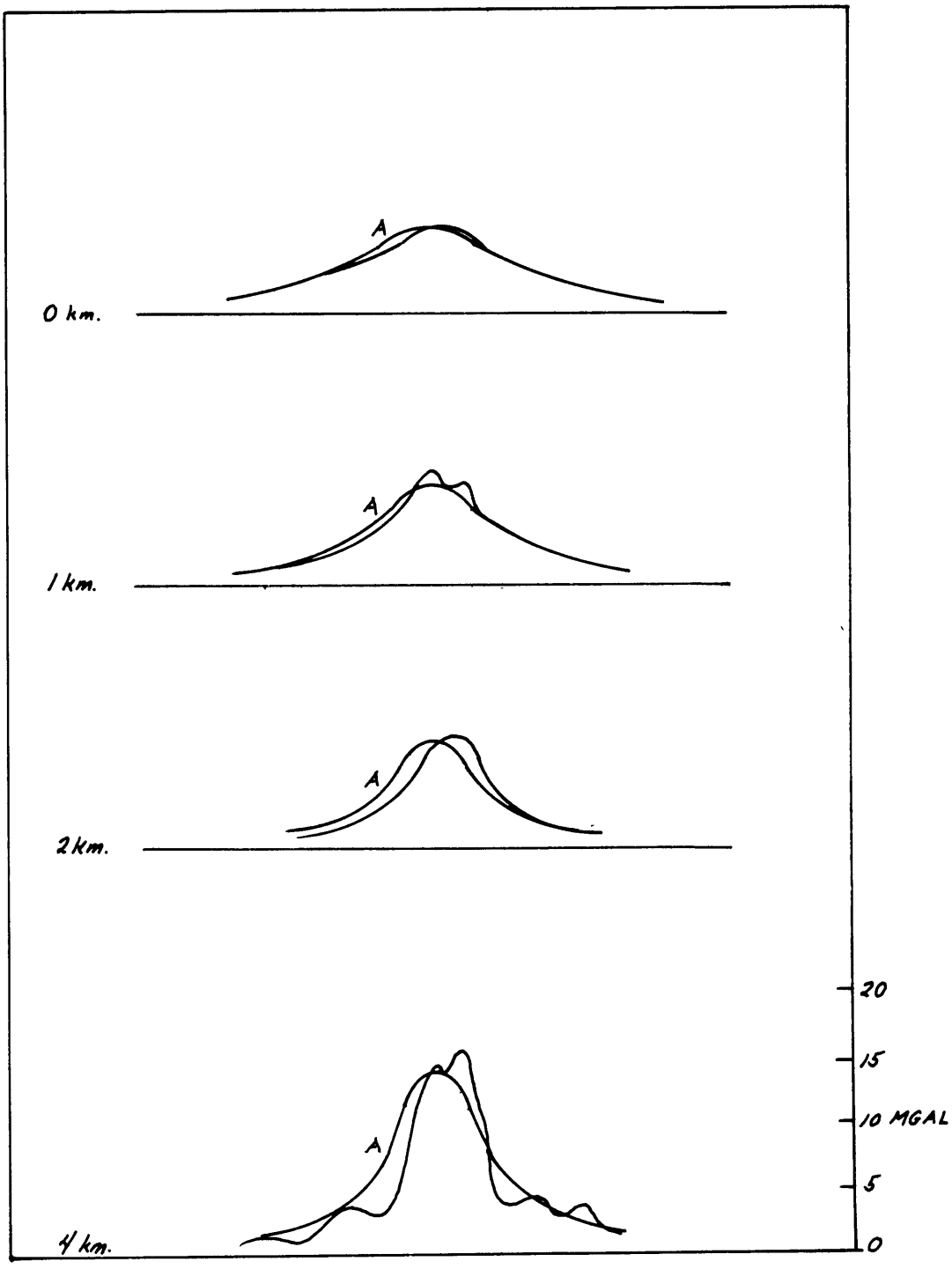

Fig. 3.34 Downward continuation with previous smoothing by eye.

is no guide to the best polynomial degree. Specifying a low degree guarantees smooth continuation but will result in the loss of the higher frequency power in the anomalies of irregular bodies. Specification of a higher degree while preserving more of the high frequency information, also preserves more of the high frequency noise.

In addition, the noise in the profile generated by the surface gravimeter is not purely random. Errors characteristically depend upon amplitude of waves and heading relative to the wave directions. A mid-profile change in either parameter would introduce lower frequency noise which could not be filtered.

PART THREE

CHAPTER ONE

MEASURING GRAVITY AT SEA

There is little difficulty in measuring accelerations with a precision of 10^{-6}g. In measuring the acceleration of gravity, however, we are measuring an acceleration in a fixed direction at a fixed point on the surface of the earth. In other words, to measure gravity at sea we need to either: 1) maintain the gravimeter in a fixed position and orientation; or 2) measure the deviations in position and orientation of the gravimeter and thereby correct the indicated readings.

1.1 Errors

In measuring gravity in a fixed position and orientation (as on the sea floor), the errors are all due to the mechanical and electrical limitations of the device. These errors are discussed in Section 2.1.

In measuring gravity from a non-fixed position, a host of additional errors may be introduced:

1.11 Vertical accelerations are indistinguishable from those due

to gravity. Unless the sensor response is linear, the signals due to random accelerations will not average to zero.

1.12 Horizontal accelerations are treated in different ways and thus have different sets of errors.

a. Gimbal mounting keeps the input vector of the sensor parallel to the sum of all accelerations. However, the vector sum of the horizontal and gravity accelerations is greater than gravity alone. We thus have the Browne error, (Browne, 1937) the time average of g cos θ. This error commonly amounts to several hundred mgal.

b. A stable platform avoids the Browne correction but introduces others. The first is the off-level error of g cos θ (Wall et al., 1966) due to the steady state misalignment of the measurement axis with the direction of local vertical.

c. Under the indluence of periodic accelerations the table may have a periodic component of tracking error, the Harrison effect (Harrison, 1954). This error is usually about 1 mgal.

d. The cross-coupling error arises when the beam, deflected slightly from the horizontal by vertical acceleration, is subjected to horizontal accelerations. The maximum cross-coupling error is about 10 mgal (Wall, et al., 1966).

1.13 Drift is a characteristic of all gravimeters. The limits on drift in both the Graf and LaCoste meters may be set at a maximum of 0.1 mgal/day. This estimate excludes the unpredictable tares.

1.14 Centrifugal acceleration of the earth's rotation about it's axis reaches a maximum of about 2,000 mgal at the equator. This is part of "gravity" as opposed to the pure Newtonian attraction "gravitation".

When a mass moves relative to the surface of the earth, however, it experiences further accelerations (Coriolis, 1844). In vector form, the Coriolis acceleration is

$$2\,\Omega \times V$$

where Ω = angular velocity of the earth

V = vector velocity of body relative to the earths' surface

In Cartesian coordinates, the three Coriolis components are:

$2\,\Omega\, v \sin \phi$ eastward

$-2\,\Omega\, u \sin \phi$ northward

$2\,\Omega\, u \cos \phi$ upward

where u = relative velocity eastward
v = relative velocity northward
ϕ = latitude

The first two components constitute the "Coriolis force" of the meteorologists. The third term combined with the centrifugal acceleration of relative motion constitute the Eötvös effect:

$$E = 2\,\Omega\, u \cos \phi + (u^2+v^2)/R$$

where R = radius of the earth

A ship drifting eastward on the equator at a velocity of 0.2 ft/sec. or 0.25 km/hr. would sense gravity reduced by -1 mgal. A ship steaming north across the equator at a velocity of 15 knots would have an error of $\pm$1 mgal if the uncertainty of heading were $\pm 0.6^{\circ}$.

1.2 Methods

1.21 Pendulum

Over 5,000 gravity stations have been occupied by the Vening-Meinesz pendulum apparatus, used aboard submarines from

1923 till 1959 (Vening-Meinesz, 1948; Worzel, 1965). The submarine hovered at depths of up to 300 feet. At depth the accelerations due to waves were normally below 6 X 10^{-3}g. The apparatus was gimbal mounted and auxiliary long-period pendulums sensed the horizontal accelerations necessary for the Browne correction. The uncertainty in free-air anomaly for the later measurements was estimated as $\pm$3.6 mgal (Worzel, 1965). The errors in the Vening-Meinesz determinations were slightly greater.

1.22 On-the-Bottom Gravimeters

Many gravity stations have been occupied in the Gulf of Mexico with the Gulf Underwater Gravimeter (Pepper, 1941) to a maximum depth of 600 feet. Developed in 1940, it was a completely remote controlled version of the Gulf land meter (Wyckoff, 1941). Data was recorded as displacement of a line on a continuously advancing film and the accuracy was essentially the same as with the land version, subject to depth correction and water conditions.

The LaCoste land gravimeter has been similarly adapted and

much use has been made of it on continental shelves. It has been of particular service in laying out sea gravity ranges (Fanning, Garoutte, 1962 a,b; Goodacre, 1964). The maximum useful depth of this meter has apparently been 1,000 feet.

Even a diver in a bell has been used for underwater gravimetry (Frowe, 1947). More recently gravimeters have been used in the new deep submersibles, but not with any regularity.

1.23 LaCoste-Romberg Surface Ship Gravimeter

Spring-type gravimeters have recently been modified for surface-ship operation by two independent designers, L. La Coste and A. Graf. Since both instruments have about the same accuracy and characteristics, exclusive of mounting, only one will be described here. There is much recent literature on both meters listed in the references. For the Graf-Askania meter, see especially: Graf (1956), Graf and Reinhard (1961), Wall et al., (1966).

The La Coste gravimeter is shown in its simplest terms in Figure 1-23. The equation of motion of the beam is:

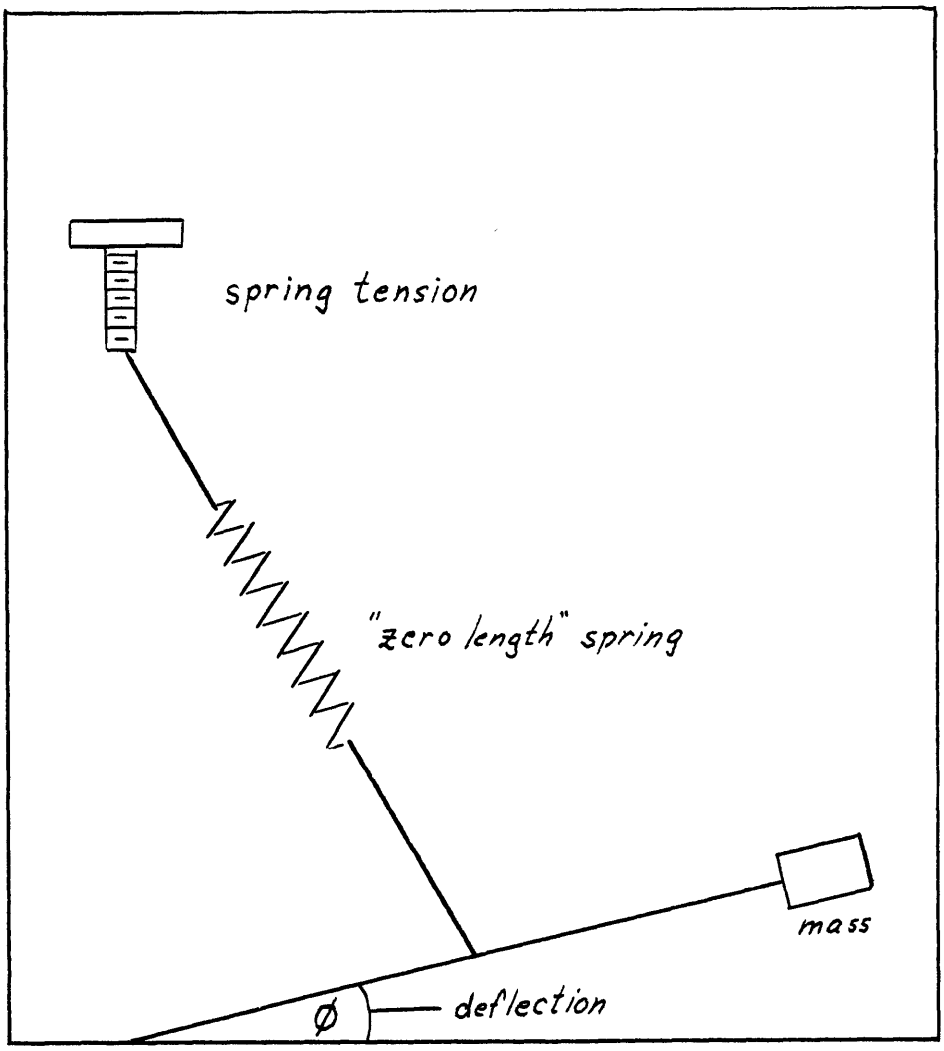

Fig. 1.23 The LaCoste-Romberg gravimeter spring.

Torque $\Gamma = I\ddot{\phi} + \beta\dot{\phi} + k\phi$

where: I = angular moment of inertia

β = damping factor

k = spring constant

Also, $\Gamma = L(g + \ddot{z} + B - C)$

where: $\ddot{z}$ = vertical acceleration

L = lever arm

B = Browne correction

C = instrument constant

Then, integrating and equating:

$$\int_{T_1}^{T_2} (I\ddot{\phi} + \dot{\phi} + k\phi)dt = L\int_{T_1}^{T_2} (g + \ddot{z} + B - C)dt$$

But $$\int_{T_1}^{T_2} (g + \ddot{z})dt = \bar{g}(T_2-T_1)$$

provided the instrument response is <u>linear</u>.

Also, $$\int_{T_1}^{T_2} Bdt = \bar{B}(T_2-T_1)$$

$$\int_{T_1}^{T_2} Cdt = \bar{R}(T_2-T_1) + \bar{B}(T_2-T_1)$$

where: R is spring setting attributed to gravity alone.

B is that attributed to the Browne correction.

Then, $L(\bar{g} + \bar{B} - \bar{R} - \bar{B})(T_2 - T_1) = L(\bar{g} - \bar{R})(T_2 - T_1)$

$$\text{or} \quad \bar{g} = \bar{R} - \frac{1}{L(T_2-T_1)} \int_{T_1}^{T_2} (I\ddot{\phi} + \beta\dot{\phi} + k\phi)dt$$

ϕ is read as a function of time and a computer returns the second term, which may be read visually from a pen recording. R is also recorded so that $\bar{R}$ may be determined visually. Then $\bar{g}$ is computed from the last equation above.

In its most refined form, navigational fixes and soundings are also fed into the computer to correct for the Eötvös effect and to calculate the Bouguer anomaly (Bernstein and Bowin, 1963).

Many of the errors due to random accelerations of the sea surface have been ingeneously and effectively eliminated in this gravimeter. These instruments still have unsolved sources of error, however:

1. Accelerations of the sea surface of over 10^{-2}g (10,000 mgal) cause increased error due to non-linearities of instrument response.

2. Although the advent of V.L.F. navigation holds much promise

for ships possessing the required electronics, the error due to the Eötvös effect has yet to be overcome.

3. Accelerations due to surface waves with periods of the order of the measuring time cannot be effectively filtered. Therefore, the measurement period required is determined by the period of the longest significant wave present. The longest period of a surface wave with acceleration > 1 mgal is usually about 60 sec. (Munk, 1962).

4. A ship of at least 500 tons displacement is required both for the elaborate instrumentation and the desired response to the sea.

5. When the Browne correction approaches 300 mgal, systematic errors of about 10 mgal are observed, due probably to inadequate horizontal accelerometer response to long period motions.

1.24 Tokyo Meter α -1

The "Tokyo Surface Ship Gravity Meter α -1" reported by Tomoda and Kanamori (1962) was the third application of the vibrating

string to surface ship gravimetry (see previous use of vibrating strings, Section 3-2). It will be described because it was the most sophisticated attempt.

The string was a strip of beryllium copper (0.015 X 0.170 X 30 mm.). The 45 gm. mass was cantilevered for cross support with an effective mass of 25 gm.. String frequency was 1800 cps.

String frequency was determined with a preset counter with a time base of 30 kc.. The preset number was either 512 or 1024 string cycles. Sampling period was thus either 0.3 or 0.6 sec. with a least significant bit equivalence of 100 mgal.

The string was mounted on a gyro-stabilized platform with an rms error of 4'. Since the string was cross supported, the Browne correction was less than 1 mgal.. Several other errors due to the nature of digital data were discussed and noted to be of the order 10 mgal. However, as was pointed out, increase in the time base frequency and decrease of sample period would reduce these errors to less than 1 mgal.

As has been the case with all other vibrating string sea gravimeters, the fly in the ointment is non-linearity.

Let the acceleration be:

$$g(t) = g_o + \ddot{z}_m \sin \frac{2\pi t}{T}$$

Using the Maclaurin's series expansion, the magnitude of the first non-linear term is $3/8(\ddot{z}/g_0)^2$.

When no correleation between sample points and acceleration phase exists (as in this case), a systematic error is introduced:

$$\Delta g = 3/8\ g_0\left(\frac{\ddot{z}_m}{g_0}\right)^2 \left[1 - \left(\frac{\sin \tau/T\,\pi}{\frac{\tau}{T}\pi}\right)^2\right]$$

With $\ddot{z}_m$ = 10,000 mgal, T = 6 sec., and τ = 0.3 sec., this error is 0.3 mgal, an acceptable figure. However, the error increases as the square of $\ddot{z}_m$. At $\ddot{z}_m$ = 100,000 mgal, Δg = 30 mgal.

CHAPTER TWO

ACCELEROMETERS AS GRAVIMETERS

The practical application of accelerometers in measuring the acceleration of gravity at the earth's surface is an innovation. Since there have been good gravimeters of the restraining spring type for several decades, a reason for this deviation must be given.

The best of the restraining-spring gravimeters are null-point devices. A null-point instrument requires either human operation or an elaborate servo mechanism. It is felt that the automation of an inherently human-mechanical system is a difficult approach (Sam Worden, personal communication). A second objection is the rather great size of present spring gravimeters.

The most important reason for rejecting a spring gravimeter is the mode of operation. Any gravity sensing element must be held in a gravity-vertical orientation. This may be accomplished in three ways: 1) servo-leveling, 2) gimbal leveling, 3) fluid leveling. The first requires excessive space and power for a free instrument.

The second is impossible to achieve with the combination of sufficient sensitivity and resistance to shock. The third (the method chosen) requires that a rigid mass be stable in a floating position. Automation of the restraining spring gravimeter, however, would require moving parts.

The advantage of null-point, spring gravimeters in the past has been their greater sensitivity. The commercially available gravimeters commonly have a sensitivity of 10^{-8}g, while inertial types have been limited to 10^{-4}g. In recent years, however, government support in the space industries has given great impetus to the latter types. A sensitivity of 10^{-7}g is now achieved with many of these improved devices. Since the ultimate accuracy of inertial guidance systems depends upon these accelerometers, it is reasonable to expect continued research and improvement of their performance during the next few years.

2.1 Performance

Once the decision was made to use an inertial accelerometer, the performance of each was considered. The factors were:

a) linearity, b) sensitivity, 3) scale factor stability, d) null point stability.

Suppose an accelerometer has a frequency output. Then the acceleration of gravity may be expressed:

$$F = K_0 + K_1 g + K_2 g^2 \cdots$$

where: K_0 = null point frequency

K_1, K_2, $\cdots$ = scale factors

a) Linearity may be defined as some ratio involving $K_{1,2\ \cdots}$ The perfectly linear device has no K factors beyond K_0, K_1. Linearity is a convenience but not a necessity where calibration is possible.

b) Sensitivity is defined as the smallest Δg which will produce a ΔF. A common figure for the most popular accelerometers is 10^{-7}g, although special types go to 10^{-12}g.

c) Scale Factor Stability is the stability of K_1, K_2, $\cdots$ expressed as g/g/time. In attempting to measure a variation of 10^{-6}g over a period of one week, an accelerometer must have a scale factor stable or predictable to 10^{-6}g/g/week.

d) Null Point Stability expresses the uncertainty in null point output as g/time. This figure, like the scale factor stability, must be known to 10^{-6}g/week. Although this stability is difficult to achieve, certain techniques of measurement sometimes allow cancellation of the term.

2.2 Types of Inertial Accelerometers

The most widely used inertial accelerometers are:

a) force balance pendulous
b) pendulous integrating gyroscope
c) vibrating string

2.21 Force Balance Accelerometer

This accelerometer, Figure 2.21, is essentially a high gain null-seeking servo. A pendulous mass is free to react along an axis of input acceleration. Motion of the mass and attached coil produces a current in the pickup coils. This pickup current is highly amplified and fed back to the restoring coilds. If the system is stable, the proof mass will seek a null. The current flowing through the restoring coils is a direct indication of the acceleration.

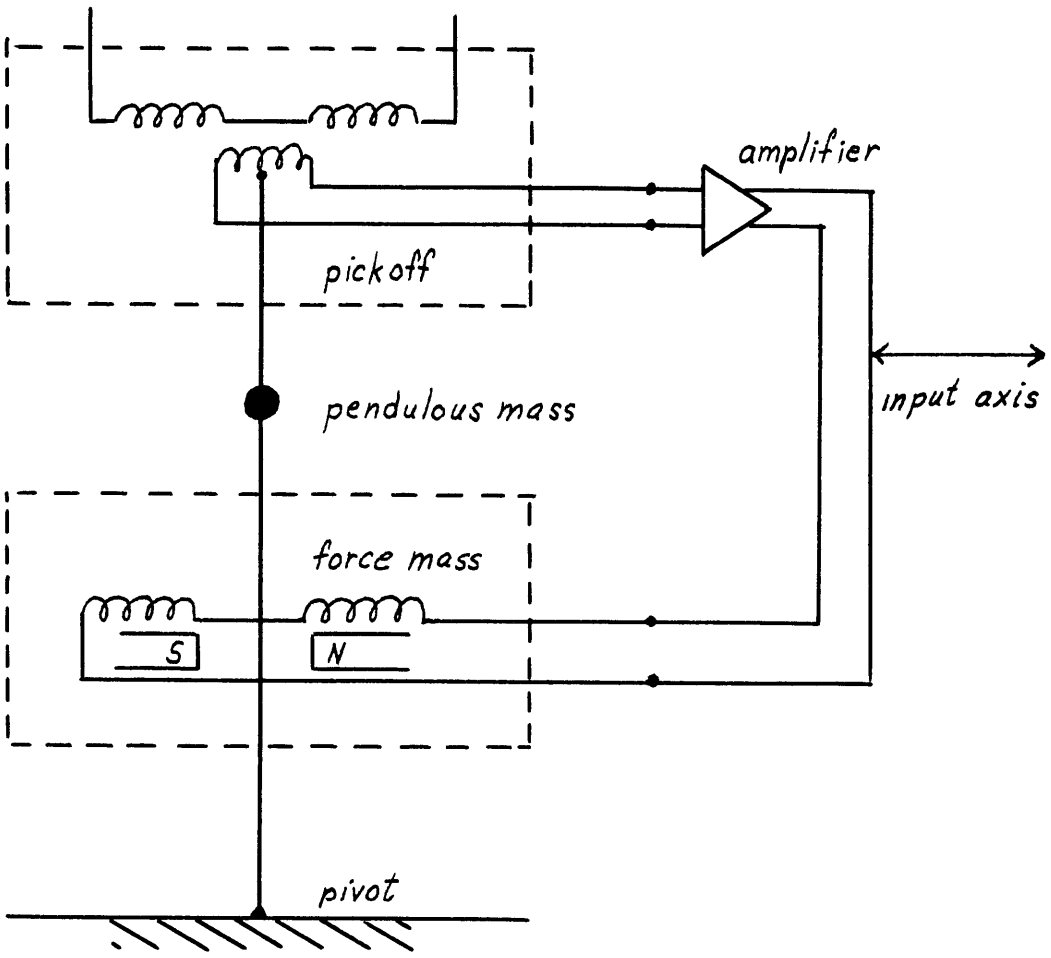

Fig. 2.21 The force-balance accelerometer.

A major problem in the force-balance accelerometer is cross-coupling. That is, the pendulous mass must be displaced from null to produce a signal. The necessary "hang-off angle" subjects the support system to a component of the acceleration in the direction perpendicular to that of the sensitive axis. To reduce this effect, very high gain amplifiers must be employed with an attendant reduction of stability.

It is well established that time is the quantity most accurately measured. For this reason, the best force balance accelerometers use rebalance forces produced by pulsed current. If the pulses are identical, the pulse frequency is the measure of acceleration.

The requirement that the pulses be identical is the second major problem in this device.

2.22 Pendulous Integrating Gyroscopes

A gyroscope with pendulosity ml is subject to a torque mgl in the field of gravity. As in Figure 2.22 this torque causes a precession of:

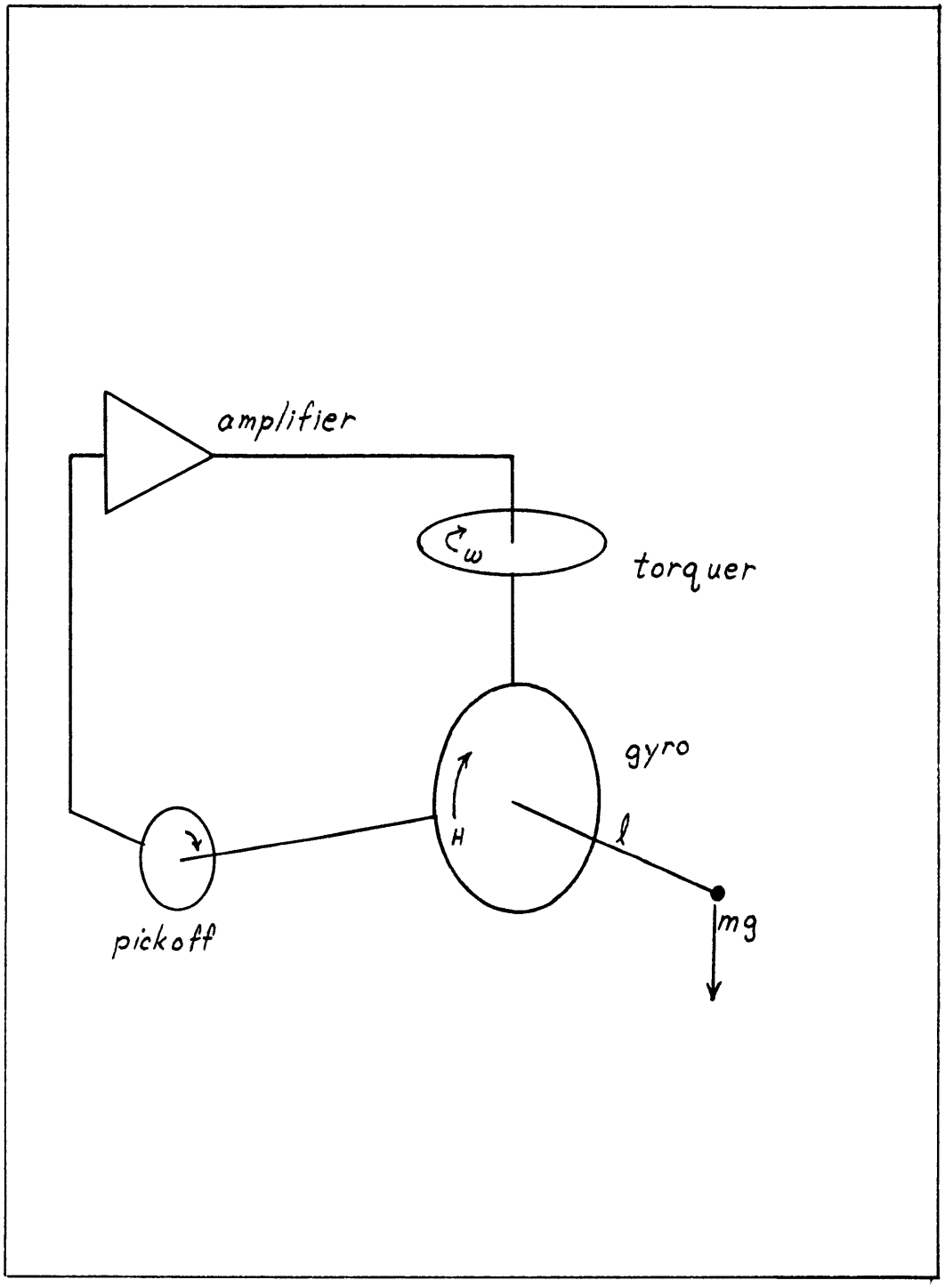

Fig. 2.22 The pendulous integrating gyro accelerometer.

$$\omega = mgl/H$$

where H is the angular momentum of the gyro rotor.

A pickup feeds a servo loop which drives the gimbal support at the angular velocity of precession ω, thereby maintaining the gyro lever arm in its null position. The angular velocity may be converted to frequency by a chopper.

The great advantage of this accelerometer is linearity. However, it suffers from the same stability problems as the others. Being a mechanical device, it cannot entirely escape the changes in dimensions caused by relaxation of residual stresses. This device has also relatively large size and power requirements.

2.23 Vibrating String

The vibrating string accelerometer will be considered in a separate section in more detail, since it was the type chosen for this study. As will become clear in the discussion, while having limitations in stability, it is by far the simplest in design and operation.

CHAPTER THREE

THE VIBRATING STRING

3.1 Theory of the Vibrating String

A string under tension has a natural frequency of vibration when excited. The frequency of vibration is a function of factors related to the dimensions, material and tension in the string.

Rayleigh (1945) has derived the natural frequency of a string suspended vertically with a mass attached at its lower end.

$$f = 1/2L\sqrt{Mg/m}\left[1 + x/L\sqrt{(ES+Mg)/Mg}\right]$$

where L = string length

M = attached mass

m = string mass per unit length

x = radius of gyration of string about mid-plane

E = string modulus of elasticity

S = cross section of the string

If a string is used under tension approaching its breaking strength (a common figure is 20%), the second term in parentheses is usually less than 0.01. Over small dynamic ranges we may therefore use the approximation:

$$f = 1/2L\sqrt{Mg/m}$$

Referring to Figure 3.1, Part One, let the tension in the string consist of two terms:

1) Mg, as before

2) T_0, prestressing by clamping both ends

Then, $f = \frac{1}{2L}\sqrt{\frac{Mg + T_0}{m}}$

For any particular string and mass, the frequency of vibration varies with the acceleration of gravity. Considering gravity as the variable, the frequency may be expressed as a Maclaurin's Series:

$$F = K_0 + K_1 g + K_2 g^2 + K_3 g^3 + \cdots$$

For the problem of determining gravity in the presence of time-varying accelerations, see Appendix C.

3.2 Previous Use of Vibrating Strings

3.21 Gilbert, 1949

Gilbert set the design criteria for several later gravimeters. His string had a length of 5 cm. and a natural frequency of 1 kc.. The string was a thin strip (.010 X .002") of beryllium copper in order that rigidity of the wire not influence the natural frequency unduly. The 65 gram copper weight was heavily damped by a magnetic

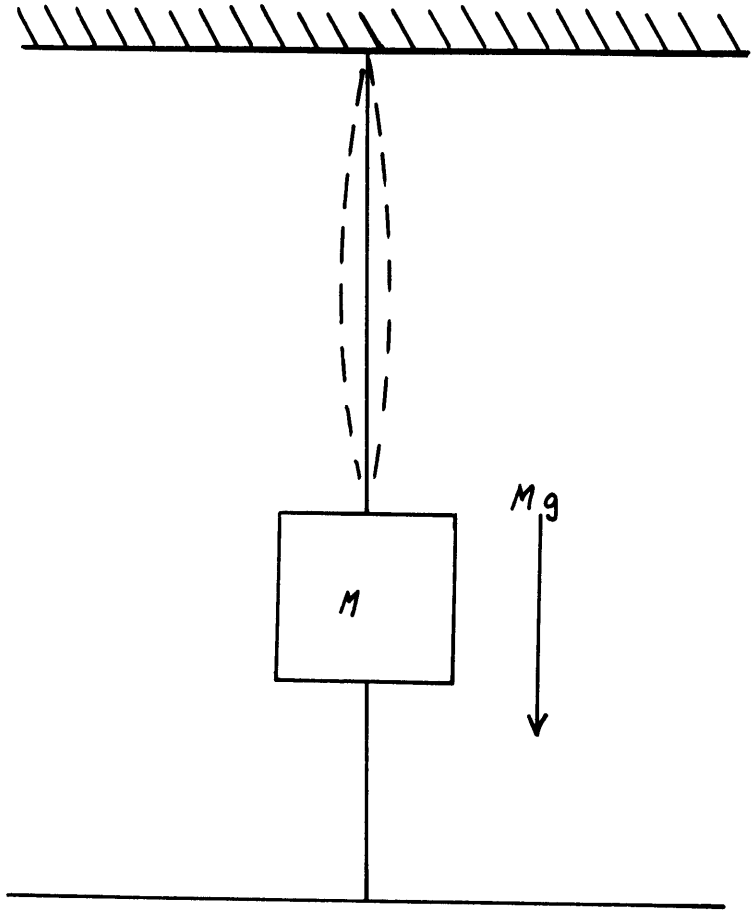
Mg
M

field to decrease pendulous swinging in the presence of horizontal accelerations. Q of the string was 20,000 when a vacuum of 2×10^{-3} mm. was held.

The string frequency produced beats with a standard 1 kc. frequency. The beat frequency was split into three phases which drove a Selsyn motor on a mechanical counter. The count was photographed at 5 second intervals and a mean taken for the value of gravity.

3.22 Lozinskaya, 1959

The vibrating string constructed by Lozinskaya is very much like Gilbert's. The string of 5.2 cm. length also had a resonant frequency of 1 kc.. The beryllium-bronze string had a rectangular cross scetion of 0.020 mm. X 0.37 mm. The 70 gm. cuprite mass was again heavily damped in a magnetic field. A vacuum of 10^{-2} mm. was maintained.

The string frequency again produced 3-phase beats against a standard 1 kc., driving a Selsyn-type motor. The only significant

change was the continuous strip photographic recording of the rotor position which preserved the sea surface accelerations more fully.

3.23 Tomoda and Kanamori, 1962

The Tokyo Surface Ship Gravity Meter α -1 once again used a Gilbert-type vibrating string (beryllium-copper, 0.015 X 0.170 X 30 mm., mass 45 gram. 1.8 kc. natural frequency, Q: 25,000 in 10^{-5}mm. vacuum). A very significant improvement, however, was the change from gimbal to stable platform mounting, eliminating the Browne correction. To allow the change of mount, all pendulous swinging of the string has to be eliminated. This was done by cross-supporting the mass and eliminating magnetic damping.

A second significant improvement was the change in frequency measurement. The beat frequency and phase detection method was replaced by preset counting. The time required for a frequency determination was thereby decreased by at least a factor of ten. The third innovation was the use of digital rather than analogue filtering.

In view of the improvements in method, the results obtained were rather disappointing. The method used, in conjunction with a few relatively easily achieved improvements in equipment, is theoretically capable of measurements in the 1 mgal range.

3.24 Goodell and Fay, 1964

Goodell and Fay were the first to make radical changes in the string itself with rather unfortunate results. The changes were to an invar string, nine inches in length, and vibrating in its ninth mode. The result of these changes was a string drift of about 100 mgals/day compared to < 1 mgal/day for the Gilbert string. Due to the linear character of the drift, a precision of about $\pm \frac{1}{2}$ mgal was still achieved in borehole measurements.

3.25 Howell, Heintz and Barry, 1965

In contrast to Goodell and Fay, the changes introduced by Howell et al were improvements. They returned to Gilbert's 5 cm. string in the first mode of vibration. They also retained the Tokyo cross support of a cantilevered mass. The big improvement was the change from beryllium copper to tungston wire, having a

greater strength and smaller temperature coefficient. The Q also went up to > 200,000 with a higher vacuum of 10^{-6}mm. In contrast to the previous borehole gravimeter, the drift was reduced to $\pm$0.1 mgal/day with an obtainable precision of $\pm$0.01 mgal.

It is interesting to note that Howell et al. are the first to mention experiments with gold plated quartz fibers, a possibility which must have occurred to others.

3.3 The American Bosch Arma VSA - A Double String

3.31 Maclaurin's series for a double string

The non-linear terms in the Taylor Series expansion reduce as the order approaches infinity, and the series converges. Let a subscript (+g) indicate a measurement made in the direction of the +g vector, while a subscript (-g) indicates the inverse. If we express the frequency of each string in the two directions as series, we have:

$$F_{1,+g} = K_{01} + K_{11}g + K_{21}g^2 + K_{31}g^3 + \cdots$$

$$F_{2,+g} = K_{02} - K_{12}g + K_{22}g^2 - K_{32}g^3 + \cdots$$

$$F_{1,-g} = K_{01} - K_{11}g + K_{21}g^2 - K_{31}g^3 + \cdots$$

$$F_{2,-g} = K_{02} + K_{12}g + K_{22}g^2 + K_{32}g^3 + \cdots$$

$$\Delta F_{+g} = (F_1-F_2)+g = (K_{01}-K_{02}) + (K_{11}+K_{12})g + (K_{21}-K_{22})g^2 + \cdots$$

$$\Delta F_{-g} = (F_2-F_1)-g = (K_{02}-K_{01}) + (K_{12}+K_{11})g + (K_{22}-K_{21})g^2 + \cdots$$

$$\Delta F_{+g} + \Delta F_{-g} = 0 + 2(K_{11}+K_{12})g + 0 + \cdots$$

Therefore, by measuring ΔF_{+g} and ΔF_{-g} and summing the results, we eliminate identically the even terms in the expansion with a resulting improvement in linearity. Even more important, however, is the elimination of the null factor. Since the null factor contributes the largest error due to instability of vibrating strings, this feature of the Arma vibrating string accelerometer makes it particularly appealing.

Two modifications are made on the double string, single mass, system to improve its performance. Two separate but equal masses, joined by a relatively soft spring, are used in place of the single

mass. See Figure 3.31. This reduces the transmission of energy from one string to the other while not causing any deterioration of the system. The second modification is the substitution of flat tapes for the strings. These tapes are mutually orthogonal, reducing the tendancy to vibrate sympathetically.

To reduce the effect of accelerations not directed along the axis of the tapes and to increase the resistance to shock it becomes necessary to restrain the masses. This is accomplished by cross support tapes perpendicular to the sensitive axis. Figure 3.31 shows the basic Arma Vibrating String Accelerometer.

3.32 Electrical Operation

Permanent magnets provide a means for vibrating the strings laterally at their natural frequencies. If a current is passed through a wire in a magnetic field, a force is produced on the wire. If the current is reversed, the force is in the opposite direction. Likewise, if a moving wire is in a magnetic field, voltages are induced in the wire. These voltages can be regenerated by stable

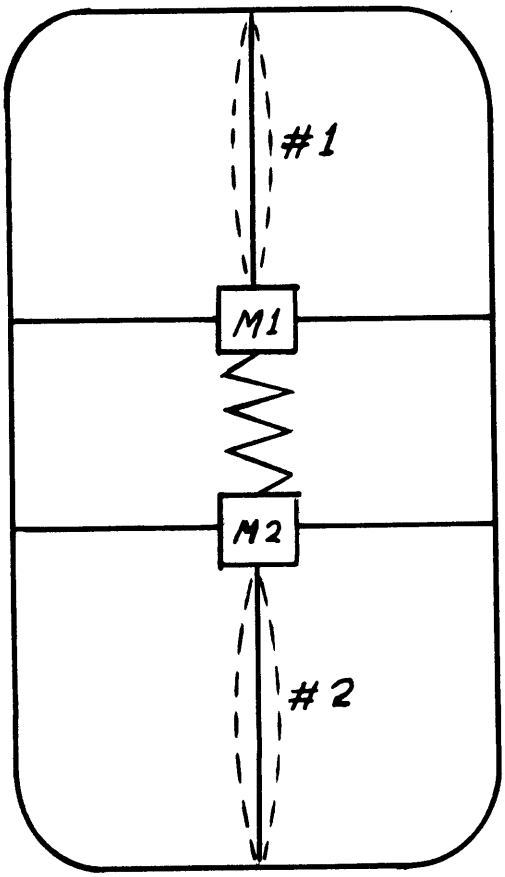

Fig. 3.31 Arma V. S. A.

high gain amplifiers and returned to the tapes to provide the energy necessary to sustain oscillation. The tape is therefore part of a tank circuit which oscillates at its natural frequency.

3.33 Calibration

Since the accelerometer scale factors are unstable to some degree, a program of periodic recalibration is necessary.

The extreme variations in g to be expected in a world wide sea gravimetry survey amount to about 7,000 mgal ($\sim$ 0.7%g). Calibration by actual measurement over a known range approximating this variation would be difficult. Fortunately, the Arma vibrating string is virtually insensitive to cross accelerations. The instrument responds to g cos θ where θ is the angle between the gravity vertical and the sensitive axis. Therefore, rotating the accelerometer sensitive axis subjects it to an apparent changing g.

The problem must be considered from two different angles:

a) What range of θ is required to simulate the range of g?

b) What accuracy in θ is required for a given accuracy of calibration?

Table 3.33

Off-level error calculations.

θ (min of arc)	error (mgal)
± 1	0.04
2	0.17
5	1.0
10	4.2
1°	131
5°	3275
5°45'	5030

a) $g_{apparent} = g \cos \theta$

$\Delta g = g - g \text{ apparent}$

$= g - g \cos \theta$

$= g (1 - 1 + \theta^2/2^1 - \theta^4/4^1 + \cdots$

$\simeq g (\theta^2/2)$

b) $g \text{ apparent} = g \cos \theta$

$dg_{apparent} = g \sin \theta \, d\theta$

let $dg_{apparent} = \pm 1$ mgal

and $d\theta = 2''$

then $\theta = 5^{\circ}45'$

By using a Vinco precision rotary head with an average tolerance of two seconds of are, the accelerometer may be calibrated with an accuracy of $\pm$ 1 mgal through a range of 5,000 mgal.

Since the term $2(K_{31} + K_{32})$ is much smaller than $2(K_{11} + K_{12})$, a redetermination of the third order term need not always be made. Since the even order, including the null, terms are cancelled in actual operation, simply measuring gravity at a known station is sufficient for recalibration.

Results of Calibration

$$2(K_{21} - K_{22}) = -16 \text{ mgal/G}^2$$

$$2(K_{31} + K_{32}) = +60 \text{ mgal/G}^3$$

$$2(K_{41} - K_{42}) = 1 \text{ mgal/G}^4$$

CHAPTER FOUR

THE INSTRUMENT

4.1 Leveling

Leveling errors may arise from two interrelated sources:

1) The accelerometer measures g cos θ where θ is the angle between the gravity vector and the accelerometer input axis. g(1 - cos θ) is termed the off-level error.

2) To eliminate the null scale factor, the accelerometer must measure +g and -g. Deviations are termed inversion error.

4.11 Off-level Error

Referring to Figure 4.11 , we see that the off-level error increases approximately as θ^2, being:

10^{-7}g for $\theta_0 = 2.2'$

10^{-6}g for $\theta_0 = 5'$

10^{-5}g for $\theta_0 = 16'$

Whether the accelerometer measures g cos (0°) of g cos (45°) is indeterminate from the frequency output alone. The effect of an arbitrary but constant θ_0 would be incorporated into the scale

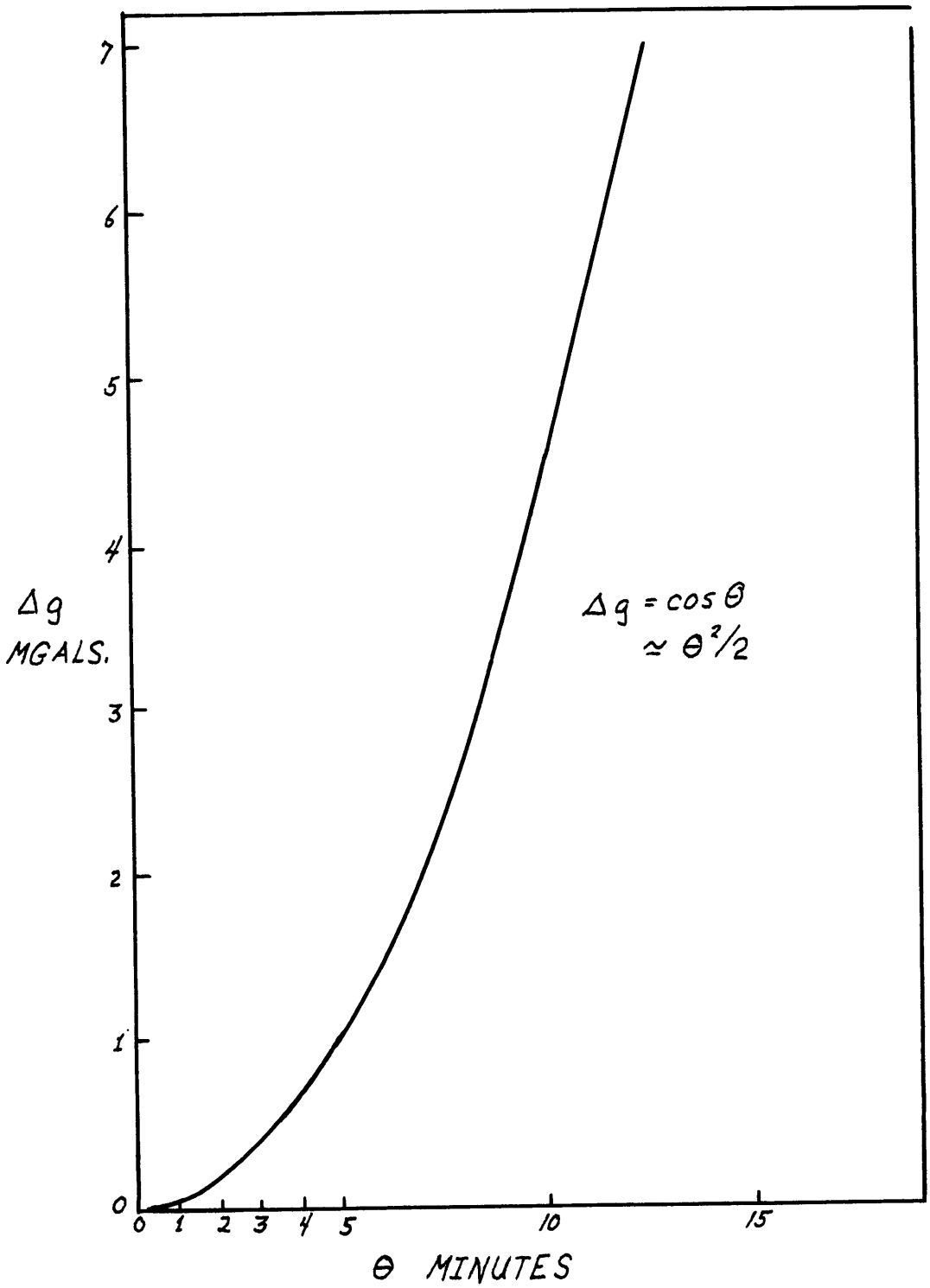

Fig. 4.11 Off-level error

factors. However, the repeatability in θ_0 required for a given repeatability in (g cos θ) increases sharply with θ_0.

For $\Delta(g \cos \theta) = \pm 10^{-6} g$

at $\theta_0 = 0^\circ$, $\Delta\theta = \pm 5'$

$\theta_0 = 5'$, $\Delta\theta = \pm 2'$

$\theta_0 = 45^\circ$, $\Delta\theta = \pm 0.3''$

Therefore, it is desirable to hold both θ_0 and $\Delta\theta_0$ as small as possible.

4.12 Inversion Error

Using the Maclaurin series expansion:

$$\Delta F + g = (F_1 - F_2)_{+g} = (K_{01} - K_{02}) + (K_{11} + K_{12})g + (K_{21} - K_{22})g^2 + \cdots \quad 4\text{-}1$$

$$\Delta F - g = (F_2 - F_1)_{-g} = (K_{02} - K_{01}) + (K_{12} + K_{11})g + (K_{22} - K_{21})g^2 + \cdots \quad 4\text{-}2$$

$$\Delta F + g + \Delta F - g = 0 + 2(K_{11} + K_{12})g + 0 + \cdots \quad 4\text{-}3$$

The precise measurement at $\theta_{0\,+g} = 0^\circ$ and $\theta_{0\,-g} = 180^\circ$ allows the complete elimination of the null frequency and all even order terms.

Now suppose $(\theta_{01,-g} - \theta_{01,+g}) \neq 180^\circ$. Let $\theta_{01,+g} = \theta_0 \neq 0$ and $\theta_{01,-g} = 180^\circ$.

Then Equations 4-1,2,3 become:

$$\Delta F_{+g} = (K_{01}-K_{02}) + (K_{11}+K_{12})g \cos\theta_0 + (K_{21}-K_{22})g^2\cos^2\theta_0 + \cdots$$

$$\Delta F_{-g} = (K_{02}-K_{01}) + (K_{12}+K_{11})g + (K_{22}-K_{21})g^2 + \cdots$$

$$\Delta F_{+g} + \Delta F_{-g} = 0 + (K_{11}+K_{12})g(1+\cos\theta_0) + (K_{22}-K_{21})g^2(1-\cos^2\theta_0) + \cdots$$

The difference between this case ($\theta_{0+g}=\theta_0$) and the ideal case ($\theta_{+g}=0^\circ$) is:

$$g(K_{11}+K_{12})(1+\cos\theta_0) - g^2(K_{22}-K_{21})(1-\cos^2\theta_0) + \cdots$$

but $\cos\theta_0 = 1 - \theta_0^2/2 + \cdots$

and $(1-\cos^2\theta_0) = \sin^2\theta_0 = \theta_0^2 - \theta_0^4/3 + \cdots$

so the difference becomes:

$$g(K_{11}+K_{12})\,\theta_0^2/2 + g^2(K_{21}-K_{22})(\theta_0^2 - \theta_0^4/3) + \cdots$$

By allowing $\theta_{0+g}=\theta_0$, some arbitrary angle near zero, we may conclude:

1) The null factor cancellation is not affected.

2) The first order term has a θ_0^2 dependence

3) Even order terms in g are no longer completely cancelled, but enter as even order (θ_0) terms.

Since even order terms are small with respect to the first order already, with small θ_0 they are negligible.

In general, then, the requirements on leveling for $\Delta g < 10^{-6}g$ are:

1) $\theta_{01,+\theta}$ and $\theta_{01,-\theta}$ should be $\pm 5'$

2) $\Delta\theta_{0,+g}$ and $\Delta\theta_{01,-g}$ should be $\pm 2'$

4.13 Leveling Mechanism

The leveling mechanism, Figure 4.13, consists of a Plexiglas cylinder floating in a bath of 100% glycerol. If the cylinder floated with stable equilibrium in a given orientation and no parameters (shape, volume, mass distribution) were changed, then this orientation would be reproducible to a high degree, depending only upon the viscosity of the fluid and the time allowed for settling. Adding two hollow end caps connected by rigid tubes, and filling one end cap completely with mercury, gives the cylinder two equilibrium orientations.

If the symmetry of construction and mass distribution of the complete assembly were perfect, the two equilibrium orientations

would be:

1) upright with the axis of symmetry coincident with the +g vector.

2) inverted with the axis of symmetry coincident with the -g vector.

In addition, if the accelerometer input axis were parallel to the cylinder axis of symmetry, the accelerometer input axis would coincide with the +g and -g vectors respectively. This case may be considered as the ideal.

How well are the above conditions approximated? And if not well approximated, how well corrected?

Symmetry of Construction

To make the cylinder axis of symmetry coincide with the gravity vector, it is not necessary that all fixed internal components have the same symmetry. It is enough that the external surface of the cylinder be symmetric and the center of mass of the complete assembly lie along this axis of symmetry. The first requirement is

fulfilled to ±0.003". The second is easily achieved by either shifting the Silcad cells between their mounting plates or adding ballast at appropriate points.

Because different ends of the cylinder are out of the fluid in the two different orientations, the ends have changing effective densities. It is therefore desirable that the end caps be identical in shape and volume. This goal is impossible to achieve to the required accuracy because the mercury cavities are hand shaped.

To correct this error, an equal and opposite dissymmetry is deliberately introduced in the mercury cavities. Plexiglas buttons of appropriate displacement are cemented into the mercury cavities. In addition, to avoid opening the mercury cavities in case of instability in the Plexiglas cylinder shape, two ¼-40 nylon plugs are threaded from outside into each mercury cavity. The adjustable projections of the plugs displace an adjustable volume of mercury, thereby shifting the center of mass of the end cap filled with mercury. The two sets of plugs act independently to shift the

center of mass in the two different orientations. The maximum mass shift achieved with these plugs is $\pm$0.2 oz. in.. With the given pendulosity of the cylinder, the shift in θ_0 is $\pm 2'$. Therefore, these plugs constitute a fine adjustment.

"Level" is determined as follows. After the accelerometer input axis is aligned with the cylinder axis, the cylinder is mounted on a precision rotary head in the vertical plane. VSA frequency is recorded as a function of angle. The frequency is an even function about vertical so splitting angles of equal frequency gives the accelerometer vertical. When the accelerometer is vertical in the first plane, the cylinder is rotated 90° in azimuth and the head is adjusted in the second plane until the frequency returns to its original maximum value. The accelerometer is then truly vertical, and the level bubble is adjusted to so indicate. The opposite bubble is set by rotating the head 180° and adjusting the bubble.

Before the Plexiglas buttons were added the floating off-level

was 12' and 5' in the two orientations. After introduction of the buttons the error was reduced to 1' in both cases. Since the nylon plugs allow an adjustment of $\pm 2'$, it is assumed that the level can be adjusted to $\pm 1'$.

There is no absolute requirement that mercury be used for leveling. A solid mass moved on a track is one alternative. Mercury is hard to keep clean when in contact with air. In addition, a leak in the mercury system could do considerable damage to the electronics by electrical shorting. On the other hand, unknowns are intriguing and mercury:

1) allows greater pendulosity per volume

2) is very precise due to its free surface

3) can be moved through small spaces

4) is a good thermal conductor

Accelerometer Axis Parallel to Cylinder Axis

The second requirement is that the accelerometer input axis be parallel to the cylinder axis of symmetry. The accelerometer is mounted in a copper thermal shroud. A single adjustment of this

mount requires several days. Therefore, the accelerometer was mounted once with the accelerometer case and shroud symmetry coincident. At the completion of the first phase of construction the symmetry axes of copper case and Plexiglas cylinder coincided within ±0.5', as measured by an indicator when the cylinder and case were rotated on a horizontal rotary head. Therefore, the misalignment between accelerometer input axis and copper case was the misalignment between accelerometer input axis and Plexiglas cylinder within ±0.5'.

Subsequent measurements showed that this initial misalignment was 10'. This figure was determined as follows. If the input axis of the accelerometer were level, the output frequency would be the null frequency. If the axis were inclined, the string would see a component of gravity (g cos θ). With the axis inclined toward the +g vector, the frequency would increase. With the axis inclined an identical amount toward -g, the frequency would be decreased by identical amount.

A flat plate was levelled to + ½'. The Plexiglas cylinder was rolled through 2π radians across the plate. A plot of output frequency versus angular rotation ϕ was made. The input axis of the accelerometer sweeps out a cone. The ideal plot would be a sine wave with the mean value, the null frequency. With the cylinder rotated to ϕ of maximum output frequency one end of the cylinder was shimmed with a feeler gage until the frequency dropped to the mean. Likewise, with the cylinder rotated to ϕ min. a feeler gage under the opposite end of the cylinder was adjusted until the frequency rose to the mean. In both cases, the gage thickness required was 0.019". It was concluded that this was the amount by which one end of the copper case must be shifted to achieve alignment of the accelerometer input axis and the cylinder axis.

The copper case was mounted in the cylinder by two symmetric nylon bushings. To achieve the .019" shift, one bushing was first bored to a larger diameter and off center by .019". Then a concentric sleeve with O.D. equal to diameter of newly bored hole

and I.D. equal to O.D. of the copper case, was inserted.

After modification, the cylinder was reassembled and re-rolled on the flat plate. The plot of frequency versus ϕ showed that the misalignment has been reduced to two minutes. This was not as small as hoped, but will cause an error of only 10^{-7}g.

4.14 Balancing the Cylinder

It was earlier remarked that the adjustment of the center of mass to coincide with the center of cylinder symmetry was easy. In principle it is; in practice it may take several days. The following program is recommended:

1) A rough balance along the cylinder axis is calculated from the measured masses of all components and their measured positions.

2) The cylinder, exclusive of mercury, is sealed and floated in water. Were the center of mass to lie equidistant between the cylinder ends, the cylinder would float horizontally.

3) Masses are attached at the light end with elastic bands until the cylinder does float horizontally - This amount of mass must either be permanently added to the light end or subtracted from the heavy.

4) After end-to-end balance is achieved the cylinder is rolled on the flat plate (±½'). Were the center of mass to lie <u>off</u> the cylinder axis, the cylinder would find only one θ of stable equilibrium. Balance is achieved through shifting batteries. The method is limited by the surface out-of-roundness and roughness of the cylinder.

5) The cylinder is again sealed and floated in water. Were the center of mass still to lie <u>off</u> the cylinder axis, the cylinder would again find only one equilibrium. This method is very precise but bothersome due to the laborious opening and resealing required.

6) After this balance is achieved the mercury is added and the cylinder floated in glycerine. Because the dissymetry

of construction has been corrected by the Plexiglas buttons in the mercury cavities, provided steps one through five havebeen done properly, the cylinder will level to within ±1 minute. The nylon plugs allow an additional adjustment through a ±2 minute range.

Once the cylinder has been balanced, only opening and changing or shifting some internal mass will require rebalancing. The original worry that a mass shift in the battery, either by chemical change, liquid loss or gassing, has been undectable, provided the cells are not abused by overcharging or reversing their bias.

4.2 Temperature Control

There are three temperature effects on the vibrating string accelerometer:

a) A scale factor temperature coefficient ($\pm 5 \times 10^{-6}$ g/°C),

b) Drift, the rate of which rises with temperature,

c) A thermal gradient coefficient (unknown magnitude).

The first control considered was an oven. This would mean

a high operating temperature which increases effect b. Second, a thermoelectric cooler was designed. By holding the ambient temperature in a narrow range and running a large module at maximum efficiency, a smaller inefficient module could perform fine control. With an ambient range of $\pm 2^{\circ}C.$, total power consumption would be two watts. Even this small figure was too large, however, for a rechargeable battery in the floating cylinder.

Next, an ice bath was considered. A crude mock-up was constructed. This consisted of a large polyurethane ice bucket containing water and ice and a second, inner polyurethane container again with water and ice. The water in the outer container was stirred at a constant rate and represented the low ($6^{\circ}C. - 2^{\circ}C.$) ambient temperature. The inner ice bath, also agitated, contained a thermistor bead in a brass thermal mass and a dummy dissipation load.

It was found that, provided a high ($> 1:1$) ice to water ratio was maintained in the inner container and both baths were agitated at constant rates, the temperature of the inner bath would reach

some rather arbitrary but constant ($\pm$.01°C.) value. The arbitrariness of the otherwise constant temperature was later found to be caused by impurities in the ice. Each time a different batch of ice was used, the temperature would level off at a different value. The differences registered were less than $\pm$0.05°C. This experiment was encouraging enough to allow the construction of an improved ice bath with the hope that it alone would prove sufficient.

The final ice bath is as appears in Figure 4.13. At typical depth of the open ocean, the bottom temperature is already less than 5°C. Since 70% of the ocean is colder than 4°C., the low ambient temperature just outside the bath will replace the first bath in the mock-up. The shape of the insulated container was dictated by the requirement that it be free to rotate inside a spherical pressure housing. Rigid urethane foam was blown into a mold consisting of two Plexiglas hemispheres (George Cram Co., Philadelphia, Penn.). Plexiglas was a poor choice since urethane foam is usually cured with steam under pressure. It was difficult

to find a company willing to try, but Techcraft, Inc., of Salem, Massachusetts did a creditable job.

The density of the foam was kept to 3.0 lb./ft.^{3}. At this density, urethane foam is the best commercial insulating material made ($K = 0.14$ BTU$^{in.}$/hr.ft.^{2o}F). Since the ice bath must support forty pounds of fluid under accelerations as high as 30 g's in any direction, the foam itself could not provide enough mechanical strength. Therefore, the foam was covered inside and out by a 1/10" layer of fibreglas. In addition, two steel plates were mounted by epoxy resin to the flat ends for the mounting of the rotation bearings.

Originally, the ice water was stirred by three paddles driven by d.c. motors exterior to the foam case. The stirring rate was held constant at 60 rpm by running the motors on mercury cells. Bronze screen cages enclosed the paddles, preventing the vibrations which would be induced by direct contact of paddles on ice. However, much difficulty was encountered with icing of the paddles and so

they were eliminated. The ice is still agitated every five minutes in the inversion process.

The amount of heat dissipated by electronics interior to the ice bath (0.6 watt) is small compared with the heat influx from the outside and the heat capacity of a full load of ice (> 500 watt-hours). With a constant inner temperature, the rate of heat flow from the outside is directly proportional to the ambient temperature. At an ambient of $\pm 2^{\circ}$C., the heat flow is about 6 watts. At 20°C. the corresponding flow is 60 watts. To avoid having to add ice every four hours, it is necessary to cool the pressure housing.

It is difficult to maintain an <u>isothermal</u> ice bath, but not so hard to keep a constant <u>average</u> temperature. This fact allows the maintenance of a constant accelerometer temperature. Temperature averaging features are utilized at every possible point. The temperature gradients existing in the ice bath are buffered by an inner bath of glycerine (highest thermal conductivity among common organic liquids), the ¼" Plexiglas cylinder walls, and the air

space. Any residual gradients are further attenuated by the 1/16" copper accelerometer shroud. It has been calculated that if the copper shroud were one solid piece and if the entire 0.6 watts of electronic dissipation were injected at one end of the shroud and removed at the other, the maximum temperature difference in the shroud would be 0.003°C. The shroud consists of two solid halves divided laterally. Good thermal contact was not achieved. The accelerometer is sensitive to longitudinal temperature gradients. The shroud should have been split longitudionally.

Because of the poor thermal contact in the shroud, thermal gradients do exist in the accelerometer. Their magnitude is equivalent to about a one mgal change from +g to -g. However, since the thermal gradients reproduce their steady state values most of their effect can be removed in the data analysis, Figure 4.2.

Provided:

1) the ice to water ratio is maintained at $> 1/1$,

2) the ambient temperature does not exceed 5°C.,

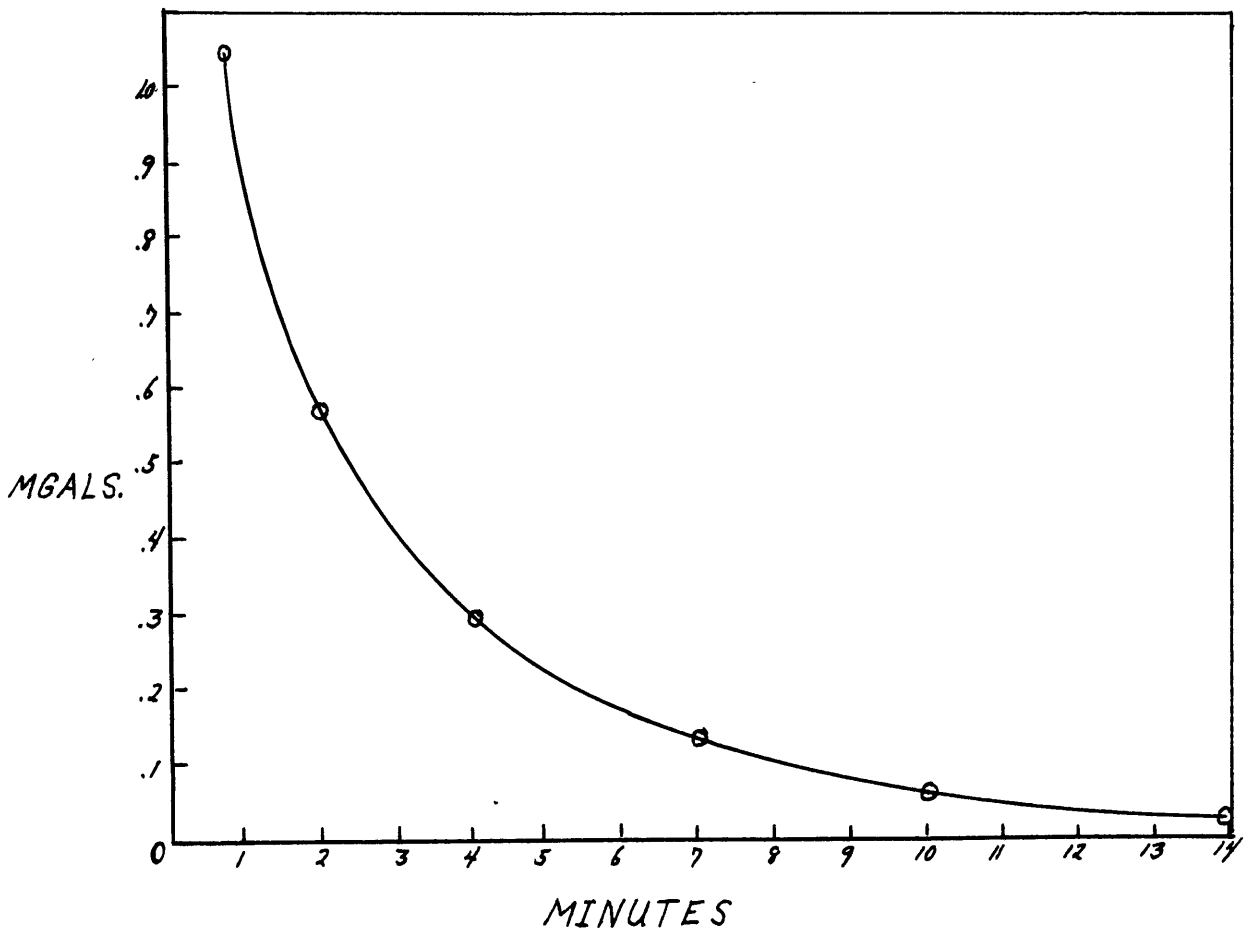

Fig. 4.2. Inversion temperature gradient effect.

3) only ice of demineralized water is used,

4) a correction is applied for the thermal gradient

-the temperature error will be about 0.2 mgal r.m.s.

In the error analysis, Chapter 6, the r.m.s. temperature error is included in the accelerometer drift, since their separation is impossible.

4.3 Signal Transmission

The vertical orientation mechanism for aligning the accelerometer axis with the local gravity vector is a pendulous cylinder floating inside a sphere. Since the vehicle has three degrees of freedom, there can be no mechanical linkage between the cylinder and sphere. This raises the problem of how to get the accelerometer signal ($\sim$ 60 cps sine wave) out to the counter. Five methods were considered in addition to wires:

a) Low frequency signals can be transmitted electromagnetically from one coil to another, provided the geometry is correct. Unfortunately, the principle of the radio direction finder

makes this application impossible. It can be shown impossible to find a geometry with any number of coils in a system with two or more degrees of freedom which has no nodes.

b) Acoustic energy can be successfully transmitted through glycerine. However, there is acoustic noise in the rest of the instrument (sequence timer) and a good signal to noise ratio would require elaborate circuitry.

c) Frequency modulation of a light source inside the clear Plexiglas cylinder could give a very clean and easily received signal. However, the amount of power required is large.

d) Frequency Modulated Radio is the most common method of telemetry. However, all of the information in the accelerometer signal is contained in the frequency and we would require a transmitter oscillator with stability equal to that of the accelerometer. An oscillator with stability of $1/10^7$/day would require at least a watt of power.

e) Amplitude Modulation of a radio frequency is simple and

consumes very little power. Using one transmitter and two orthogonal receivers a signal can be transmitted in any orientation on a minimum of power.

Only two receivers are required because, with the instrument lying on its side, the Plexiglas cylinder has only two degrees of freedom. Adding the signals of two orthogonal antennae would yield the same result as two coils - the possibility of nodes. Fortunately, in the case of A.M. transmission, the signals may be added after demodulation, insuring a signal in any orientation.

Two ferrite antennae are used on the transmitter. They are placed on opposite sides of the Plexiglas cylinder and keep the amplitude of the received signal more nearly constant. The transmitter, Figure 4.3, has only a single stage and draws 2 ma. on 4.2 volts. Battery life is 30 days.

The receivers are typical ten transistor Japanese radios. Unmodified, their performance at 60 cps. is poor (down 20 db.). By simple capacitive tuning of the last two audio transformers,

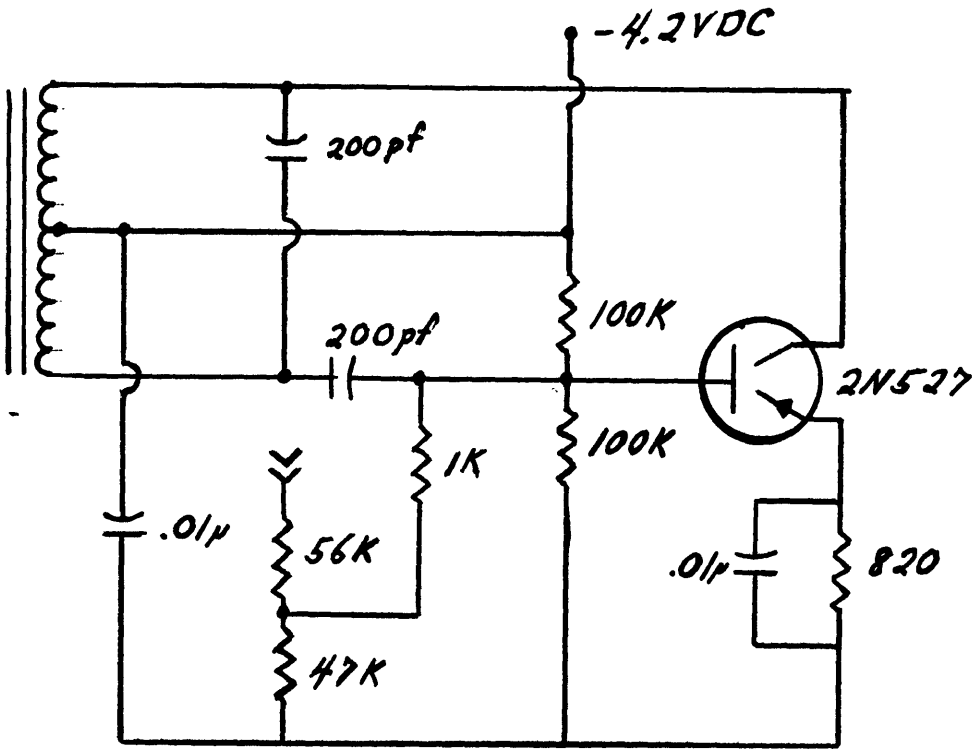

Fig. 4.3. The amplitude modulated transmitter.

the response is made to peak at 60 cps. component results in a sine wave. In this simple manner a drastic reduction in noise is effected.

To improve the signal for the logic section, the sine wave overdrives a two stage amplifier to produce a square wave. The jitter in the square wave is less than 0.03% even in the presence of laboratory 60 cps noise.

4.4 Frequency Measurement

Data from the accelerometer is in the f.m. mode. A frequency of approximately 64 cps results from the $\pm$1g acceleration. To measure g to 0.1 mgal or 10^{-7}g we must determine frequency to $1/10^{7}$.

Magnetic tape recording of the signal was initially considered. Recording the accelerometer frequency on one channel and a standard frequency on a second channel allows the effect of variable tape speed to be reduced to about 0.001%. An accuracy of $1/10^{7}$ could then be achieved in 100 seconds. Magnetic tape recorders have one good and several bad features. By examining different sections of the recording, it can be determined whether the accelerometer is

at rest. Bad features are combinations of high cost, high power consumption and size. An instrument suitable for this application would typically cost $5,000, consume 30 watts and displace 0.2 cu. ft.

After the magnetic tape recorder, the accelerometer frequency would be determined with a preset digital counter. As a preset counter can be built for less cost and the same power consumption and displacement as a tape recorder, the direct incorporation of such a counter is indicated.

With a preset counter, frequency is obtained indirectly. The counter consists of two registers. The preset of "gating" register counts cycles of the unknown frequency. It registers a cycle each time the voltage of the signal crosses a fixed point in a fixed direction. With a clean signal this counting process can be very precise. A typical precision is $\pm$0.0003 cycle. The second register counts cycles of a higher frequency stable oscillator (usually 1 mc. or 100 kc.). The first cycle in the gating register enables or gates the second register on. Similarly, the nth cycle gates

the second register off. Since the frequency of the stable oscillator is precisely known, the count in the second register is precise time.

We therefore have time per n cycles of signal or (1/f). For an accuracy of $1/10^7$ in g we need $1/10^7$ in f. The present instrument uses a 125 kc. stable oscillator with a gating precision of $\pm$.0003 cycle and n = 3072. This results in a counting of $\pm$.10 mgal rms.

The logic diagram is shown in Figure 4.4. The notation as listed in Table 4.4 is that used by Digital Equipment Corp., supplier of the logic modules. A frequency measurement is accomplished as follows:

1) The mechanical sequence timer connects +10V and -15VDC.
2) The 125 kc. stable oscillator signal is continuously amplified and standardized by PA1 and blocked by DG2.
3) The gravity signal is on PG2 continuously. The Schmitt trigger generates a negative pulse each time the signal goes more positive than -1.0V after having been more

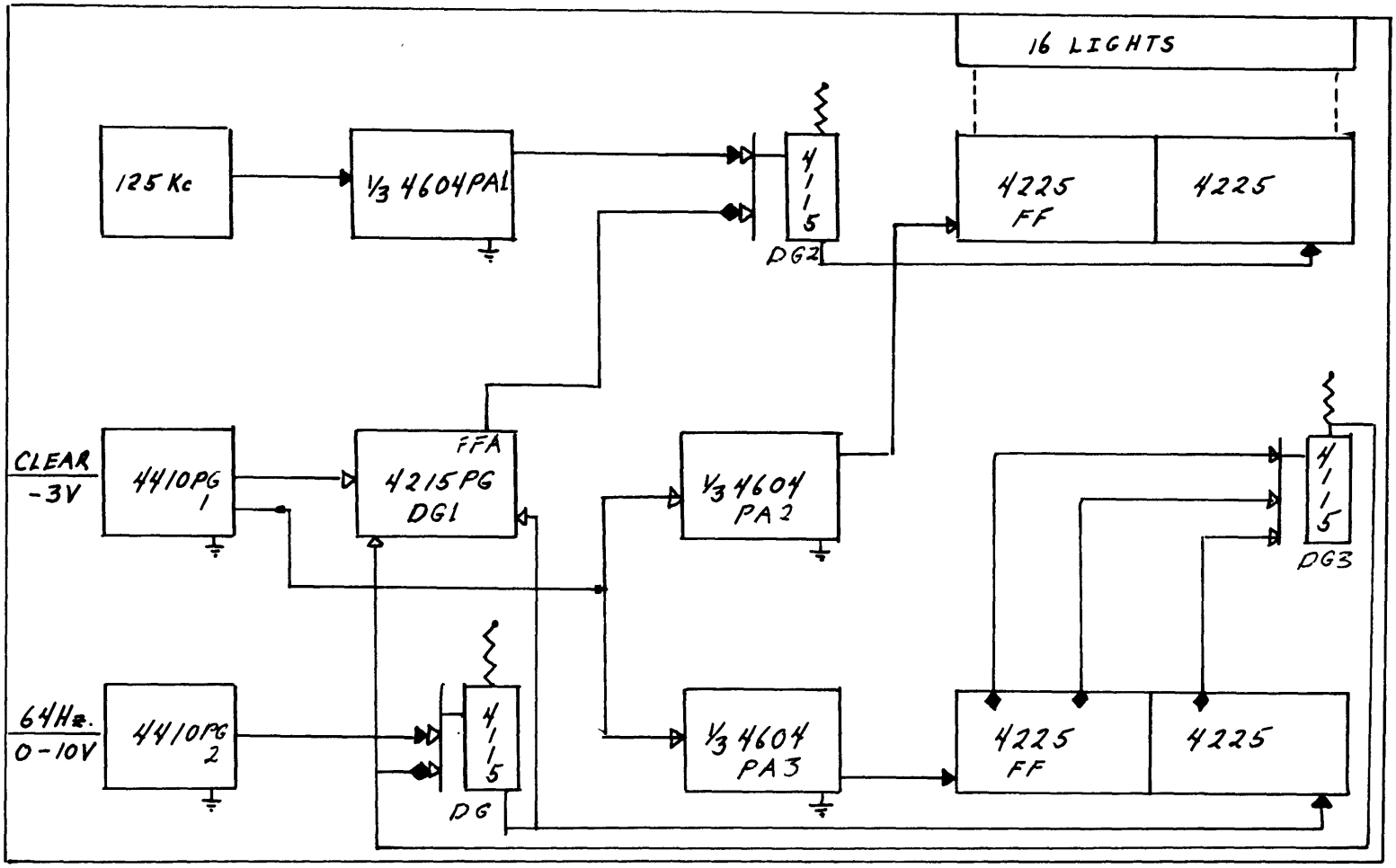

Fig. 4.4. The Digital Equipment Corp. preset counter.

negative than -2.5V.

4) The sequence time applies a -3V level to PG1 which generates a standard negative pulse. This is the clear and set pulse. The pulse then goes to PA2 and PA3 where it is amplified and inverted. The amplified pulses serve to clear all 32 flip-flops in the registers. The same clear and set pulse sets FFA in the one state, this enabling DG2. Consequently, with the generation of the clear and set pulse, both the gating and timing registers begin counting.

5) After n cycles have entered the gating register, DG3, a negative AND, generates a positive pulse. The combination of positive pulses DG1 and DG3 switches FFA to the zero state.

6) The disabling of DG2 caused by the FFA zero state blocks further 125 kc. pulses from PA1.

7) All flip-flop states are maintained until either cleared or shut down.

8) The sequence timer turns on the light drivers (L1 - L16)

for ten seconds, recording the binary count on film.

9) The sequence timer fires the solenoid twice causing the accelerometer to invert and to level to $\pm 1'$.

10) After a suitable period allowed for vertical stabilization of the accelerometer, steps 1-8 are repeated, measuring (-g).

11) Steps 1-10 are repeated as many times as desired.

Although not incorporated in the present instrument, the preset counter can be used as such for the depth determination. Exactly as with the gravity measurement, the frequency of an f.m. pressure transducer (such as the Bissett-Berman vibrating string) can be determined.

A significant improvement which could be easily made on the present timing system would be the incorporation of a third timer controlling the interval between readings. Presetting the interval between gravimeter readings would allow occupation of successive stations without hoisting the gravimeter all the way to the surface.

In reconnaissance work no time would be saved, but for the closely spaced stations of a profile over a small feature, this ability would be invaluable.

Table 4.4

Logic Notation - Digital Equipment Corporation

PA - Pulse Amplifier

The pulse amplifiers perform pulse amplification and optional inversion and standardize pulse height and width. Maximum pulse rates are 1 mc. Standard pulses are 0.4 micro seconds and 2.5 volts. Pulses are produced with input level changes of 2.5 volts in only one direction.

PG - Pulse Generator

The pulse generators convert external signals to standard pulses. A Schmitt trigger produces a standard pulse each time the input goes more positive than -1.0V after having been more negative than -2.5V. An optional integrating circuit is included to filter constant bounce on switch closures. Pulse generators are used when: 1) high triggering accuracy is needed, 2) input risetimes are long, 3) inputs are generated by switch closures.

DG - Diode Gate

Diode gates contain an arbitrary number of diodes in varying logic configurations. These particular gates are connected as OR logic for positive levels and AND logic for negative levels. The output of the DG is ordinarily a negative level. When all diode gates are negative (negative AND) the output becomes a positive level.

FF - Flip-Flop

Flip-flops are bi-stable logic elements consisting of two transistor inverters interconnected. In a sense, each inverter controls the other. The flip-flop has two output states:

1) positive level or zero

2) negative level or one

Each input pulse changes the ouptut state. Connected in series, flip-flops constitute a binary counter.

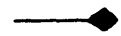
negative level

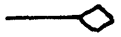
positive level


negative pulse

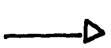
positive pulse


negative-going level change, leading edge

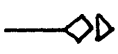
positive-going level change, leading edge

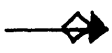
negative-going level change, trailing edge

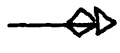
positive-going level change, trailing edge


branch point


no connection

CHAPTER FIVE

THE VEHICLE

5.1 Pressure Case

Only the simplest geometries can be treated analytically in pressure vessel design. Even then, a confidence level of about 80% should be used. Experimentally confirmed formulae for these simplest geometries are found in Mark's Mechanical Engineers' Handbook (1958).

5.11 Formulas and Materials

Notation: O.D. = outside diameter
I.D. = inside diameter
W = wall thickness
L = cylinder length
P = hydrostatic pressure
T = yield strength of material
E = modulus of elasticity
R_2, R_1 = outer and inner radii

Thin-walled Cylinder (O.d./W) > 10; L/O.D. = 2.5

Buckling Pressure $P = 5E(W/O.D.)^3$

Yield Collapse $P = 2WT/O.D.$

Thin-walled Sphere (O.D./W) > 10; T > 1.05P

Yield Collapse $R_2/R_1 = (T/(T-1.05P))^{1/3}$

Flat Round Plate

Yield Collapse $T = \frac{10P(I.D.)^2}{32W^2}$

Material

Three popular high-strength materials have been considered. Their mechanical properties are given in Table 5.11-1. A common low-strength aluminum alloy has been included to show their high strengths. Other popular materials are polyvinal chloride (PVC), Fiberglas and glass. Since these materials are very variable, they will not be included.

Figures 5.11-1,2 and Tables 5.11-2,3 are given to aid computations in the case of a cylinder. Figures 5.11-3,4 and Table 5.11-4 are given for the thin walled sphere.

Table 5.11-1

Strengths of Commercially Available Alloys

ASTM & SAE #	Ultimate Tensile	Yield Strength, Tension	Shear Strength
6061-T6 Al.	45,000 psi	40,000 psi	30,000 psi
7075-T6 Al.	83,000	73,000	48,000
1100-0 Al.	13,000	5,000	9,000
17-4 PH St.		180,000	

TABLE 5.11-2

Yield Collapse Pressure for 30" Cylinder

(W/O.D.) =	0.025	.050	.075	.100	.125
T = 180,000 psi	9,000 psi	18,000	27,000	36,000	45,000
75,000	3,600	7,200	10,800	14,400	18,000
50,000	2,500	5,000	7,500	10,000	12,500
40,000	2,000	4,000	6,000	8,000	10,000
30,000	1,500	3,000	4,500	6,000	7,500
20,000	1,000	2,000	3,000	4,000	5,000

TABLE 5.11-3

Buckling Pressure of 30" Long Cylinder

(W/O.D.) =	0.025	.050	.075	.100	.125
E = 10,500,000	820 psi	6,500	22,150	52,500	--
30,000,000	2350	18,700	56,700	--	--

TABLE 5.11-4

Yield Collapse Pressure for Spheres

(O.D./I.D.) =	1.020	1.039	1.080	1.166	1.200
T = 180,000 psi	18,780	35,300	--	--	--
72,000	--	7,530	14,100	25,400	28,350
50,000	--	5,240	9,800	17,600	22,600
40,000	--	4,190	7,850	14,100	16,200
30,000	--	3,140	5,890	10,580	12,140
20,000	--	2,090	3,920	7,050	8,100

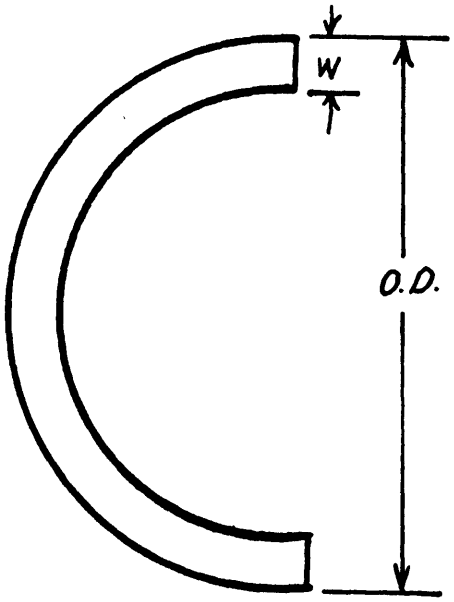

BUCKLING PRESSURE

$P = KE(W/OD)^3$

WHERE $K = 5$ for 30" CYL.

E = MOD. OF ELAST.

YIELD PRESSURE

$P = 2TW/OD$

WHERE T = YIELD STRENGTH

Fig. 5.11-1 The thin-walled cylinder.

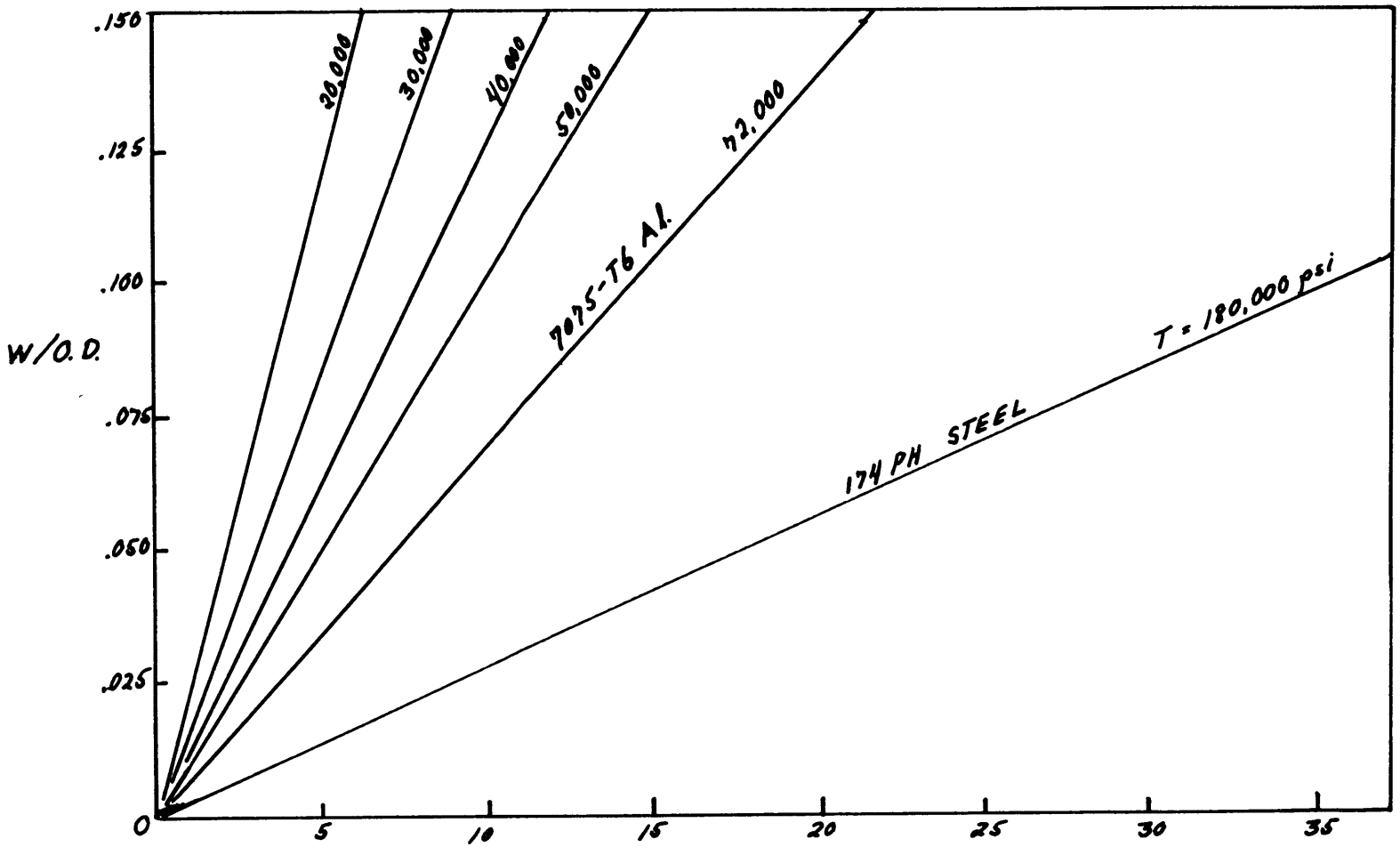

Fig. 5.11-2. CYLINDER COLLAPSE PRESSURE (10^3 PSI)

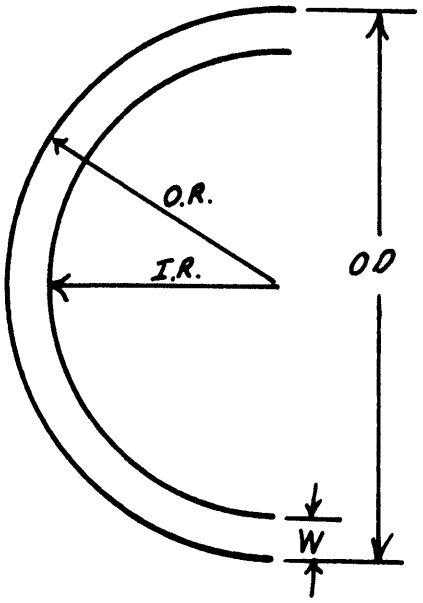

$$O.R./I.R. = \left[T/(T-1.05P)\right]^{1/3}$$

WHERE: T = YIELD STRENGTH

P = COLLAPSE PRESSURE

Fig. 5.11-3. Thin-walled sphere.

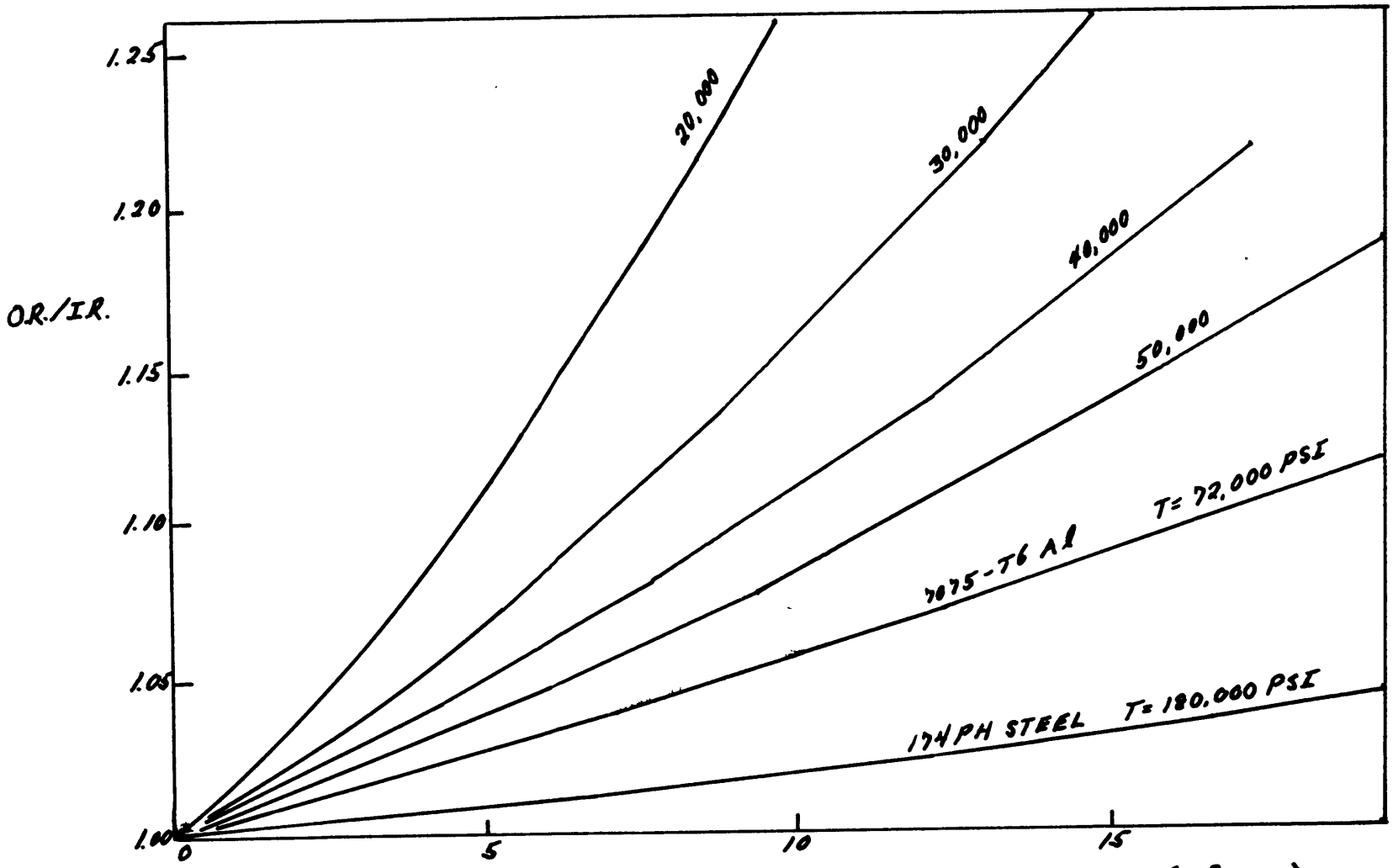
1.25
1.20
1.15
1.10
1.05
1.00
O.R./I.R.
20,000
30,000
40,000
50,000
7075-T6 Al
T= 72,000 PSI
17-4PH STEEL
T= 180,000 PSI
0
5
10
15
SPHERE COLLAPSE PRESSURE (10³ PSI)

Fig. 5.11-4.

An important figure of merit for the comparison of materials in pressure vessels is (yield strength/wt.). The highest strength steel and aluminum alloys are about equal in this respect. The next important consideration is ease of fabrication. In the simple geometries, close tolerances must be held in the (W/O.D.) ratio. Since (W/O.D.) is always greater in aluminum, machining tolerances are correspondingly less stringent.

The sphere manufactured by Phoenix Metal Products, Milwaukii, Wisconsin has the dimensions: 19-3/8" I.D., 1.0" wall, $\pm$0.002' outer sphericity. The material is 7075-T6 aluminum and, according to our formula for thin-walled spheres, test pressure is 12,500 psi with a safety factor of 36%.

Each hemisphere is fitted with a reinforced tapered plug. The plug on the top hemisphere has a 3/8" - 16 stainless eye bolt for ease in handling. Sealing at low pressures is effected by 1/8" O-ring, the hemispheres being held together by six clamps. Sealing at pressures greater than 10 psi is metal-to-metal. The O-ring

seals are made against a 21-3/8" O.D. parting plate. The parting plate also serves as an alignment jig for the hemispheres and as a platform for the instrumentation.

5.12 Corrosion Protection

There are three common methods of corrosion protection for aluminum in sea water:

a) Anodizing is cheap but has several disadvantages. It is rather soft protection, subject to abrasive wear, and worn spots are sometimes hard to detect.

b) Paint is an even softer protection. However, a surface break can be easily discerned.

c) A martin hardcoat is extremely tough and durable, but it must be waxed periodically as it is full of small pores.

The Martin hardcoat was applied to all surfaces of the hemispheres and parting plate.

5.2 Suspension

The accelerometer has a shock limit of 5 g's to recalibration and 30 g's to breaking. These are very low figures considering the

difficulty of handling at sea.

The easiest point at which to introduce shock mounting is between pressure vessel and vehicle. The web bag enclosing the sphere is attached to stainless eye bolts on the vehicle by ½" rubber shock cord. The suspension has a maximum play of one inch laterally and four inches vertically (along axis of vehicle). With an important exception, the motion of the system may be considered simple harmonic (as a mass on a spring). The exception is the case of overload when the pressure case strikes the vehicle.

For simple harmonic motion:

$$X = A \sin \omega t$$

where A is amplitude of motion

$$V = dx/dt = \omega A \cos \omega t$$

$$a = d^2x/dt^2 = -\omega^2 A \sin \omega t$$

but $\omega = 2\pi / \tau$ where τ = period

and $\tau = 4T$ where T is time required to stop motion

so, $$a = -\left(\frac{-A\pi^2}{4T^2}\right) \sin \omega t$$

$$\text{or maximum } |a| = A\pi^2/4T^2$$

$$\text{maximum } |v| = A\pi/2T = V \text{ initial}$$

Maximum /a/ versus Vinitial for A = 1 in. and A = 4 in. is presented in Table 5.2 and Figure 5.2. From the curves, the accelerometer would receive a shock necessitating recalibration if the vehicle came to an instantaneous stop from a horizontal velocity of 3.6 ft./sec/ ($\sim$ 2 knots) or a vertical velocity of 7.2 ft./sec. ($\sim$ 4 knots). A destructive shock could be received from a vertical velocity of 18 ft./sec. ($\sim$ 10 knots).

The exception to simple harmonic motion is overload when the case contacts the vehicle. The spring constant in the vertical is 1200 lb./in., or in this case 5.2 g's/in. with a 230 lb. mass. The acceleration must be about 21 g's for the suspension system to overload in the vertical direction. In the lateral direction the suspension is not nearly as stiff. For this reason, soft rubber blocks are placed between the case and the vehicle. Without them, overload would occur at 3 g's; with them it theoretically never occurs,

Table 5.2-1

Shock calculations for the accelerometer.

V initial (ft./sec.)	max. /a/ with A = 4 in.	max. /a/ with A = 1 in.
1	0.1 g	0.4 g
3.3	1.0	4.0
5.0	2.3	9.2
7.1	4.7	18.8
10	9.4	37.2
18	30	120

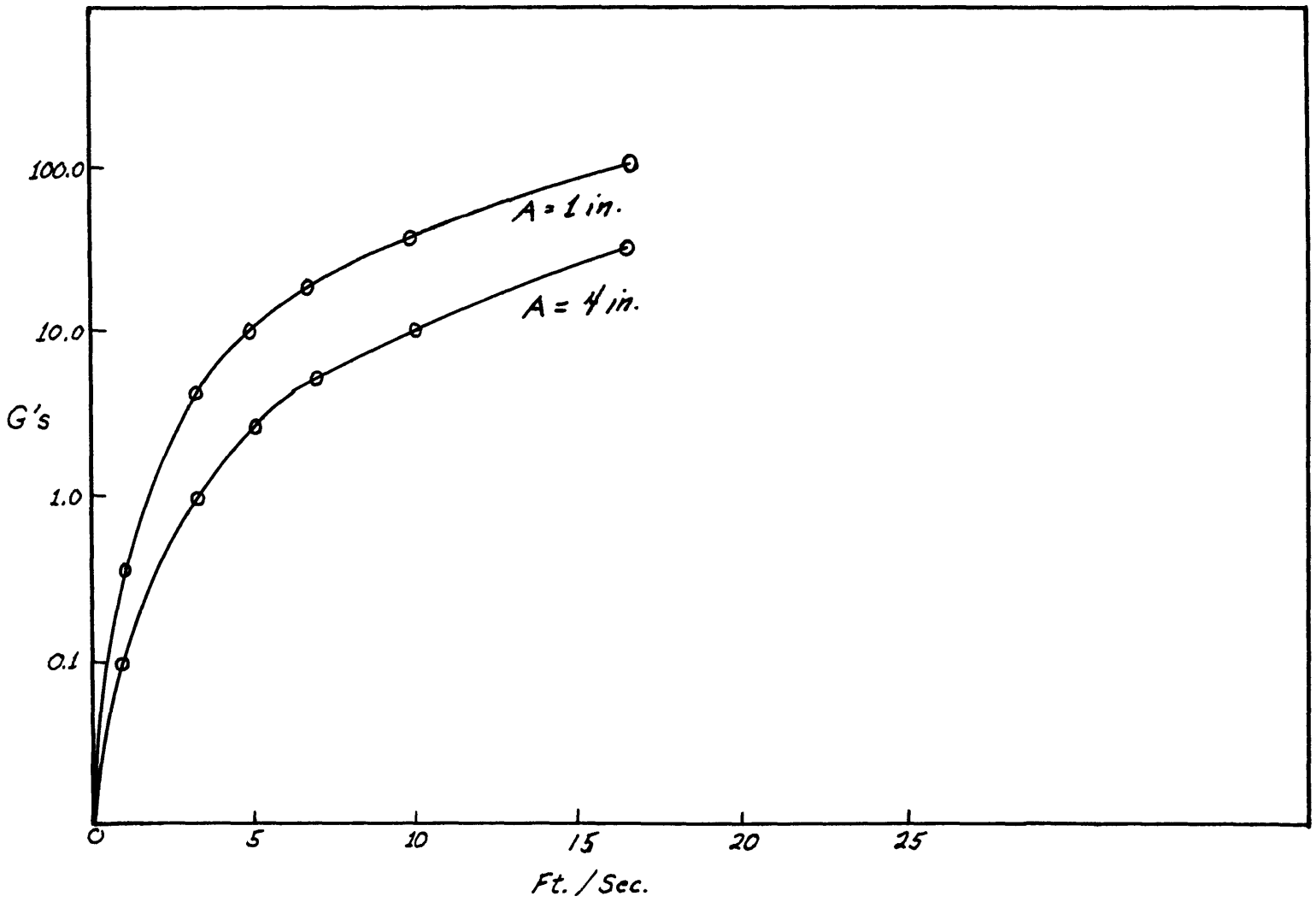

Fig. 5.2. Shock vs. initial velocity of instrument.

although very large g forces may be experienced. Because of the vibrating string cross tapes, however, the accelerometer is not nearly as fragile in the lateral direction. The figure, although not specified, is greater than 50 g's.

Only the shock absorption by the suspension system has been considered. Inside the pressure case two further effects occur: 1) The ice bucket assembly can flex as much as ¼". 2) The viscous glycerine in which the cylinder floats with 1/8" clearance will act as a dashpot.

5.3 Flotation

Without a flotation element, the complete instrument in water is approximately neutrally buoyant. For a return velocity of 10 ft./sec. fifty pounds of positive buoyancy is required. The characteristics of a flotation element should include:

1) corrosion resistance
2) shock resistance
3) buoyancy of 50 pounds
4) collapse pressure of > 10,000 psi
5) safety in handling

Table 5.3

Buoyancy Elements

Material	Buoyancy/ Surface Wt.	Buoyancy/ Volume	Cost/ Buoyancy (1964)
Gasoline	0.37 lb./lb.	17.3 lb./ft.^{3}	0.07$/lb.
Glass Spheres	1.20	34.9	$ 5.00
Lithium	0.93	33.3	10.75
Solid Polyethylene	0.12	6.9	2.08
Epoxy Foam (micro-spheres in epoxy)	0.49	20.4	25.08

. Gasoline is by far the cheapest but a dangerous material at sea. Solid Lithium is a little tried material which, according to the Lithium Corp. of America, can be guaranteed absolutely safe when hermetically sealed in aluminum cannisters. However, its price is slightly high. Epoxy foam would be very desireable for small floats due to its toughness, but is prohibitevely expensive for a large float. Polyethylene cannot achieve the desired buoyancy in the volume available.

Glass spheres have only one bad feature - handling. Although glass has a compressive strength better than the best steel, once its surface tension has been broken it is very succeptible to shock. Therefore, special care must be taken in its mounting. It was felt that a framework of Plexiglas would suffice for the mounting. Plexiglas was chosen because it has relatively high strength, corrosion resistance, and machinability and it has an effective specific gravity in water of only 0.18.

The spheres were obtained from the Corning Glass Works. Six

have an O.D. of 10¼", wall of 5/16", dry weight of 8.7 lb. and buoyancy 10.8 lb. The anticipated collapse pressure is ~15,000psi. The 16" sphere has a ½" wall and buoyancy of 46 lb. The material is Corning #7740 chemical resistant borosilicate glass (Pyrex).

The spheres were nested for maximum density packing in a framework of 3/8" Plexiglas sheet and stainless steel rods. The holes in the sheets and the spacers were cut to maintain ½" clearance between all spheres. The rack of spheres is attached to the Fiberglas nose cone with stainless fittings. A clearance of ½" is also maintained between the spheres and vehicle and the top shpere and the weight release. Channel rubber lines the Plexiglas plates as protection against shock when the vehicle flexes under rough handling.

The top sphere has been replaced by a split 9½" sphere containing a one watt-second strobe flash and a one watt citizens band radio transmitter and a second by a 9½" sphere containing a 40 watt pinger.

Total buoyancy with four 10½" and one 16" spheres is approximately 100 pounds. Fifty pounds is thus allowed for ballast which may be shifted for optimum balance of the vehicle.

5.4 Weight Release

In choosing a release for the anchor weight, the common electrically fired "squibs" and solenoids were considered rather critically. It was decided that their convenience was outweighed by their poor reliability. A reliability of 99% is low for a device with a price of over $30,000.

The utmost in reliability is the "automatic marine time release device (Van Dorn, 1953). Rather than fight corrosion, it depends upon it. As modified for this application, a drawing appears in Figure 5.4.

The body of the device consists of two jaws, closed at one end by a releasing pawl and containing a jaw opening spring (steel electrode) and an axial spring restraining rod (magnesium electrode). As these two alloys are widely spaced in the electrochemical series,

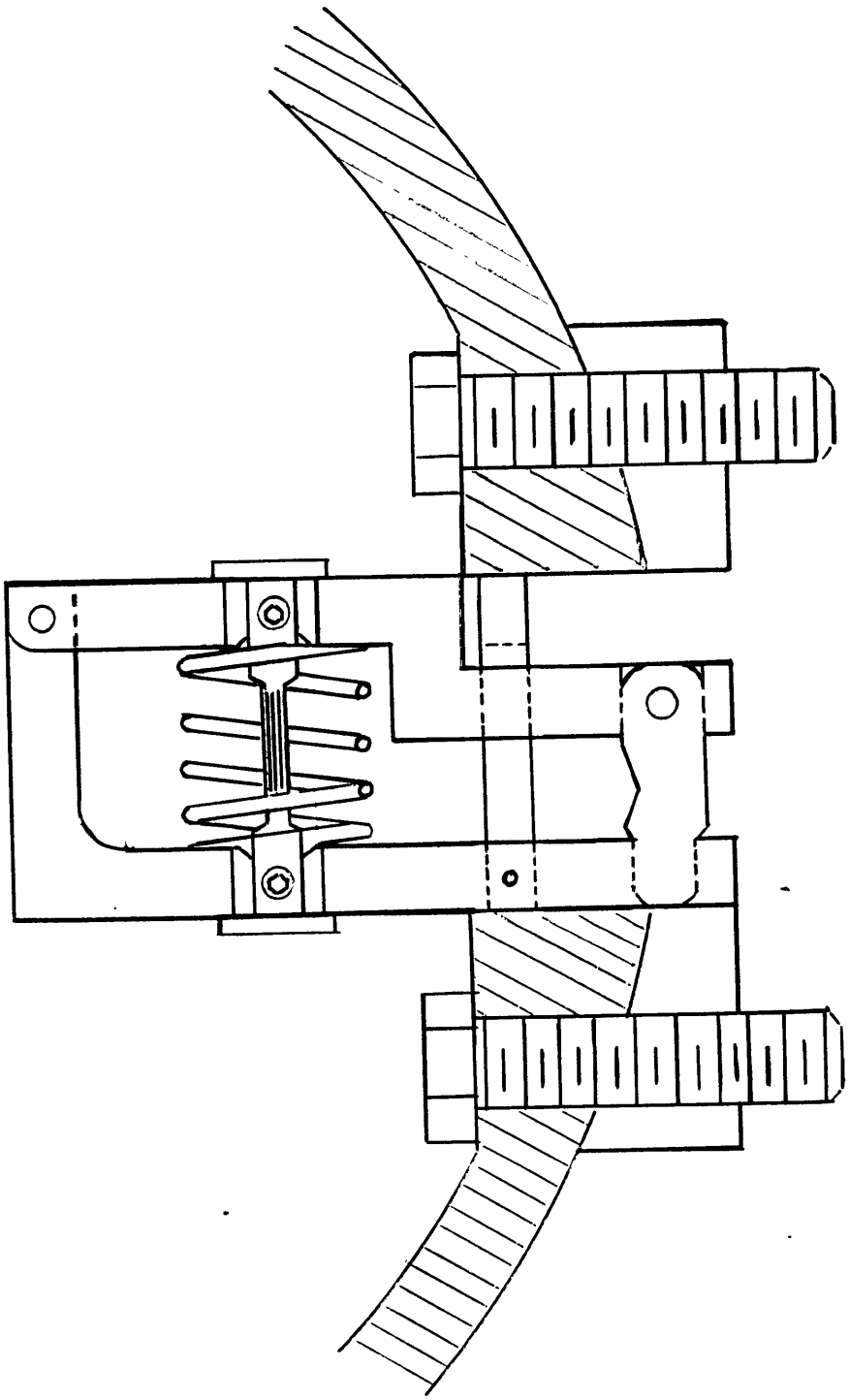

Fig. 5.4. The modified Van Dorn magnesium weight release.

an electrolyte (sea-water) causes the rapid deterioration of the magnesium rod. When the rod is reduced to its breaking point, the jaws are forced open, releasing any attached weight.

All of the critical features are retained in this modified design. The most critical for repeatability is constant tension on the magnesium rod regardless of orientation or weight of the anchor.

The spring, supplied by Hardware Products Co., Boston, is stainless steel with a spring constant of 70 pounds per inch. The magnesium rod, supplied by A. R. Purdy Co., Lyndhurst, N.J., is ¼" extruded round alloy AZ-31B. The jaws are brass for good electrical contact.

The primary factor controlling release time is the diameter of the machined magnesium rod. In tests conducted by Van Dorn and Bradner, the operation of the release was found to be virtually independent of pressure and the normal ranges of salinity, slightly dependent upon temperature, but strongly dependent upon contact resistance. Provided care was taken to keep all surfaces clean

(removing precipitates with dilute nitric acid and degreasing contacts with an orgainc solvent) Van Dorn found that machining with a tolerance of 0.001" yielded a mean error of less than 2%.

Tests conducted on the modified release at M.I.T. showed that Van Dorn's report omitted or assumed one important consideration. In addition to rod diameter, the release times were found to be dependent upon the geometry of the electrochemical cell. At diameters close to the breaking point, variations in the width of the machined portion could cause variations of up to 50% in the release time. In particular, when the machined portion is but a small gap ($< 1/8$"), the thinned portion is protected from corrosion by the adjacent thick portion which is closer to the steel electrode. On the other hand, attempts to widen the thinned portion result in variable cross-section as the rod, close to its breaking point, flexes away from the machining tool.

Future users might find it profitable to investigate the availability of magnesium wire in the cross section desired when

working close to the breaking point. Another possibility would be the use of an electric release with the magnesium release as a fail-safe.

CHAPTER SIX

ERROR ANALYSIS

6.1 Instrument Errors

6.11 Accelerometer

The construction and causes of drift in the vibrating string were discussed in Chapter Three. The major part of the drift in a simple string appears in the first order term of the Maclaurin's series, $K_1 g$. The Arma vibrating string is prestressed and so the major instability for each string occurs in the term K_0. Taking the difference frequency for the two strings reduces the null term to $(K_{01}-K_{02})$. The instability of this term is reduced in proportion to which the two strings are identical. By inverting the strings for each measurement the null term is eliminated identically and do we are concerned, in practice, with only the first order term, $2(K_{11}+K_{12})$.

It is interseting to note that the drift in the difference frequency alone, Figure 6.11, is an order of magnitude worse than

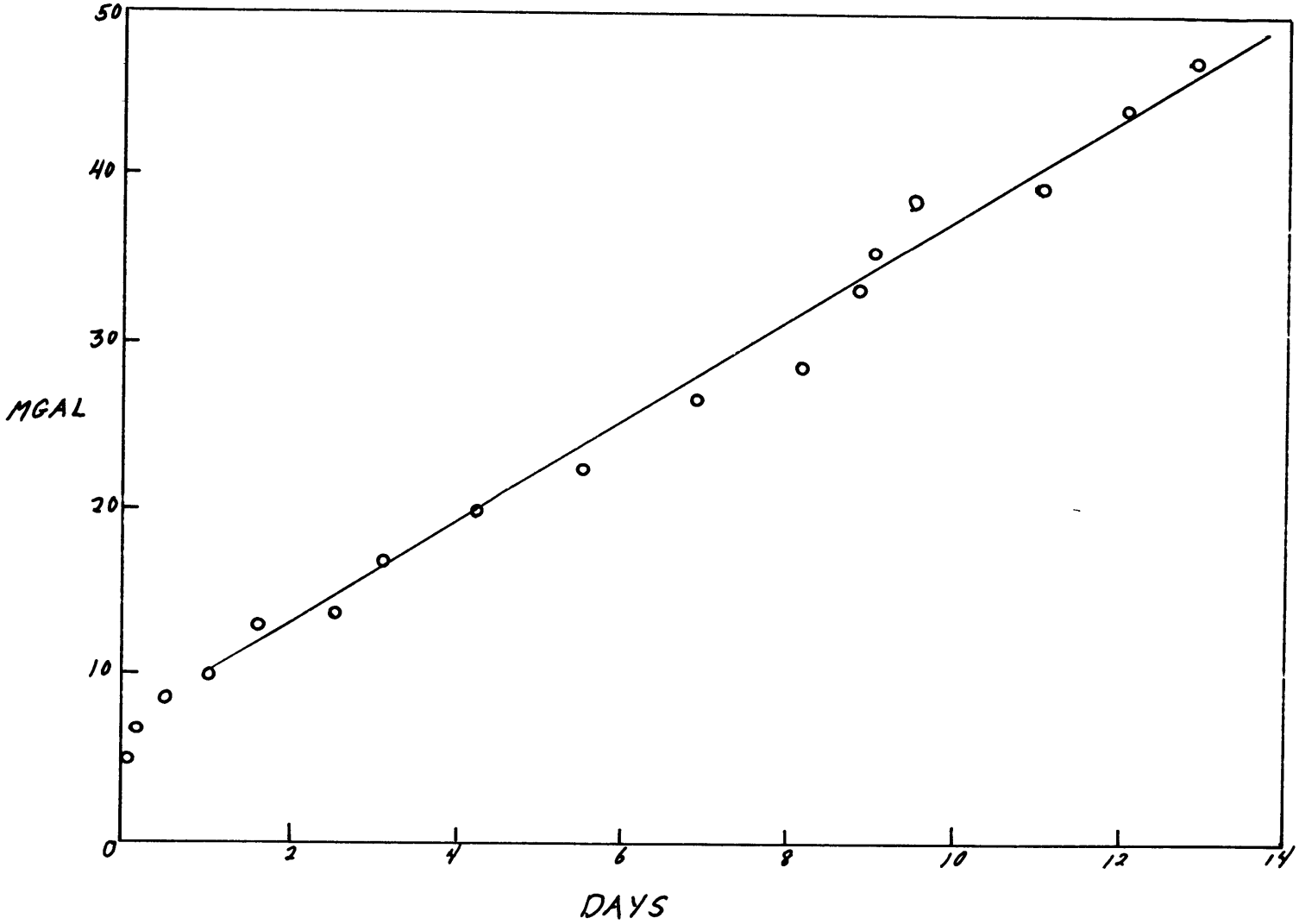

Fig. 6.11. Accelerometer difference frequency drift.

the drift with inversion. The inversion drift, Part 1, Figure 3, was found by taking nine values over a twenty-two day period while maintaining a constant temperature. Each value is the mean of five successive readings.

The jump in the readings after the second day is, no doubt, a tare inflicted during handling. Drift must be considered exclusive of tares since they are so unpredictable. A major tare may be detected by comparing the linear portions of drift before and after the cruise. With no tares, the two lines should be segments of the same straight line.

None of the points, three through nine, deviate more than ±0.8 mgal from any straight line drawn through any two ante- and post-dated points. On the basis of this curve, the error, after correction for linear drift, is less than ±0.8 mgal for two weeks.

6.12 Supply Voltage

A typical discharge curve for the silver-cadmium battery is shown in Part 1, Figure 4-3. If the battery were always charged

under identical conditions the discharge curves would be identical. This requirement may be difficult to fulfill since charging periods dictated more by available time than state of charge. In any case, the curve is always smooth.

The supply voltage dependence of the accelerometer frequency was found by running the voltage through a range of 20.0 to 34.0 volts in steps of 1 volt with a Keithley precision power supply (accuracy of 10 millivolts) and observing frequency with a preset counter. This was done six times to allow for drift correction. The voltage effects on ΔF_{+g} and ΔF_{-g} were found separately and then combined for the overall effect.

To correct a measurement to $\pm$0.1 mgal we need to read supply voltage to $\pm$0.05 volts. The supply voltage is biased with a battery of either nineteen or twenty-two Eveready E4 mercury cells (25.65 or 29.70 volts) and the difference is read with a $\pm$1.5% Simpson meter on the 2.5 Volt scale. Voltage is measured at each lowering and values for the actual time of measurement are found by

interpolation.

6.13 Off-level Error

The error due to off-level is 10^{-8}g for $\pm$1' and 10^{-7}g for $\pm$2.2', (Section 4.11). With clean mercury in the cavities, the off-level is commonly less than 1'. With older mercury, the error rises to an apparent plateau of about 2'. The maximum off-level error is therefore less than 0.1 mgal.

6.14 Oscillator Drift

The stable oscillator (Manson Labs FFO-144A) is rated at $1/10^8$/day. The actual drift, after a twenty-four hour warmup, was observed to be about $3/10^8$/week when compared with a Hewlett-Packard oscillator rated at $1/10^8$/week. Ideally, the oscillator should run continuously for twenty-four hours before any measurements. However, from a cold start (20°C.) the oven reaches temperature within 50 minutes and the oscillator error at that time is less than 0.1 mgal, Figure 6.14).

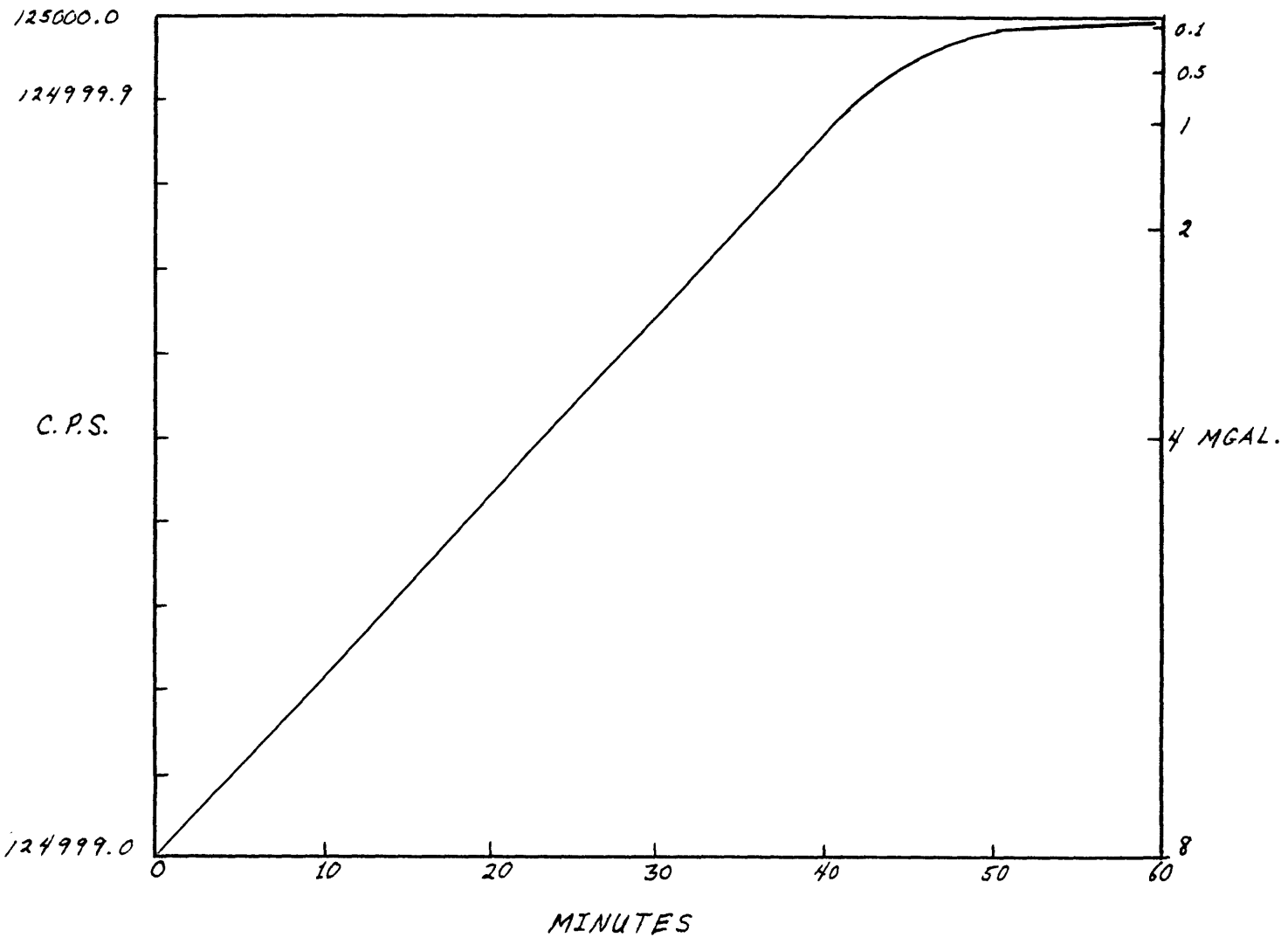

Fig. 6.14. Stable oscillator warmup from 20°C.

6.15 Counter

The counter error is of three parts:

a) a ±1 count ambiguity inherent in all digital counters,

b) precision (voltage level repeatability) of the Schmitt trigger,

c) jitter in the accelerometer signal.

One count is equivalent to about 0.1 mgal. Trigger repeatability at constant temperature is less than ±10 millivolts. With a signal amplitude of 10 volts, the phase repeatability is less than ±0.001 radian or ±0.00016 cycle. With a count of 3072 cycles, trigger error reduces to ±0.05 mgal. Jitter has been measured at ±0.0005 cycles under laboratory conditions. Underwater, in the sealed aluminum ball, the jitter should be further reduced. Based on the maximum figure of ±0.0005 cycles, jitter error is less than ±0.15 mgal.

The sum of the maximum individual errors is ±0.30 mgal and being random, the error for three consecutive measurements is less than ±0.20 mgal.

6.2 Reduction Errors

6.21 Position Relative to Ship

Figure 6.21 shows the method of locating the acoustic sound source (pinger) on the bottom. The ship (A) proceeds on a straight course, towing one or two hydrophones. The signals from the hydrophones appear on a Precision Depth Recorder (hereafter, P.D.R.) filtered for 4.2 kc. The P.D.R. has a constant sweep rate. The pinger has been calibrated to have the same repetition rate at the bottom ambient temperature.

Using only one hydrophone, approach or recession from the pinger will appear as opposite slopes in the P.D.R. record (Doppler effect). When the distance between pinger and hydrophone is not changing the slope becomes zero. This is the point when the pinger is directly abeam the ship. The abeam line is a line of position (LOP). After passing this point the ship changes course 90^{o} and a new LOP is found. The intersection of LOP's is the pinger position.

With two hydrophones boxing may be accomplished even when the

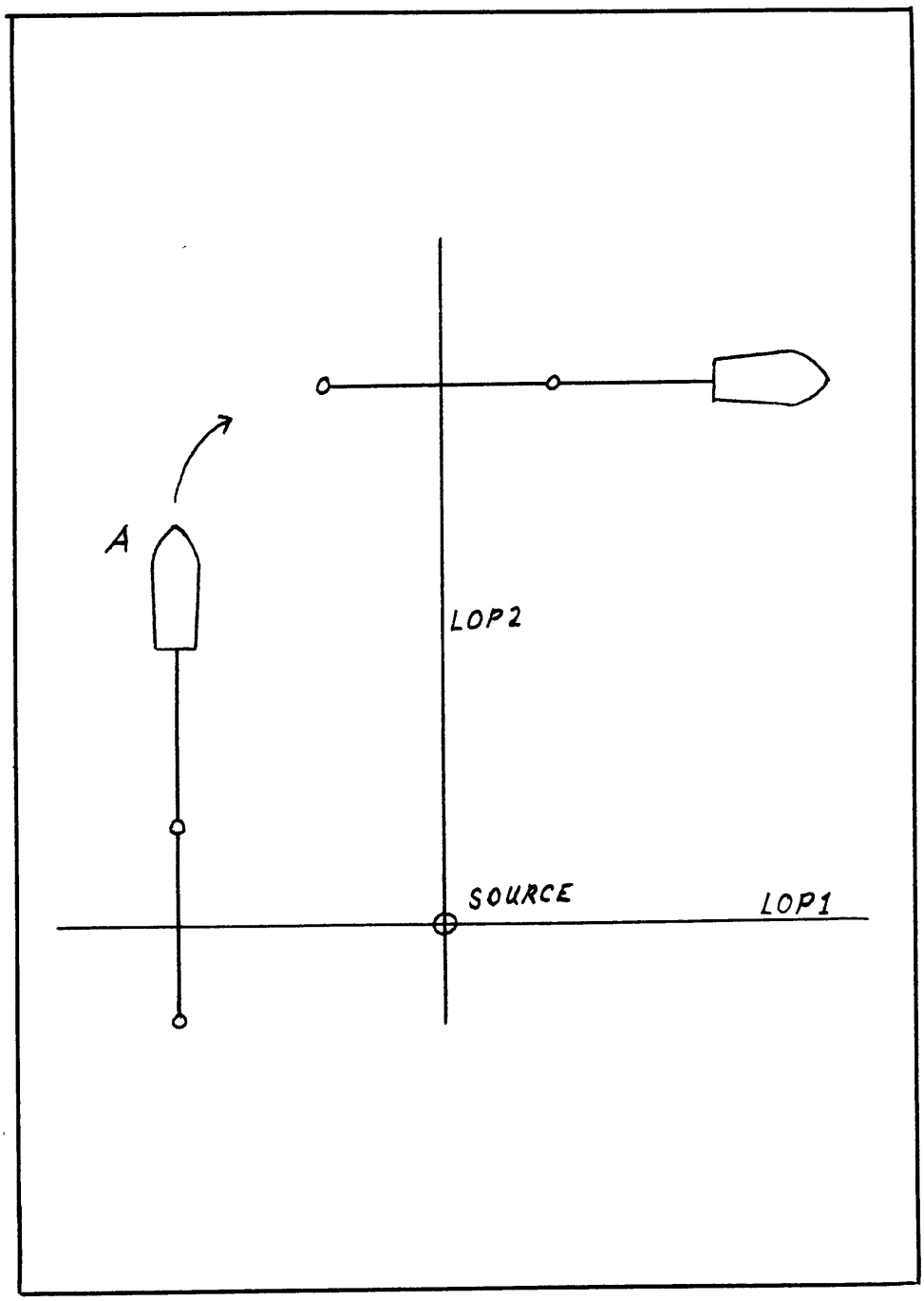

Fig. 6.21. "Boxing"the sound source.

pinger and PDR sweep rates are somewhat different. The hydrophones are recorded for short periods in alternation. Each hydrophone may yield a sloped segment. However, the offset between adjacent segments will be zero only when the pinger is directly abeam the line between the two hydrophones. Care must be taken that the gain of the two hydrophones be identical. Otherwise, a higher gain signal may appear to be arriving sooner.

A time difference of 0.01 second may be easily read from the P.D.R. At close ranges, the pinger lies at a steep angle and refraction of the sound path may be ignored. Given the time uncertainty and the depth, the uncertainty in relative position is a simple trigonometric calculation. For example, using $\pm$0.01 second and 3,000 fathoms, the uncertainty is $\pm$ 1400 feet. At a latitude of 20° the uncertainty in latitude correction is $\pm$0.20 mgal.

Less frequently, the differences in arrival time of the hydrophones are observed on a dual-beam oscilloscope. Theoretically, the major source of error is then the difference in depth of the

hydrophones. Practically, however, it is impossible to obtain a clean enough signal to fulfill the theoretical promise. Proponents of this method claim an uncertainty of about ±700 feet in 3,000 fathoms.

6.22 Position of the Ship

At mid-latitudes, the latitude correction based upon ship's position may be the major source of error. At latitude 45° this correction is about 1.3 mgal/mile and anything less than one mile accuracy is unacceptible. At the other extreme, radar navigation will reduce this error to the order of ±0.1 mgal. The most common of good long range navigation systems at present is Loran C. V.L.F. navigation is useful provided the positioning of the data points on the bottom is not critical, as the ships position can only be determined after the event.

The most useful navigation system available on a Woods Hole Oceanographic vessel is Geon (Gyro Erected Optical Navigation) with an r.m.s. error of ±0.15 mile. Error limits may be set at ±0.2 mile for a 20° latitude error of ±0.2 mgal.

6.23 Depth Correction

The depth correction amounts to 1 mgal/14.7 feet. In nine cases out of ten, it is only relative depth which is required. Relative depth of the gravimeter may be obtained in two ways.

a) In most deep ocean areas water properties change very slowly horizontally. Thus, for determination of relative depth by relative echo times, they often need not be considered. With a narrow beam sonar and a level bottom with little relief, the relative depth may be read to the order of the relief within the sonar beam or ± 5 feet, whichever is greater. When the bottom slopes more than 1°, indicated depths are not to be trusted, as first arrivals are not necessarily indicative of true depth.

b) When bottom relief is considerable, the protected and unprotected reversing thermometer pair may be used as a pressure transducer. It is a common belief among oceanographers that the reversing thermometer has a precision on only 1% as a pressure transducer. This is true enough when used on a hydrographic wire with its extreme vibrations. Calibration under laboratory conditions, however, reveal a precision of better than 0.1% (Folsom, 1963).

We are interested in precision of depth measurement. Therefore, in addition to precision of pressure measurement we must consider variations in the density field.

$$P = \int \rho \, dz = \bar{\rho} z$$

$$dP = \bar{\rho} \, dz + z d\bar{\rho}$$

$$dz = dP/\bar{\rho} - z(d\bar{\rho}/\bar{\rho})$$

The error of thermometer repeatability is $(dP/\bar{\rho})$

The error of density variation is $z(d\bar{\rho}/\bar{\rho})$

Let $z = 20{,}000$ feet

$$\frac{dP}{P} = \pm 0.001$$

$$\bar{\rho} = 1.0$$

$$d\bar{\rho} = \pm 0.0001 \quad (d\bar{v}_t = \pm 00.10)$$

Then $(dP/\bar{\rho}) = \pm 20$ feet or ± 1.36 mgal

$z(d\bar{\rho}/\bar{\rho}) = \pm 1$ foot or ± 0.06 mgal

The variation in $\bar{\rho}$ may be considered as the upper bound for a scale investigation in most areas. Therefore the depth error by thermometer is ± 0.068 mgal/1000 feet.

REFERENCES

Allan, T.D., P. Dehlinger, C. Gantar, J.C. Harrison, C. Morelli, and M. Pisani, Comparison of Graf-Askania and LaCoste and Romberg surface-ship gravity meters on the R.V. Aragonese, J. Geophys. Res., 67, 5157 - 5162, 1962.

Bernstein, R., and C.O. Bowin, Real-time digital computer acquisition and computation of gravity data at sea, I.E.E.E. Trans. on Geo. Sciences Electronics, Vol. GE-1,1, 1963.

Bertrand, G., principle of a method for rapid measurement of the relative value of g, C.R. Acad. Sci., paris, 207, 356 - 357, 1938.

Beyer, L.A., R.E. von Huene, T.H. McCulloh, and J.R. Lovett, Measuring gravity on the sea floor in deep water, J. Geophys. Res., 71, 2091 - 2100, 1966.

Browne, B.C., The measurement of gravity at sea, Monthly Not. Roy. Astr. Soc. Geophys. Suppl. London, 3, 271 - 279, 1937.

Bunce, E.T., and D.A. Fahlquist, Geophysical investigations of the Puerto Rico Trench and outer ridge, J. Geophys. Res., 67, 3955 - 3971, 1962.

Campbell, G.A. and R.M. Foster, Fourier Integrals for Practical Application, Van Nostrand, New York, 177 pp., 1948.

Coriolis, G.G., Traite de la Mecanique de Corps Solides, Paris, 1844.

Dean, W.C., Frequency analysis for gravity and magnetic interpretations, Geophysics, 23, 97 - 127, 1958.

Dehlinger, P. Reliability at sea of gimbal-suspended gravity meters with 0.7 critically damped accelerometers, J. Geophys. Res., 69, 5383 - 5394, 1964.

Ewing, J.I., J.L. Worzel, and M. Ewing, Sediments and oceanic structural history of the Gulf of Mexico, J. Geophys. Res., 67, 2509 - 2527. 1962.

Fanning, K.F. and S.K. Garoutte, Gravity meter operational check range, Rhode Island Sound area, reprint G-1-62, U.S. Naval Oceanographic Office, Washington, 1962a.

Fanning, K.F. and S.K. Garoutte, Gravity meter evaluation and training range, Chesapeake Bay, reprint G-2-62, U.S. Naval Oceanographic Office, Washington, 1962b.

Folsom, T.R., Transducers for oceanic research - a wide scope, in Marine Sciences Instrumentation, Vol. 2, edited by R.D. Gaul, Plenum Press, New York, 1963.

Frowe, E., Adiving bell for underwater gravimeter operation, Geophysics, 12, 1 - 12, 1947.

Gilbert, R.L.G., A dynamic gravimeter of novel design, Proc Phys. Soc. Lond. B,62, 445 - 454, 1949.

Gilbert, R.L.G., Gravity observations in a borehole, Nature, 170, 424 - 425, 1952.

Godby, E.A., R.C. Baker, M.E. Bower, and P.J. Hood, Aeromagnetic reconnaisance of the Laborador Sea, J. Geophys. Res., 71, 511 - 517, 1966.

Goodacre, A.K. A shipborne gravimeter testing range near Halifax, Nova Scotia, J. Geophys. Res., 69, 5373 - 5381, 1964.

Goodell, R.R., and C.H. Faye, Borehole gravity meter and its application, Geophysics, 29, 774 - 782, 1964.

Graf, A., and S. Reinhard, Improvements of the sea gravimeter Gss-2, J. Geophys. Res., 66, 1813 - 1821, 1961.

Grant, F.S., and G.F. West, Interpretation Theory in Applied Geophysics, McGraw-Hill, New York, 583 pp., 1965.

Harrison, J.C., A laboratory investigation of the second order corrections to gravity measured at sea, Monthly Not. Roy. Astr. Soc. Geophys. Suppl., 7, 22 - 31, 1954.

Hayes, H.C., Method and apparatus for determining the force of gravity, U.S. Patent No. 1,995,305, 1935.

Heiskanen, W.A., and F.A. Vening-Meinesz, The Earth and its Gravity Field, McGraw-Hill, New York, 470 pp., 1958.

Hubbert, M. King, A line-integral method for computing the gravimetric effects of two dimensional masses, Geophysics, 13, 215 - 225, 1948.

LaCoste, L.J.B., Surface-ship gravity measurements on the Texas A. and M. College ship, the "Hidalgo", Geophysics, 24, 309 - 322, 1959.

Langseth, M.G., P.J. Grim, and M. Ewing, Heat flow measurements in the East Pacific Ocean, J. Geophys. Res., 70, 367 - 380, 1965.

Lozinskaya, A.M., A string gravimeter for measurements of gravity at sea, Isv. Akad. nauk SSSR, ser. geofiz., Moskva, 3, 398 - 409, 1959.

Marks, L.S., Mechanical Engineers' Handbook, 6th ed., McGraw-Hill, New York, 1958.

Morelli, C., Gravity measurements on surface-ships, Le Petrole et la Mer, Sect. 1, No. 107, 1 - 9, 1965.

Munk, W.H., Long ocean waves, in The Sea, Vol. 1, edited by M.N. Hill, 647 - 663, Interscience, New York, 1962.

Nettleton, L.L., Geophysical Prospecting for Oil, McGraw-Hill, New York, 444 pp., 1940.

Nettleton, L.L., Regionals, residuals, and structures, Geophysics, 19, 10 - 22, 1954.

Northrop, J., R.A. Frosch, and R. Frassetto, Bermuda-New England seamount arc, Bulletin G.S.A., 73, 587 - 594, 1962.

Pepper, T.B., The Gulf Underwater Gravimeter, Geophysics, 6, 34 - 44, 1941.

Peters, L.J., The direct approach to magnetic interpretation and its practical application, Geophysics, 14, 290 - 320, 1949.

Rayleigh, J.W.S., The Theory of Sound, Dover, New York, 320 pp., 1945.

Shurbet, G.L., and J.L. Worzel, Gravity anomalies associated with seamounts, Bulletin G.S.A., 66, 777 - 782, 1955.

Swartz, C.A., and V.M. Sokoloff, Filtering associated with selective sampling of geophysical data, Geophysics, 19, 402 - 419, 1954.

Talwani, M., J.L. Worzel, and M. Landisman, Rapid gravity computations for two-dimensional bodies with application to the Mendocino submarine fracture zone, J. Geophys. Res., 64, 49 - 59, 1959.

Talwani, M., G.H. Sutton, and J.L. Worzel, A crustal section across the Puerto Rico Trench, J. Geophys. Res., 64, 1545 - 1555, 1959.

Talwani, M., and M. Ewing, Rapid computation of gravitational attraction of three-dimensional bodies of arbitrary shape, Geophysics, 25, 203 - 225, 1960.

Tomoda, Y., and H. Kanamori, Tokyo surface-ship gravity meter Y-1, The Ocean Research Institute, Univ. of Tokyo, Collected Reprints, Vol. 1, 116 - 145, 1962.

Vening-Meinesz, F.A., Theory and Practice of Pendulum Observations at Sea, Publ. Neth. Geod. Comm., Waltman, Delft, 95 pp., 1929.

Vening-Meinesz, F.A., Gravity Expeditions at Sea, 1923 - 1938, Vol. 4, Publ. Neth Geod. Comm., Waltman, Delft, 233 pp., 1948.

Van Dorn, W.G., The marine release-delay timer, Scripps Institution of Oceanography Reference 53-23, 1953.

Wall, R.E., M. Talwani, and J.L. Worzel, Cross-coupling and off-leveling errors in gravity measurements at sea, J. Geophys. Res., 71, 465 - 483, 1966.

Worzel, J.L., and J.C. Harrison, Gravity at sea, in The Sea, Vol. 3, edited by M.N. Hill, 134 - 174, Interscience, New York, 1963.

Worzel, J.L., Gravity at sea, U.S. Nat. Rep. 1960 - 1963, Trans. A.G.U., 44, 356 - 358, 1963.

Worzel, J.L., Pendulum Gravity Measurements at Sea, 1936 - 1959, Wiley, New York, 422 pp., 1965.

Wyckoff, R.D., The Gulf Gravimeter, Geophysics, 6, 13 - 44, 1941.

ACKNOWLEDGEMENTS

This work was performed under Office of Naval Research contract Nonr 1841(74). Machine computations were done at the Computation Center of the Massachusetts Institute of Technology.

The accelerometer was generously loaned by the U.S. Air Force. Invaluable aid was rendered by the accelerometer manufacturer, Arma Division, American Bosch Arma Corporation in the person of Dr. Robert Bock.

The two theses advisors, Dr. William S. von Arx and Dr. Frank Press cleared the path of several seemingly insurmountable obstacles. Valuable suggestions were made by many fellow graduate students, particularly Mr. George Beardsley and Mr. Thomas Sanford.

Needless to say, major credit goes to the author's wife Susan who, with the patience of Job, waited.

BIOGRAPHICAL SKETCH

Charles Goddard Wing was born on April 26, 1939 in Portland, Maine. He graduated from Hartford Public High School, Hartford, Connecticut in 1957. Bowdoin College in Brunswick, Maine was attended on a National Merit Scholarship from 1957 to 1961. Elected to Phi Beta Kappa in the Junior year, he received the A.B. in physics with highest honors in 1961.

He entered Massachusetts Institute of Technology in 1961 on a National Science Foundation Fellowship. From 1962 to 1966 he was supported by a research assistantship in the Department of Geology and Geophysics.

He was married in 1962 to Susan Black of Winchester, Massachusetts. They have two sons, Charles H. and Gregory T.

APPENDICES

APPENDIX A

Gravity Interpretation - Two Dimensions

The time required per measurement with the on-the-bottom gravimeter practically limits investigations to single profiles. With a single profile, reasonable interpretations are best made in the case of two dimensional structures. By "two dimensional" is meant a structure where the ratio of maximum to mean dimension is greater than five (Grant and West, 1965). Hubbert (1948) showed that the gravitational attraction of a two dimensional structure could be computed by a line integral around the structure periphery. Talwani, et al.(1959) developed an algorithm for machine computation of the line integral.

Let such a two dimensional structure be represented by Figure A-1 where $-\infty < y < \infty$

and let ρ = const. = $\Delta\rho$

then, $$U(x,z) = -G\,\Delta\rho \int_{s} dx_o\, dz_o \int_{-\infty}^{\infty} \left[(x-x_o)^2+(y-y_o)^2+(z-z_o)^2\right]^{-\frac{1}{2}} dy_o$$

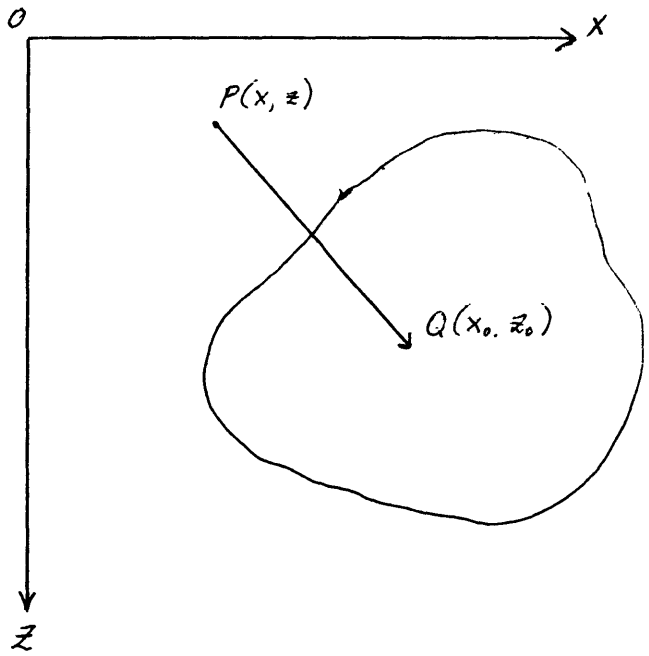

Figure A-1 A two dimensional body.

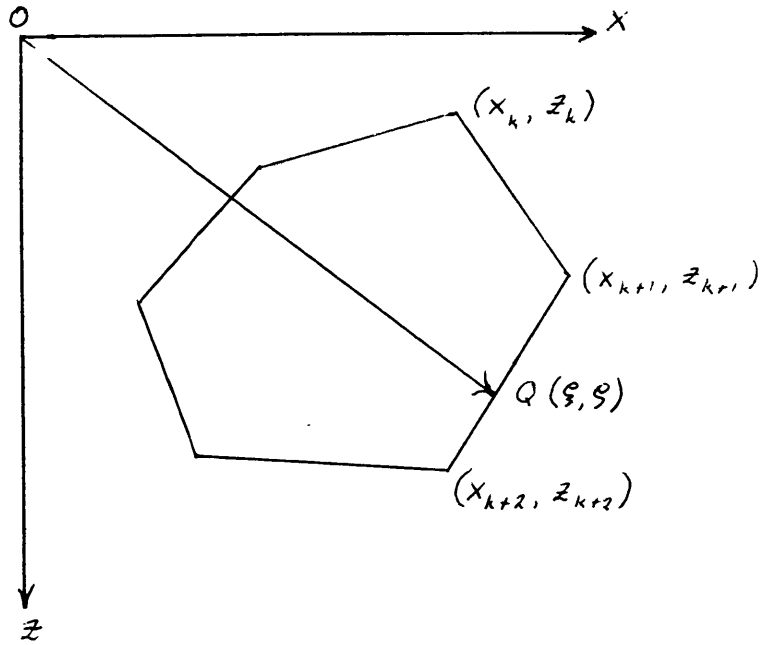

Figure A-2 A two dimensional polygon.

Move the origin so that $P(x,z) = P(0,0)$

$$U_p = 2G\Delta\rho \int \log_e R \, dx_0 \, dz_0$$

$$\Delta g_p = \partial U_p / \partial z = 2G\Delta\rho \int \frac{\partial R/\partial z}{R} dx_0 \, dz_0$$

where $R = (x_0^2 + z_0^2)^{1/2}$

$$\Delta g_p = 2G\Delta\rho \int \frac{z_0 \, dx_0 \, dz_0}{x_0^2 + z_0^2}$$

$$= 2G\Delta\rho \oint \tan^{-1}(x_0/z_0) \, dz_0$$

Now let the body be approximated by an n-sided polygon as in Figure A-2. Let the coordinates of the vertices by (x_k, z_k). The equations of the sides are: $\zeta = a_k \xi + b_k$

where $$a_k = \frac{x_{k+1} - x_k}{z_{k+1} - z_k}$$

$$b_k = \frac{x_k z_{k+1} - x_{k+1} z_k}{z_{k+1} - z_k}$$

then $$\Delta g_p = 2G\Delta\rho \oint \tan^{-1} \zeta/\xi \, d\xi$$

$$= 2G\Delta\rho \sum_{k=1}^{n} \int_{z_k}^{z_{k+1}} \tan^{-1}(a_k + b_k/\xi) \, d\xi$$

$$= 2G\Delta\rho \sum_{k=1}^{n} \frac{b_k}{1+a_k^2} \left[\tfrac{1}{2} \log_e \left(\frac{x_{k+1}^2 + z_{k+1}^2}{x_k^2 + z_k^2} \right) + a_k \left(\tan^{-1} \frac{x_{k+1}}{z_{k+1}} - \tan^{-1} \frac{x_k}{z_k} \right) \right]$$

There follows a listing of a Fortran II program based upon this algorithm.

```
*      M4795-4398,FMS,DEBUG,2,2,1000,0        CHARLES WING X5738
*      XEQ
*      LABEL
CDG2
C         TWO DIMENSIONAL GRAVITY PROGRAM WHERE
C         X ARRAY IS X COORDINATES OF ORIGINAL POLYGON
C         Z ARRAY IS Z COORDINATES OF ORIGINAL POLYGON
C         N = NUMBER OF POLYGON SIDES
C         L = NUMBER OF COMPUTED POINTS (ANOMALIES)
C         SX,SZ ARE COORDINATES OF L POINTS
C         G = GRAV. CONST.  0.2035 FOR 100 FEET. 6.670 FOR 1 KM.
C         NPOLY = NUMBER OF POLYGONS
C         MAIN PROGRAM
      DIMENSION X(100),Z(100),SX(100),SZ(100),DGZ(100),N(1),L(1),DR(1),N
     1P1(1),G(1),GRAV(50,100)
  100 READ 4, L,NPOLY,G
      READ 3, (SX(I),I=1,L)
      READ 3, (SZ(I),I=1,L)
      DO 50 NP=1,NPOLY
      READ 1,NAME,N,NP1,DR
      READ 3, (X(I),I=1,NP1)
      READ 3, (Z(I),I=1,NP1)
      PRINT 7,NAME
      PRINT 2,N,L,DR
      PRINT 8
      PRINT 9
      DO 30 J=2,L
      SUM = 0.0
      DO 20 K=1,N
      H=(Z(K+1)-Z(K))/(X(K+1)-X(K))
      IF (H) 71,79,72
   71 C=3.141593 + ATANF(H)
      GO TO 79
   72 C= ATANF(H)
   79 IF (X(K)) 90,90,91
   90 A=3.141593 + ATANF(Z(K)/X(K))
      GO TO 94
   91 IF (Z(K)) 92,93,93
   92 A=6.283186 + ATANF(Z(K)/X(K))
      GO TO 94
   93 A= ATANF(Z(K)/X(K))
   94 IF (X(K+1)) 95,95,96
   95 B=3.141593 + ATANF(Z(K+1)/X(K+1))
      GO TO 99
   96 IF (Z(K+1)) 97,98,98
   97 B=6.283186 + ATANF(Z(K+1)/X(K+1))
      GO TO 99
   98 B= ATANF(Z(K+1)/X(K+1))
   99 IF (X(K+1)-X(K)) 81,85,81
   81 IF(Z(K+1)-Z(K)) 82,86,82
   82 D=X(K+1)+Z(K+1)*((X(K+1)-X(K))/(Z(K)-Z(K+1)))
      E=(COSF(A)*(TANF(A)-TANF(C)))/(COSF(B)*(TANF(B)-TANF(C)))
      IF (E) 83,83,84
   83 E=0.0001
   84 F=D*SINF(C)*COSF(C)*(A-B+TANF(C)*LOGF(E))
```

```
      GO TO 87
   85 F=X(K)*LOGF(COSF(A)/COSF(B))
      GO TO 87
   86 F=Z(K)*(B-A)
   87 SUM = SUM + F
      DG = 2.0*G*DR*SUM
   20 CONTINUE
      DGZ(J-1)=DG
      SFT = -(SX(J)-SX(J-1))
      CALL SHIFT(X,SFT,NP1)
      SFT = -(SZ(J)-SZ(J-1))
      CALL SHIFT(Z,SFT,NP1)
      PRINT 11, SX(J-1),SZ(J-1),DGZ(J-1)
      GRAV(NP,J-1) = DGZ(J-1)
   30 CONTINUE
   50 CONTINUE
      PRINT 12
      PRINT 9
      DO 70 J=2,L
      SUM = 0.0
      DO 60 NP=1,NPOLY
   60 SUM = SUM + GRAV(NP,J-1)
      PRINT 11, SX(J-1), SZ(J-1), SUM
   70 CONTINUE
      GO TO 100
    1 FORMAT (A6,I3,I3,F5.2)
    2 FORMAT (1H012HPOLYGON HAS I3,8H SIDES. 18HDATA COMPUTED FOR I3,9H
     1POINTS. 18HDENSITY CONTRAST =F5.2)
    3 FORMAT (9F8.2)
    4 FORMAT (I3,I3,F8.4)
    7 FORMAT (1H120HRESULTS FOR POLYGON A6)
    8 FORMAT (1H040HVERTICAL GRAVITY ANOMALIES VS X AND Z MG)
    9 FORMAT (1H06X,1HX9X,1HZ9X,4HMGAL)
   11 FORMAT (2F10.1,F10.2)
   12 FORMAT (1H014HTOTAL ANOMALY.)
      END
      SUBROUTINE SHIFT(A,S,N)
      DIMENSION A(1)
      DO 40 I=1,N
      A(I) = A(I)+S
   40 CONTINUE
      RETURN
      END
*     DATA
```

APPENDIX B

Gravity Interpretation - Three Dimensions

A similar three dimensional algorithm has been written by Talwani, et al. (1960). The n-sided polygons in this case lie in the x - y plane and are stacked in the z-direction.

Let V be the anomaly due to unit thickness of ABCDEF at point P in Figure B-1. Then the total gravity anomaly at P due to a stack of polygons will be:

$$\Delta g_p = \int_{z\ \text{bottom}}^{z\ \text{top}} V(Z)dz$$

V is proportional to the solid angle subtended by ABCDEF at P.

$$V(z) = G\Delta\rho \left[\oint d\psi - \oint \frac{z\, d\psi}{(r^2+z^2)^{1/2}} \right]$$

On side BC:

$$r = p_i / \sin(\phi_i - \psi_{i+1} + \psi_i)$$

Then for the portion BC:

$$V_{BC} = V_{i,i+1} = G\Delta\rho \left[\psi_{i+1} - \psi_i - \sin^{-1} \frac{z\cos\theta_i}{(p_i^2+z^2)^{1/2}} + \sin^{-1} \frac{z\cos\phi_i}{(p_i^2+z^2)^{1/2}} \right]$$

And for the whole polygon ABCDEF

$$V = \sum_{i=1}^{n} V_{i,i+1}$$

Also

$$\sum_{i=1}^{n} (\psi_{i+1} - \psi_i) = 2\pi$$

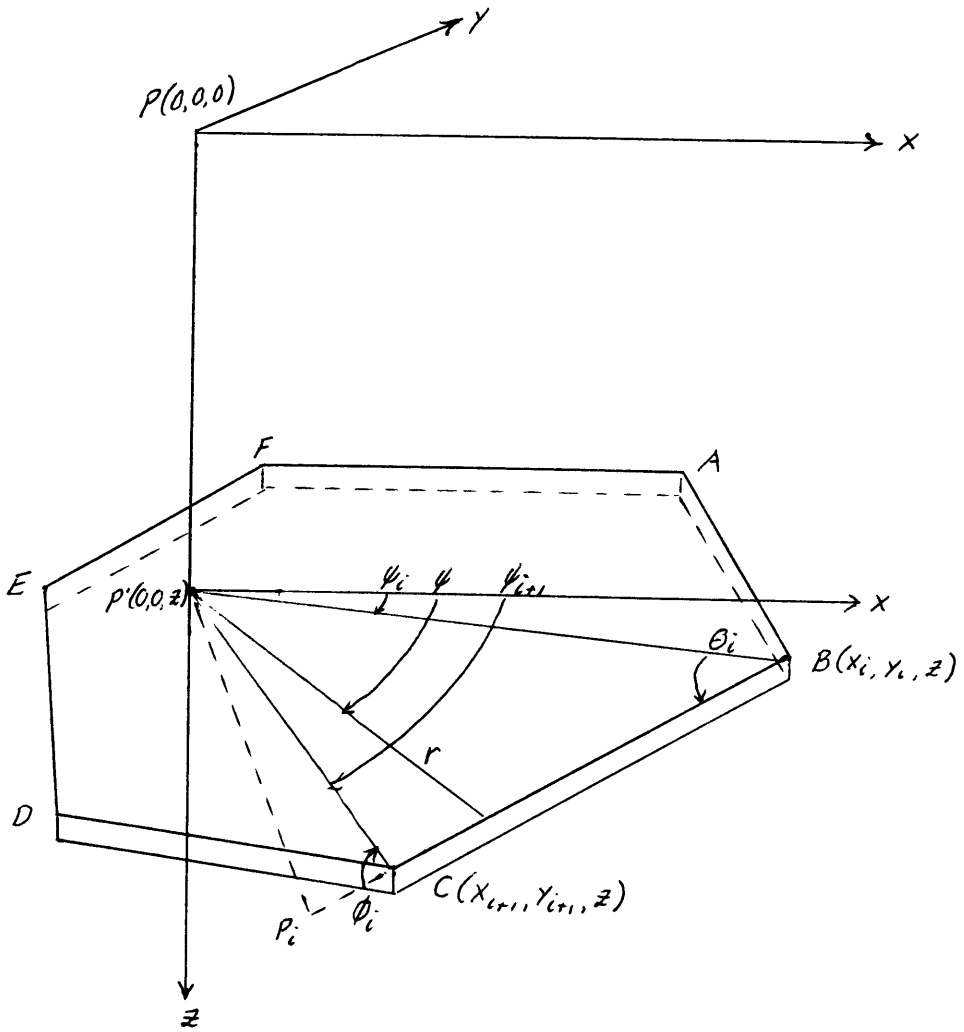

Figure B-1 A three dimensional polygon.

For machine computation ψ_i, θ_i, ϕ_i, P_i must be expressed in terms of x_i, y_i.

Then, $$V = G\Delta\rho \sum_{i=1}^{n} \left[W\cos^{-1}\left\{ \left(x_i/r_i\right)\left(x_{i+1}/r_{i+1}\right) + \left(y_i/r_i\right)\left(y_{i+1}/r_{i+1}\right) \right\} - \sin^{-1}\left\{ \frac{z q_i S}{(p_i^2 + z^2)^{1/2}} \right\} + \sin^{-1}\left\{ \frac{z f_i S}{(p_i^2 + z^2)^{1/2}} \right\} \right]$$

where: $S = 1$, $p_i > 0$
$S = -1$, $p_i < 0$
$W = 1$, $m_i > 0$
$W = -1$, $m_i < 0$

$$p_i = \frac{y_i - y_{i+1}}{r_{i,i+1}} x_i - \frac{x_i - x_{i+1}}{r_{i,i+1}} y_i$$

$$q_i = \frac{x_i - x_{i+1}}{r_{i,i+1}}\left(x_i/r_i\right) + \frac{y_i - y_{i+1}}{r_{i,i+1}}\left(y_{i+1}/r_i\right)$$

$$f_i = \frac{x_i - x_{i+1}}{r_{i,i+1}}\left(x_{i+1}/r_{i+1}\right) + \frac{y_i - y_{i+1}}{r_{i,i+1}}\left(y_{i+1}/r_{i+1}\right)$$

$$m_i = \left(y_i/r_i\right)\left(x_{i+1}/r_{i+1}\right) - \left(y_{i+1}/r_{i+1}\right)\left(x_i/r_i\right)$$

$$r_i = \left(x_i^2 + y_i^2\right)^{1/2}$$

$$r_{i+1} = \left(x_{i+1}^2 + y_{i+1}^2\right)^{1/2}$$

$$r_{i,i+1} = \left[(x_i - x_{i+1})^2 + (y_i - y_{i+1})^2 \right]^{1/2}$$

When V(z) has been obtained, a numerical integration must be performed for $$\Delta g_p = \int_{z_{bottom}}^{z_{top}} V(z)\,dz$$ The method of integration used depends upon the degree of accuracy desired, but a simple Simpson's rule will usually suffice. A Fortran II program using this algorithm also follows.

The investigation of a three dimensional structure where none of the parameters are known can only be undertaken with a two-dimensional gravity coverage. However, if the structure outline were know (by seismic profiling), then a single gravity profile could yield the density contrast, $\Delta\rho$. In such a case the three dimensional gravity program can be used to compute the single gravity profile.

```
*      M4795-4398,FMS,DEBUG,2,2,1000,0        CHARLES WING X5738
*      XEQ
*      LABEL
CDG3
C      THREE DIMENSIONAL GRAVITY PROGRAM WHERE
C      X(I,J) ARE X COORDINATES OF POLYGON J
C      Y(I,J) ARE Y COORDINATES OF POLYGON J
C      N = NUMBER OF POLYGON SIDES
C      NP1 = N+1
C      NZ = NUMBER OF POLYGONS
C      H = POLYGON THICKNESS
C      L = NUMBER OF DG POINTS
C      G = GRAV. CONST.  0.2035 FOR A(100FT), 6.670 FOR ( 1.0 KM)
C      SX,SY = COORDINATES OF DG POINTS
C      DR(J) = DENSITY CONTRAST OF  POLYGON J
C      MAIN PROGRAM BEGINS HERE
       DIMENSION N(1),NP1(1),NZ(1),L(1),DR(20),SX(100),SY(100),X(36,20),Y
      1(36,20),Z(20),V(20,100),DG(100),H(1)
  150  READ 1,N,NP1,NZ,L,H,G
       READ 2,((X(I,J),I=1,NP1),J=1,NZ)
       READ 2,((Y(I,J),I=1,NP1),J=1,NZ)
       READ 2,(Z(I),I=1,NZ)
       READ 2,(SX(I),I=1,L)
       READ 2,(SY(I),I=1,L)
       READ 3,(DR(J),J=1,NZ)
       PRINT 4,N,NZ,L
       PRINT 5
       LM1 = L-1
       DO 100 K=1,LM1
       DO 30 J=1,NZ
       SUM = 0.0
       DO 20 I=1,N
       RI = SQRTF(X(I,J)**2+Y(I,J)**2)
       RP = SQRTF(X(I+1,J)**2+Y(I+1,J)**2)
       RIP=SQRTF((X(I,J)-X(I+1,J))**2+(Y(I,J)-Y(I+1,J))**2)
       P=((Y(I,J)-Y(I+1,J))*X(I,J)-(X(I,J)-X(I+1,J))*Y(I,J))/RIP
       Q=((X(I,J)-X(I+1,J))*(X(I,J)/RI)+(Y(I,J)-Y(I+1,J))*(Y(I,J)/RI))/RI
      1P
       F=((X(I,J)-X(I+1,J))*X(I+1,J)+(Y(I,J)-Y(I+1,J))*Y(I+1,J))/(RIP*RP)
       O=(Y(I,J)*X(I+1,J)-Y(I+1,J)*X(I,J))/(RI*RP)
       IF(P) 40,40,50
   40  S=-1.0
       GO TO 60
   50  S=1.0
   60  IF(O) 70,70,80
   70  W=-1.0
       GO TO 90
   80  W=1.0
   90  SUM = SUM+W*ACOSF((X(I,J)*X(I+1,J)+Y(I,J)*Y(I+1,J))/(RI*RP))-ASINF
      1((Z(J)*Q*S)/SQRTF(P**2+Z(J)**2))+ASINF((Z(J)*F*S)/SQRTF(P**2+Z(J)*
      2*2))
   20  CONTINUE
       V(J,K)=G*DR(J)*SUM
   30  CONTINUE
       ODD = 0.0
```

```
      EVEN = 0.0
      NZM1 = NZ-1
      DO 130 J=2,2,NZM1
      EVEN = EVEN+V(J,K)
  130 CONTINUE
      NZM2 = NZ-2
      DO 140 J=3,2,NZM2
      ODD = ODD + V(J,K)
  140 CONTINUE
      DG(K)=(V(1,K)+V(NZ,K)+4.0*EVEN+2.0*ODD)*(H/3.0)
      SFT= -(SX(K+1)-SX(K))
      CALL SHIFT(X,NZ,NP1,SFT)
      SFT = -(SY(K+1)-SY(K))
      CALL SHIFT(Y,NZ,NP1,SFT)
      PRINT 6,SX(K),SY(K),DG(K)
  100 CONTINUE
      PRINT 7
      PRINT 8, ((V(J,K),J=1,NZ),K=1,LM1)
      GO TO 150
    1 FORMAT (4I5, F5.1, F7.4)
    2 FORMAT (9F8.1)
    3 FORMAT (12F6.2)
    4 FORMAT(1H112HPOLYGON HAS I3,18H SIDES. THERE ARE I3,38H POLYGONS.
     1ANOMALIES ARE COMPUTED FOR I3,8H POINTS.)
    5 FORMAT(1H05X,1HX8X,1HY8X,5HMGALS)
    6 FORMAT(3F9.1)
    7 FORMAT (1H 17HV(J,K) AS STORED.)
    8 FORMAT (11F9.2)
      END
      SUBROUTINE SHIFT(A,NZ,NP1,SFT)
      DIMENSION A(36,20)
      DO 110 J=1,NZ
      DO 110 I=1,NP1
      A(I,J)=A(I,J)+SFT
  110 CONTINUE
      RETURN
      END
*     DATA
```

APPENDIX C

DOWNWARD CONTINUATION PROGRAM

Dean (1958) has shown that all of the common operations performed on gravity data have their analogues in linear electric filters.

Let $V_o(t)$ = output of the linear filter
$V_i(t)$ = input " " " "
$W(\tau)$ = weighting function, the response to an impulse

Then
$$V_o(t) = \int_{-\infty}^{\infty} V_i(t-\tau)W(\tau)\,d\tau \qquad (1)$$

A function of time may be expressed as a function of frequency by the Fourier transform,

$$V(\omega) = \int_{-\infty}^{\infty} V(t)e^{-i\omega t}dt \qquad (2)$$

and conversely

$$V(t) = 1/2\pi \int_{-\infty}^{\infty} V(\omega)e^{+i\omega t}d\omega \qquad (3)$$

Taking the Fourier transform of the convolution (eq. 1)

$$V_0(\omega) = V_i(\omega)Y(\omega) \qquad (4)$$

where $Y(\omega)$, the frequency response, is the Fourier transform of the weighting function.

The same theory applies to functions of space variables. Using space variables x,y, the equation for continuation of the vertical gravity component is (Peters, 1948):

$$F_z(x,y,z) = -1/2\pi \int_{-\infty}^{\infty}\int_{-\infty}^{\infty} F_z \frac{(x-a,y-b)z\ da\ db}{(z^2+a^2+b^2)^{3/2}}$$

or

$$V_o(x,y) = \int_{-\infty}^{\infty}\int_{-\infty}^{\infty} V_i(x-a,y-b)W(a,b)dadb$$

The weighting function is $\frac{-z/2\pi}{(x^2+y^2+z^2)^{3/2}}$

and the frequency response is the Fourier transform

$$e^{+z\sqrt{u^2+v^2}} \quad \text{(Campbell and Foster, 1948)}$$

For downward continuation, z = +h

$$Y_{down} = e^{+h\sqrt{u^2+v^2}}$$

For upward continuation, z = -h

$$Y_{up} = e^{-h\sqrt{u^2+v^2}}$$

In the analogous two dimensional case

$$Y_{down} = e^{+hu}$$

$$Y_{up} = e^{-hu}$$

ALGORITHM

$$Y_{down} = e^{+hu}$$

$$= \sum_{n=-N}^{+N}{}' W_n e^{-iun\Delta x}$$

$$= W_o + 2\sum_{n=1}^{N-1} W_n \cos um\Delta x + W_N \cos uN\Delta x$$

$$W_n = 1/N\left[\tfrac{1}{2} + \sum_{k=1}^{N-1} e^{hk\Delta u}\cos(kn\pi/M) + \tfrac{1}{2}(e^{hN\Delta u})\cos n\pi\right]$$

where $\Delta u = \pi/N\Delta x$

$$G_{bottom}(m\Delta x) = \sum_{n=-N}^{+N} W_n G_{surface}(m\Delta x - n\Delta x)$$

With smoothing, $Y_{down}(u) = e^{+hu}\cdot e^{-au^2}$

```
*      M4795-4398,FMS,DEBUG,2,2,1000,0        CHARLES WING X5738
*      XEQ
*      LABEL
CDG6
C         2D DOWNWARD CONTINUATION WITH NORMAL ERROR CURVE SMOOTHING
C         H = DEPTH OF CONTINUATION IN KM.
C         DU = PI/M*DX
C         DX = DATA SPACING IN KM.
C         M = NUMBER OF COEFFICIENTS - 1
C           = NUMBER OF CONTINUED POINTS
      DIMENSION GS(100),GB(100),W(100)
  100 READ 1, N,H,DU,M3,AW
      READ 2,(GS(I),I=1,M3)
      PI = 3.1415926
      M=N
      MM1=M-1
      MP1=M+1
      DO 20 I=1,M
      SUM = 0.0
      DO 30 J=1,MM1
      FJ=J
      FI=I
      FM=M
      E=(H*FJ*DU-(AW*FJ*DU)**2)
      F=(H*FM*DU-(AW*FM*DU)**2)
      A=EXPF(E)*COSF(FJ*FI*PI/FM)
      SUM=SUM+A
   30 CONTINUE
      W(I)=(0.5+SUM+0.5*EXPF(F)*COSF(FI*PI))/FM
   20 CONTINUE
      SUM = 0.0
      DO 40 J=1,MM1
      FJ=J
      E=(H*FJ*DU-(AW*FJ*DU)**2)
      B=EXPF(E)
      SUM = SUM + B
   40 CONTINUE
      WO=(0.5+SUM+0.5*EXPF(F))/FM
      DO 50 I=1,M
      SUM = 0.0
      DO 60 J=1,N
      NM=N+I-J
      NP=N+I+J
      C=W(J)*(GS(NM)+GS(NP))
      SUM = SUM + C
   60 CONTINUE
      NI=N+I
      GB(I)=SUM+WO*GS(NI)
   50 CONTINUE
      PRINT 10
      PRINT 11,WO
      PRINT 12,(W(I),I=1,M)
      PRINT 13
      PRINT 14,(GB(I),I=1,M)
    1 FORMAT (I3,F5.2,F10.8,I3,F5.2)
```

```
    2 FORMAT (12F6.2)
   10 FORMAT (1H022HVALUES OF WO AND W(N).)
   11 FORMAT (F18.8)
   12 FORMAT (4F18.8)
   13 FORMAT (1H136HDOWNWARD CONTINUED ANOMALIES, GB(I).)
   14 FORMAT (F10.2)
      GO TO 100
      END
*     DATA
```

APPENDIX D

A Double String Surface-Ship Gravity Meter

D.1 Previous attempts to use a vibrating string for surface ship gravimetry have all failed because of a single fact: the single string is non-linear. A double string sensor is proposed which, due to its great increase in linearity, is capable of an accuracy of $\pm$1 mgal in the presence of $\pm$100,000 mgal wave accelerations.

D.2 Linearity of the Single String

The frequency of the vibrating string as given before is:

$$f = \frac{1}{2L}\sqrt{Mg/m}$$

For convenience we change notation:

G = acceleration of gravity

g = disturbing acceleration of waves

Then $f = \frac{1}{2L}\sqrt{M(G+g)/m}$

$= K(G+g)^{\frac{1}{2}}$

Expand in powers of (g/G):

$$f_{+g} = KG^{\frac{1}{2}} \left[1 + \frac{1}{2}(g/G) - \frac{1}{8}(g/G)^2 + \frac{3}{48}(g/G)^3 - \frac{5}{128}(g/G)^4 + \cdots\right]$$

$$f_{-g} = KG^{\frac{1}{2}} \left[1 - \frac{1}{2}(g/G) - \frac{1}{8}(g/G)^2 - \frac{3}{48}(g/G)^3 - \frac{5}{128}(g/G)^4 - \cdots\right]$$

When $g = 0$, the mean frequency is $\frac{f_0 + f_0}{2} = KG^{\frac{1}{2}}$

When $g \neq 0$

$$\frac{f_{+g} + f_{-g}}{2} = KG^{\frac{1}{2}} \left[1 - \frac{1}{8}(g/G)^2 - \frac{5}{128}(g/G)^4 - \cdots\right]$$

The difference in the mean is the <u>non-linear error</u>:

$$-KG^{\frac{1}{2}} \left[\frac{1}{8}(g/G)^2 + \frac{5}{128}(g/G)^4 + \cdots\right]$$

When $g = \pm 100{,}000$ mgals, the error = -1254 mgals

In using the single string either an analogue operational amplifier or a computer program must correct for this error. In either case, as Tomoda and Kanamori (1962) have pointed out, a systematic error in correcting the non-linearity exists, due to the finite spacing of sample points.

$$\Delta g/G = \frac{3}{8}(g/G)^2 \left[1 - \left(\frac{\sin\frac{\tau\pi}{T}}{\frac{\tau\pi}{T}}\right)^2\right]$$

where τ = sample period

T = period of disturbance

With g = 100,000 mgals and T = 6 sec., for Δg = 1 mgal, we must have τ = 0.06 seconds. This results in about 10^4 data points over a ten minute period. It would require a good sized computer to apply corrections and digitally filter.

D.3 Linearity of the Double String

Using the Maclaurin's series notation for the individual string frequency, Section 3.31:

$$F_{1,+g} = K_{01} + K_{11}(G+g) + K_{21}(G+g)^2 + K_{31}(G+g)^3 + K_{41}(G+g)^4 + \cdots$$

$$F_{2,+g} = K_{02} - K_{12}(G+g) + K_{22}(G+g)^2 - K_{32}(G+g)^3 + K_{42}(G+g)^4 + \cdots$$

$$F_{1,-g} = K_{01} + K_{11}(G-g) + K_{21}(G-g)^2 + K_{31}(G-g)^3 + K_{41}(G-g)^4 + \cdots$$

$$F_{2,-g} = K_{02} - K_{12}(G-g) + K_{22}(G-g)^2 - K_{32}(G-g)^3 + K_{42}(G-g)^4 - \cdots$$

$$\Delta F_{+g} = (F_{1,+g} - F_{2,+g}) = (K_{01}-K_{02}) + (K_{11}+K_{12})(G+g) + (K_{21}-K_{22})(G+g)^2 + (K_{31}+K_{32})(G-g)^3 + (K_{41}-K_{42})(G+g)^4 + \cdots$$

$$\Delta F_{-g} = (F_{1,-g} - F_{2,-g}) = (K_{01}-K_{02}) + (K_{11}+K_{12})(G-g) + (K_{21}-K_{22})(G-g)^2 + (K_{31}+K_{32})(G-g)^3 + (K_{41}-K_{42})(G-g)^4 + \cdots$$

Keeping only terms in g,

$$\Delta F_{+g} = (K_{11}+K_{12})g + (K_{21}-K_{22})(2Gg+g^2) + (K_{31}+K_{32})(3G^2g+3Gg^2+g^3)$$
$$+ (K_{41}-K_{42})(4G^3g+6G^2g^2+4Gg^3+g^4)$$

$$\Delta F_{-g} = -(K_{11}+K_{12})g + (K_{21}-K_{22})(-2Gg+g^2) + (K_{31}+K_{32})(-3G^2g+3Gg^2-g^3)$$
$$+(K_{41}-K_{42})(-4G^3g+6G^2g^2-4Gg^3+g^4)$$

$$\frac{\Delta F_{+g} + \Delta F_{-g}}{2} = (K_{21}-K_{22})g^2 + (K_{31}+K_{32})(3Gg^2) + (K_{41}-K_{42})(6G^2g^2+g^4) + \cdots$$

We may use the following figures attained in the Arma Lot D vibrating string accelerometer as representative:

$$(K_{21}-K_{22}) = -8 \text{ mgal}/G^2$$

$$(K_{31}+K_{32}) = +30 \text{ mgal}/G^3$$

$$(K_{41}-K_{42}) = 1 \text{ mgal}/G^4$$

Then the <u>non-linear error</u>

$$\frac{\Delta F_{+g} + \Delta F_{-g}}{2} = -(8 \text{ mgal}/G^2)g^2 + (30 \text{ mgal}/G^3)3Gg^2 = +82 \text{ mgal}(g/G)^2$$

For example, if g = ±100,000 mgals, error = +0.82 mgal

if g = ±50,000 mgals, error = +0.20 mgal

Therefore, for g = ±100,000 mgal, non-linearity need not be considered in the double string.

D.4 Drift

The drift of the vibrating string is not as small as in either the LaCoste or Graf meters. The drift of the null term $(K_{01}-K_{02})$ may amount to as much as 1mgal/day, while the drift of the first order term $(K_{11}+K_{12})$ will be an order of magnitude less. However, a redesign of the accelerometer for 1g measurements should reduce total drift to about 1mgal/weel.

In addition, correction for null-term drift is possible at sea provided the accelerometer is periodically inverted. The null correction is accomplished by stopping the ship and inverting the gravimeter 180°. Using the series:

$$\Delta F_{+g} = (K_{01}-K_{02}) + (K_{11}+K_{12})g + \cdots 0(0)$$

$$\Delta F_{-g} = (K_{02}-K_{01}) + (K_{11}+K_{12})g + \cdots 0(0)$$

$$\Delta F_{+g} - \Delta F_{-g} = 2(K_{01}-K_{02}) + 0 + 0(0)$$

The difference of the differences yields the null term which is independent of the force of gravity or the disturbing accelerations. With a corrected drift of the order 1mgal/week, 90% of which is

linear, the double string is competetive with the LaCoste and Graf meters.

D.5 Filtering

It will now become clear that the two unique properties of the double string, extreme linearity and f.m. output, give it the advantage in data reduction.

The Graf and LaCoste meters use mechanical and analogue filters in obtaining the steady state value of G in the presence of $\pm$100,000 mgal disturbances. For an accuracy of $\pm$1 mgal, these filters must be linear to $\pm 1/10^5$. This proves difficult, if not impossible. Analogue and mechanical filters must be used because the output signal is analogue.

The double string, however, has a digital output. Digital filters can be made to have any property desired, especially linearity.

One possible method of filtering will now be described: The input signal to the gravimeter, Figure D.5-a, is the gravitational acceleration G with wave accelerations of up to 100,000 mgal

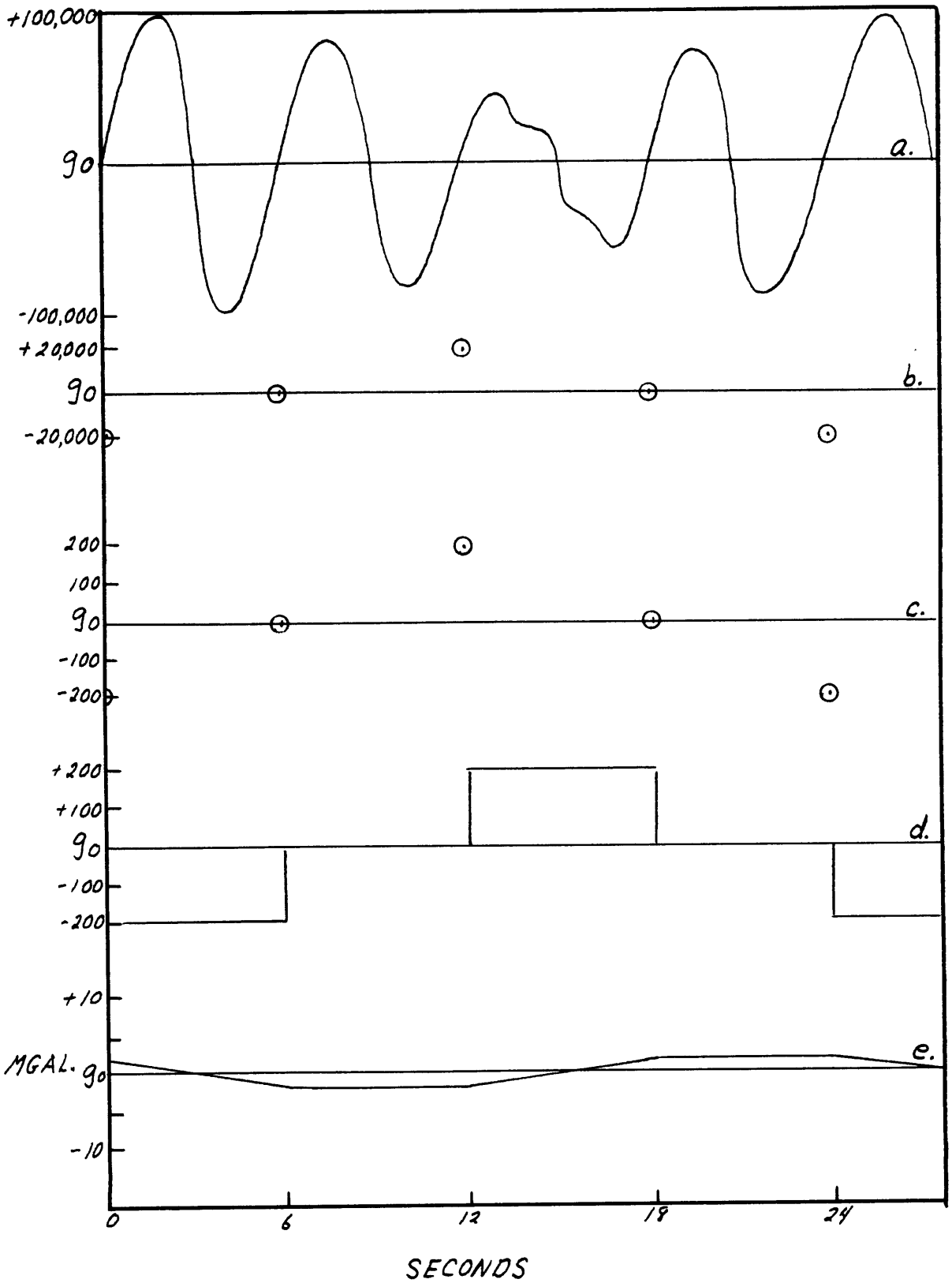

Fig. D-1. Filtering steps in proposed gravimeter.

superimposed. At one extreme, if the wave accelerations were purely sinusoidal, and if we chose our measuring periods to be exactly one wave period long, the contribution of the disturbing wave accelerations would integrate to zero.

In the other extreme, we would extend our measuring period to infinity. The mean acceleration of the waves approaches zero as the measurement period approaches infinity.

Unfortunately, neither of the two above cases may be used at sea. The first is simply not true and the second is impractical. We must use a compromise approach.

D.5-1 First Step

The output of the double string is a frequency. That frequency is measured with a preset counter. If the mean frequency due to the wave train in Figure D.5-a were measured at random intervals or at fixed intervals having no correlation with the wave phase, the scatter of the measurements would be nearly the same as the amplitude of the wave, ±100,000 mgals. However, most wave trains do have a

dominant sinusoidal component. In Figure D.5-a the dominant component has a period of six seconds. As a compromise with the first extreme, then, we choose our measurement intervals to be approximately the same as the period of the disturbing acceleration.

The choice of measurement period can be made automatically by a second vertical analogue accelerometer. We let the integrated output voltage from the second accelerometer fire a Scmitt Trigger. The trigger voltage may be chosen to correspond to a wave velocity of zero. The Scmitt trigger, through logic circuitry, controls the preset counter. Then the preset counter output is the mean string difference frequency between succeeding wave velocity zeros. If the second accelerometer and the associated electronics were perfect, the above method would be limited only by the ± 1 preset count ambiguity. As an extremely conservative figure, the scatter in acceleration measurements would be reduced by 70 - 80%. A more likely figure would be 95%. In the following discussion it should be remembered that the likely performance is nearly an order of magnitude better.

D.5-2 Second Step

In the average case we have so far reduced the ±100,000 mgal disturbing accelerations to a mean reading every six seconds of magnitude 20,000 - 30,000 mgals, Figure D.5-b.

We now take a running mean of the preceding 100 mean accelerations. This may be accomplished by either a 100 register push-down list in a computer or a continuous loop magnetic tape. To the preceding sum of 100 means, the latest mean period is added; the 100th is subtracted; and the sum is divided by 100. By the nature of the mean, the scatter in measurements is now reduced by a factor of 100 to 200-300 mgals, Figure D.5-c.

It is important to note that up to this point the information has not been distorted in any way as it would be with a mechanical or analogue filter. By the nature of digital operations, not a single bit of information has been lost.

D.5-3 Third Step

At this point we must turn to the electric filter to obtain the

final data form, a strip chart recording. Digital to analogue conversion with a precision of 0.01% is routine. Input to the electric filter will be voltage values with scatter of ±200-300 mgal and periods of about six seconds, Figure D.5-d.

We choose a filter with a time constant of five minutes. The input period for each data point will be six seconds or 2% of the time constant. A signal of ±300 mgals will therefore change the filter output by about ±6 mgals. The analogue signal from the filter will appear with a scatter of ±4-6 mgals on a strip chart recorder as in Figure D.5-e. The best straight line, drawn by eye will be the value of G.

The total filtering time for ±100,000 mgals is 15 minutes. This assumes there are no significant accelerations with periods greater than 15 minutes. No gravimeter will ever overcome this difficulty by any method other than a longer filtering time. In addition, the above analysis assumes a constant value of G over the 15 minute period, but again, all gravimeters make this assumption.

Wave accelerations of smaller magnitude allow shorter filtering times. The filtering time in the double string may be varied very simply, while mechanical filtering is difficult to change. This is an important consideration. The filtering time should always be set at the minimum practical value in order that variation in G not be filtered and consequently distorted and delayed more than is necessary.

D.6 Additional Errors

Other gravimeters must apply corrections for:

a) Browne effect, if hung in gimbals,

b) Harrison effect if mounted on a stable platform with periodic stabilization error,

c) cross-coupling effect when the weigh-beam displacement is correlated with horizontal accelerations.

The double string is small enough (2" diameter X 5" length and 1 lb. weight, including oven) to be mounted on a very precise stable platform ($\pm 1'$). It therefore has no Browne error or Harrison error. In addition, the sensing mass is cross-supported

so that there is negligible cross-coupling.

The LaCoste-Romberg and Graf meters are very complicated electromechanical devices. Aside from the electronic components, they have had a rather poor reliability record. In contrast, the Arma Lot D double string proved to have a mean time between failures of $>$ 50,000 hours.